

University of Jordan
Faculty of Graduate Studies



Handwritten notes in the left margin: $\frac{1}{2}$, $\frac{1}{4}$, $\frac{1}{8}$, and $\frac{1}{16}$.

Wavelet Analysis of Dynamic Response : Flow Induced Vibration of a Single Cylinder in a Cross Flow

Nabeel Hamdi Abdullah Shabaneh

Supervised by

Prof. Bassam Ali Jubran

Co-Supervised by

Dr. Moh'd Nader Hamdan

عميد كلية الدراسات العليا

Submitted in Partial Fulfillment of the Requirements for the Degree of
Master of Science in Mechanical Engineering
Faculty of Graduate Studies,
University of Jordan.

April / 1995.

COMMITTEE DECISION

This thesis was defended successfully on 24, April 1995.

COMMITTEE MEMBERS

SIGNATURE

1. Prof. Bassam Ali Jubran



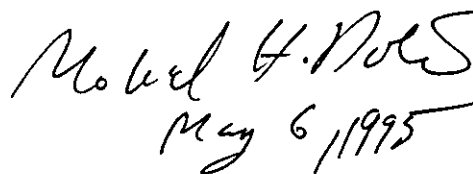
2. Dr. Moh'd Nader Hamdan



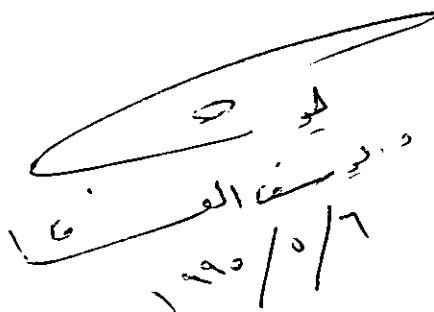
3. Dr. Mazen Al-Qaisi



4. Dr. Mohammad H. Dado



5. Dr. Yousef Al-Assaf



DEDICATION

**To My
Parents
Brothers
and
Sisters
With
Love.**

ACKNOWLEDGMENTS

It is a pleasure to express my deepest gratitude to Prof. Bassam A. Jubran and to Dr. Mohammad N. Hamdan, whom without their support and valuable advice, my work could have been more difficult. It is also a pleasure to thank Dr. Yousef Al-Assaf for his support and encouragement. In addition, it is a pleasure to express my appreciation to both Dr. Ali Badran and Dr. M. A. Hamdan for their administrative assistance.

The gracious help of those at the Mechanical Engineering Laboratories, the Industrial Engineering Laboratories and the Engineering Computer Laboratories is highly appreciated.

I am completely indebted to my family members for their constant support and encouragement during my long preparation for this work.

Special thanks to all my friends, who helped me to accomplish this work; especially Nasser A. Qasem, Moh'd Abu-Samak and Ahmad S. Salaymeh.

TABLE OF CONTENTS

COMMITTEE DECISION.....	ii
DEDICATION	iii
ACKNOWLEDGMENTS.....	iv
TABLE OF CONTENTS	v
LIST OF FIGURES.....	viii
NOMENCLATURE.....	xi
ABSTRACT IN ENGLISH.....	xiv
CHAPTER 1 : INTRODUCTION	1
1.1 Introduction	1
1.2 Objectives of the Thesis	3
1.2 Layout of the Thesis.....	4
CHAPTER 2 : FLOW INDUCED VIBRATION	6
2.1 Introduction	6
2.2 The Flow Induced Vibration Phenomena.....	7
2.3 Forms of Flow Induced Vibration.....	9
2.3.1 Vortex Shedding.....	9
2.3.2 Fluid-Elastic Excitation (Galloping)	10
2.3.3 Flutter	11
2.3.4 Acoustic Excitation	11
2.4 Vibrations Induced By an Oscillating Flow	12
2.5 Literature Survey.....	12
CHAPTER 3 : SIGNAL PROCESSING	22
3.1 Introduction :	22
3.2 Classical Methods	22
3.2.1 the Autocorrelation.....	23
3.2.2 The Power Spectrum	23
3.3 Joint Time-Frequency Analysis	25

3.3.1 The Short-Time Fourier Transform.....	26
3.3.2 Gabor Transform & Zak Transform.....	27
3.3.3 The Wavelet Transform	31
3.4 Literature Survey	38
CHAPTER 4 : CHAOS	43
4.1 Introduction	43
4.2 Chaos Descriptors	44
4.3 Properties Of Chaos	45
4.3.1 Chaotic Attractors	45
4.3.2 Structural Stability And Bifurcations.....	46
4.3.3 Stability And Lyapunov Exponents	48
4.3.4. Fractal Dimension	50
4.4 Routes To Chaos	52
4.5 Literature Survey.....	53
CHAPTER 5 : EXPERIMENTAL SETUP & PROCEDURE.....	57
5.1 Introduction	57
5.2 Apparatus	57
5.3 The Test Model	57
5.4 Instrumentation.....	59
5.5 Experimental Procedure	59
5.6 Instrumentation and WT Program Testing.....	60
5.7 Repeatability of Measurements.....	61
CHAPTER 6 : RESULTS AND DISCUSSION.....	65
6.1 Introduction	65
6.2 Signal Processing Results.....	65
6.3 Chaotic Behavior Investigations	72
CHAPTER 7 : CONCLUSIONS & RECOMMENDATIONS.....	94
7.1 Introduction	94
7.2 Conclusions	94

7.3 Recommendations	95
REFERENCES	97
APPENDIX A	110
APPENDIX B	118
APPENDIX C	132
ABSTRACT IN ARABIC.....	138

LIST OF FIGURES

Figure (2.1) : A Classification of Flow Induced-Vibrations [1].....	19
Figure (2.2) : Illustration of the Vortex Shedding Mechanism [1].....	20
Figure (3.1) : The Gabor Transform Algorithm [70].	39
Figure (3.2) : Time-Frequency Resolution of (a)STFT and (b)Wavelet Transform [77].....	40
Figure (3.3) : The Wavelet Transform Algorithm [13].....	41
Figure (5.1) : Experimental Setup.	61
Figure (5.2) : End plates detail [60].....	61
Figure (5.3) : The end plates and the circular cylinder used.	62
Figure (5.4) : The instruments used in the experimental investigations.....	62
Figure (5.5) : A schematic diagram for the test cylinder used in this work. ..	63
Figure (5.6) : A flow chart of the instrumentation setup used in this work. ..	63
Figure (6.1) : The time series, the corresponding autocorrelation, and the corresponding power spectrum at a free stream velocity of 19.00m/s.....	73
Figure (6.2) : The 3D-Gabor plot at a free stream velocity of 19.00m/s.....	74
Figure (6.3) : The 3D-wavelet plot using the modulated Gaussian as a mother wavelet at a free stream velocity of 19.00m/s.	75
Figure (6.4) : The 3D-wavelet plot using the Mexican hat as a mother wavelet at a free stream velocity of 19.00m/s.....	75
Figure (6.5) : The 3D-wavelet plot using the eighth derivative of the Gaussian as a mother wavelet at a free stream velocity of 19.00m/s.....	76
Figure (6.6) : The 3D-wavelet plot using Daubechies' tight frame as a mother wavelet at a free stream velocity of 19.00m/s.	76

- Figure (6.7) : The 3D-phase-plot of the wavelet on the range (0-180o) using the modulated Gaussian as a mother wavelet at a free stream velocity of 19.00m/s..... 77
- Figure (6.8) : The 3D-phase-plot of the wavelet on the range (-180o-0) using the modulated Gaussian as a mother wavelet at a free stream velocity of 19.00m/s..... 77
- Figure (6.9) : The time series, the corresponding autocorrelation, and the corresponding power spectrum at a free stream velocity of 4.98m/s..... 78
- Figure (6.10) : The 3D-wavelet plot using the modulated Gaussian as a mother wavelet at a free stream velocity of 4.98m/s. 79
- Figure (6.11) : Another view of Figure (6.10) using a shorter time scale..... 79
- Figure (6.12) : The time series, the corresponding autocorrelation, and the corresponding power spectrum at a free stream velocity of 5.50m/s..... 80
- Figure (6.13) : The 3D-wavelet plot using the modulated Gaussian as a mother wavelet at a free stream velocity of 5.50m/s. 81
- Figure (6.14) : The time series, the corresponding autocorrelation, and the corresponding power spectrum at a free stream velocity of 24.08m/s..... 82
- Figure (6.15) : The 3D-wavelet plot using the modulated Gaussian as a mother wavelet at a free stream velocity of 24.08m/s. 83
- Figure (6.16) : The first time series, the corresponding autocorrelation, and the corresponding power spectrum at a free stream velocity of 26.00m/s..... 84
- Figure (6.17) : The second time series, the corresponding autocorrelation, and the corresponding power spectrum at a free stream velocity of 26.00m/s..... 85

- Figure (6.18) : The 3D-wavelet plot of the first time series using the modulated Gaussian as a mother wavelet at a free stream velocity of 26.00m/s..... 86
- Figure (6.19) : The 3D-wavelet plot of the second time series using the modulated Gaussian as a mother wavelet at a free stream velocity of 26.00m/s..... 86
- Figure (6.20) : (a) Phase plot, (b) Poincaré map, and (c) the correlation dimension factor at a free stream velocity of 4.98m/s. 87
- Figure (6.21) : (a) Phase plot, (b) Poincaré map, and (c) the correlation dimension factor at a free stream velocity of 5.50m/s. 88
- Figure (6.22) : (a) Phase plot, (b) Poincaré map, and (c) the correlation dimension factor at a free stream velocity of 19.00m/s. 89
- Figure (6.23) : (a) Phase plot, (b) Poincaré map, and (c) the correlation dimension factor at a free stream velocity of 24.08m/s. 90
- Figure (6.24) : (a) Phase plot, (b) Poincaré map, and (c) the correlation dimension factor at a free stream velocity of 26.00m/s. 91
- Figure (6.25) : The correlation dimension factor versus the free stream velocity..... 92

NOMENCLATURE

- $a(\tau, \omega)$: The cross-ambiguity function.
 a_{mn} : Gabor coefficients.
 \bar{C} : Closed trajectory solutions (limit cycles) in the phase space.
 $C(r)$: The correlation function.
 D : The diameter of the circular cylinder.
 D_2 : The order-2 information dimension.
 $D_{x_0} \phi$: The derivative of the solutions in the phase space with respect to the initial conditions.
 f_n : The natural frequency of the cylinder.
 f_{nz} : The translational-mode natural frequency.
 $f_{n\theta}$: The rotational-mode natural frequency.
 f_s : The sampling frequency.
 f_v : The Karman vortex-shedding frequency.
 f_o : Centered frequency of the wavelet.
 $G(\omega)$: The Fourier Transform of the synthesis window.
 $G^*(\omega)$: The Fourier Transform of the analysis window.
 $g(t)$: The synthesis window.
 $g^*(t)$: The analysis window.
 g_{mn} : Gabor bases.
 $H(\omega)$: The Fourier Transform of the mother wavelet.
 $h(t)$: The mother or basic wavelet.
 $h_{a,b}(t)$: The family of wavelets constructed from the mother wavelet by shift in time b , and dilation in scale a .
 \mathbf{I} : The identity matrix.
 $L^2(\mathbf{R})$: The Hilbert space of the square integrable functions.
 $P_{m,n}$: The discrete wavelet transform phase coefficients taken at a scale factor of m and at a time shift factor of n .

- p : The period of a periodic solution.
 Re : Reynolds number.
 $R_x(\tau)$: The autocorrelation function.
 S_t : The Strouhal number.
 $S_x(f)$: The power spectrum.
 S_α : Linear subspaces of a tangent initial conditions space.
 $T_x M$: The tangent space of the matrix \bar{X} .
 $T_{x_0} M$: The tangent space of the initial conditions matrix \bar{X}_0 .
 t : Time.
 t_n : Sampling rate of the Poincaré map.
 U_∞ : The free stream flow velocity.
 $WT_{a,b}$: The continuous wavelet transform shifted in time by b , and dilated by a scale parameter a .
 $WT_{m,n}$: The discrete wavelet transform coefficients taken at a scale factor of m and at a time shift factor of n .
 $X(\omega)$: The Fourier Transform of the time signal.
 \bar{X} : N-dimensional matrix.
 $x(t)$: The time signal.
 $Z(f)$: The Zak Transform of a function f .
 $Z_{r,s}$: The Gabor coefficients after implementing the Zak Transform.

Greek Symbols

- δ : The logarithmic decrement.
 ε : Small perturbations.
 $\phi_\tau^f(\bar{x})$: Solutions in the phase space for a vector field \bar{f} .
 λ_i : Lyapunov exponents.
 μ_i : The eigenvalues of the monodromy matrix.
 ω : Frequency.

ABSTRACT

Wavelet Analysis of Dynamic Response : Flow Induced Vibration of a Single Cylinder in a Cross Flow

Nabeel Hamdi Abdullah Shabaneh

Supervised by
Prof. Bassam Ali Jubran

Co-Supervised by
Dr. Moh'd Nader Hamdan

Published experimental data indicates that the vibration signals of an elastically mounted single cylinder in a cross flow are in general nonstationary. This important issue has been thus far ignored, where stationarity of the signals is often proposed to allow implementation of the available classical methods, such as autocorrelation and power spectrum functions.

The present work attempts to shed some lights on the dynamic process of flow induced vibration of an elastically mounted single cylinder in a cross flow using the newly developed joint time-frequency analysis techniques (JTFA), such as Gabor and wavelet transforms. Gabor transform and various wavelet transforms are implemented and the results are compared to those of the classical methods (autocorrelation and power spectrum). The wavelet transforms, which possess good time-frequency localizations, are found to be the most powerful techniques to analyze and reveal the many aspects of the complex dynamic characteristics of nonstationary signals under consideration. More specifically, the modulated Gaussian wavelet is found to be the most suitable wavelet to

analyze the flow induced vibration process. Also, the nonlinearity of the process under consideration is investigated by both classical and JTFA methods.

It is found that for certain system parameters the nonlinearity may lead the system into chaos. Furthermore, phase-plane portraits, Poincaré maps and fractal dimensions have been used to confirm the chaotic behavior of the response of the system under investigation. Recommendations for further investigations are discussed.

CHAPTER 1

INTRODUCTION

1.1 INTRODUCTION

Flow induced vibration arises in many practical engineering systems, such as heat exchangers, power transmission lines, bridges and tall towers. For example, when an elastically mounted cylinder is placed in a cross-flow (bluff body) it is generally known that as the flow separates from either side of the cylinder, vortices are shed alternately resulting in an oscillating external force which causes the cylinder to oscillate [1].

It is to be noted that large amplitude vibrations due to vortex shedding are observed when the flow free stream velocity reaches a critical value. Resonant oscillations can be excited by the incident flow if a bluff cylinder structure is flexible and lightly damped. As a consequence of this flow induced resonance, the body and wake oscillate at the same frequency as they interlock in a "somewhat" complex feedback loop, a phenomenon generally known as lock-on, where the frequency is near one of the structure characteristic frequencies [2,3]. One of the approaches traditionally used to analyze the collected data (time-series) of flow induced vibration is the spectral distribution using the Fourier transform (FT) and, sometimes, the autocorrelation function. The FT does not reveal any information about localization in time, since it assumes that the signal analyzed to be of infinite duration and the window used is representative throughout the signal, i.e. it assumes the signal to be stationary. This assumption can not hold for nonstationary signals, wherein transient effects are of much concern. Because of the many pitfalls of the FT analysis [4], new joint time-frequency analysis (JTFA), such as the Gabor transform (GT) and the wavelet transform (WT), have been recently introduced [5,6].

Among these JTFA, the wavelet transform (WT) appears to be the most powerful tool yet presented for the analysis of the dynamic behavior of nonstationary signals (process). Wavelet transforms are rapidly finding applications in many branches of science, such as fluid mechanics, structural dynamics, sound and vision processing, acoustics, random vibrations and many others [4,7-10]. One of the major characteristics of the WT is its good time-frequency localization, i.e. it has good time-frequency resolution [6].

Moreover, any system which is nonlinear as the one presented in this study may show chaotic behavior for certain combinations of system parameters [11,12]. A nonlinear system undergoing chaotic behavior is characterized by a broad banded and fluctuating power spectrum, where various harmonics are continuously excited and then become unstable and bifurcates to other harmonics. Since the frequency spectrum is time varying (usually rapidly), JTFA becomes a must for a realistic and rigorous study of chaotic systems. In general, any nonlinear system may be studied via qualitative or quantitative techniques to investigate its dynamic stability. The main classical tools frequently used to study the stability and the chaotic behavior of the systems are the phase-space portraits, the Poincaré maps and the fractal dimensions. It is shown in this work that WT can be used as another powerful and useful tool in the analysis of the chaotic behavior of the system under consideration, i.e. it can be used more efficiently than classical methods to construct bifurcation diagram.

To the best of the present author's knowledge, the problem of flow induced vibration, as pointed out above, has been analyzed using classical methods. Only, in the recent work presented by Abu-Samak [13] at the University of Jordan, the WT has been introduced in the study of flow induced vibration of an elastically mounted cylinder. The present work is a continuation of the "somewhat" preliminary work in [13], where the data

3. The use of a more realistic and appropriate discretization scale for the time series, so as to extend the frequency range over which the data is valid.
4. Considering new values of free stream velocities in the same range considered in [13], for which the process shows different and interesting dynamics.
5. The addition of 3D joint time-frequency-phase analysis, not considered in [13], which represents a plot of the imaginary part of the complex wavelet ignored in [13], and is particularly suited to the detection of singularities in the signal, if any [6].
6. To explore the possibilities of using GT in the dynamic analysis of the process and to compare the results with those obtained using the WT. The necessary software needed to implement GT analysis is developed and tested in this work.
7. To carry out a more detailed and rigorous investigation of the type of nonlinearity which may be present in the process and to examine the range of parameters over which the process undergoes chaotic motion.

1.2 LAYOUT OF THE THESIS

The thesis is divided into seven chapters, of which this introduction is the first. Chapter two gives a review of the flow-induced vibration phenomena as well as a literature survey at the end. On the other hand, chapter three elucidates several concepts of signal processing methods and algorithms used in this work; however, at the end of the chapter a separate literature survey concerning the new signal processing methods is supplemented. Chapter four lays down the theory behind chaotic behavior of systems in general as well as the methods adopted in this work for

chaotic investigations, whereas at the end of the chapter a literature survey concerning the chaotic behavior of systems is presented.

Chapter five discusses the experimental work carried out in this work. The instrumentation and the experimental procedures used are thoroughly detailed. Moreover, in chapter six the experimental results and their analysis obtained are represented and discussed thoroughly.

Finally, chapter seven is devoted to the conclusions and the recommendations which may be useful for future investigations.

CHAPTER 2

FLOW INDUCED VIBRATION

2.1 INTRODUCTION

Flow induced vibration arises in many practical engineering systems, such as heat exchangers, power transmission lines, bridges and tall towers. For example, when an elastically mounted cylinder is placed in a cross-flow it is generally known that as the flow separates from either side of cylinder, vortices are shed alternately resulting in an oscillating external force which causes the cylinder to oscillate [1].

It is well known that an oscillating aerodynamic force is induced on a structure which vibrates in a steady flow. The structure can achieve aerodynamical stability if the oscillating aerodynamic force tends to abate the structure vibrations, whereas if this force tends to augment the structure vibrations, aerodynamical stability can not be achieved and thus the structure is termed as aerodynamically unstable. For sufficiently small vibration amplitudes, the aerodynamic force may be modeled as a linear function of the angle of flow relative to the structure, for example the airfoil flutter. However, if the flow separates from the structure cross-section, then the aerodynamic force is nonlinear function of the flow angle, and the structure is said to be a bluff [1].

The viscous flow past a two-dimensional bluff body and the resulting recirculating region behind the bluff body have been a subject for numerous investigations [1,14-17]. Over a wide range of Reynolds numbers (from 50 and up to 10^6 and even higher), the physics of street formation and the near-wake flow have been experimentally studied [18-26]. It is well known that the flow depends on, for example, Reynolds

number, surface roughness of the bluff body, blockage, free stream turbulence, the aspect ratio and the end plates conditions.

Vortex shedding theory is very complex, and the exact solution to the fluid elastic problem has not, yet, been developed. A promising new investigations which examined oscillating flow problems have begun to relate vortex motions to the forces exerted on the cylinder [14,16,27]. These vortex motions are explained in terms of the relevant dimensionless parameters.

Furthermore, recent experiments [14,15] ensure that a bluff body in a perturbed incident flow consisting of a mean flow with a periodic component superimposed upon it is identical, under suitable conditions, to the vortex resonance of a cylinder oscillating in line with an incident uniform flow.

In general, cylinder vibration in a cross-flow near the vortex shedding frequency can enlarge the spanwise correlation of the wake, augment the drag force, increase the vortex shedding and force the vortex shedding frequency to deviate from the stationary cylinder shedding frequency to the cylinder vibration frequency, called lock-on effect; which is also present if the vibration frequency is equal to a multiple or submultiple of the shedding frequency [1].

Also, it is to be noted that large amplitude vibrations due to vortex shedding are observed when the flow reaches a critical value. These vibrations have a destructive effects on cables, bridges and other structures, which make the study of the flow induced vibration of a practical importance.

2.2 THE FLOW INDUCED VIBRATION PHENOMENA

If a cylinder is set normal to a uniform flow direction, the fluid structure dynamic interaction will induce a transverse oscillation of the cylinder.

approximate theoretical model for the fluid-structure interaction problem with some success.

The main reason for the difficulty of developing a successful model is due to the relatively large number of parameters affecting the amplitude of the vibrating body. These parameters include; the reduced velocity, the mass ratio, Reynolds number and the damping factor.

454187

2.3 FORMS OF FLOW INDUCED VIBRATION

There are four forms of flow induced vibration ; namely , vortex shedding, fluid elastic excitation or galloping, flutter and acoustic excitation. Following is a brief description of each.

2.3.1 VORTEX SHEDDING

Vortex shedding has been the most common form of fluid dynamic excitation for a single a cylinder. Blevins [1] described the mechanism of separation and vortex shedding. He claimed that when the fluid flows toward the leading edge of a bluff body the fluid pressure rises from the free stream pressure to the stagnation pressure. This will develop boundary layers on both sides of the cylinder. These boundary layers separate from each side of the cylinder surface near the widest section and from two free shear layers which bound the wake. Since the innermost portion of the free shear layers moves much slowly than the outer most portion of the layers which are in contact with the free stream, the free shear layers tend to roll up into descent, swirling vortices. The shedding of the formed vortices alters the pressure distribution, and the cylinder experiences a time varying force at the frequency of vortex shedding. Fig.(2.2) illustrates this mechanism.

Lock-on phenomena is an important feature of vortex-shedding excitation. If the frequency of the vortex-shedding is in resonance with the natural frequency of the member that produces it, large amplitude oscillations with consequent large stresses can develop. These oscillations begin when the velocity increases or decreases so that the shedding frequency approaches the natural frequency of the structure. Lock-on occurs over a certain range of velocities depending on the structural and flow properties. This is the difference between the lock-on and the usual case of resonance which exhibits a single resonance point.

As the lock-on phenomena begins and the motion of the vortex shedding locks into the structural frequency, a feed path is completed so that the motion of the structure controls the vortex shedding. Lock-on phenomenon disappears beyond a critical condition due to the limited capacity of the oscillating structure to alter the frequency of vortex shedding.

2.3.2 FLUID-ELASTIC EXCITATION (GALLOPING)

The flow induced vibration of bluff structure is commonly referred to as stall flutter or galloping. For any lightweight, flexible structure exposed to a flow, galloping may arise. Various cross sections, such as square, rectangular, right angle, and stalled aerofoil are potentially unstable in the presence of aerodynamic galloping.

The main assumption of galloping analysis is that the fluid force on the structure is determined solely by the instantaneous relative velocity and the angle of the attack of the flow to the structure. This implies that the information about the fluid force can be measured by wind tunnel test on stationary model held at various angles.

The most fascinating feature of the interference galloping is that both the mean position of the motion and the body's oscillation frequency may vary appreciably with increasing flow velocity. Another notable feature is that

the vibration amplitude always approach asymptotically a constant value. The instability is either in the form of a vortex resonance or a galloping. The cylinder never exhibits a combined vortex resonance and a galloping or a vortex resonance followed by a galloping [17].

Galloping vibration can be prevented by increasing the internal damping of the structure, reducing the flow velocity, stiffening the structure, increasing the mass of the structure without lowering its natural frequency or damping, and changing the orientation of the structure to the flow or the contours of the structure in order to stabilize it.

2.3.3 FLUTTER

Flutter has been defined as the dynamic instability of an elastic body in an airstream and is produced by aerodynamic force which result from the deflection of the elastic body from its undeformed state [2].

Flutter can occur in any engineering application of more than two degrees of freedom, such as long-span suspension bridges and turbine blades. The main reason of flutter is due to coupling interaction of bending and torsion modes.

The aerodynamic forces of aircraft flutter are often sufficiently large to produce large shifts of the natural frequency, while in the galloping vibration they are usually small to produce significant shifts of the natural frequencies. Also, aerodynamic flutter is produced by more than one mode of vibration, but galloping vibrations affect a single mode.

2.3.4 ACOUSTIC EXCITATION

The application of an appropriate sound field to the flow about a cylinder can induce vortex lock-on and resonance in the wake. There are even fewer reported studies of the effect of sound than rotational oscillations. It was observed that the vortex lock-on was induced by the

velocity rather than the pressure, and the lock-on occurred at a frequency less than Strouhal frequency. Turbulence in the free stream suppressed the influence of sound on the vortex shedding. The results suggest that the induced sound field velocity must exceed the turbulence velocities so that the sound causes vortex shedding along the span of the cylinder [28].

2.4 VIBRATIONS INDUCED BY AN OSCILLATING FLOW

It has been observed that an oscillating flow, for example ocean waves, can cause a destruction of structures [28,29]. Oscillating flows, which may arise in acoustics and turbulence as well, usually involve nonlinear vibration problems, which in turn have not been fully explored yet. Despite the huge literature on estimating the forces on stationary structures, little theoretical and experimental work on the complex dynamic response of elastic structures to oscillating flows is available.

In order to reduce the vibrations induced by an oscillating flow, either the amplitude of fluid oscillation is reduced, which is usually not possible, or the structure is modified. The structure can be modified by one or more of the following; avoiding resonance by increasing the fundamental frequency of the structure up to at least five times that of the oscillating flow, increasing the ratio of the structural mass to the displaced fluid mass, increase the damping of the structure and modify the cross section so that the inertial and drag coefficients of the cross section are reduced [1].

2.5 LITERATURE SURVEY

It is well known that the response of structures interacting with fluid flow is essentially nonlinear. Also, the fluid flow and the structure are interactive systems; and their interaction is dynamic [1]. Structure

deformation is caused by the exerted fluid forces. In turn, this causes a change in the pressure distribution, and some interesting effects arise; following a brief of some related studies.

Resonant oscillations can be excited by the incident flow if a bluff cylinder is flexible and lightly damped, or rigid and flexibly mounted. As a consequence of this flow induced resonance, the body and wake oscillations have the same frequency; usually termed lock-on, which is near one of the structure characteristic frequencies [2,3]. Sarpkaya [30] and Bearmann [18] introduced extensive reviews of vortex shedding and vortex induced vibration.

The results of recent experiments about the vortex shedding phenomena and bluff body wakes flow control are reported by Griffin and Hall [27,31-33]. They observed both symmetric and asymmetric vortex patterns over a wide range of oscillation conditions. For a bluff body oscillating in-line with the incident flow, vortex lock-on was observed at $f = 2, 3$ and $4 f_n$, with an asymmetric street formed at twice the basic Strouhal frequency and a symmetric street formed at three times the basic Strouhal frequency. The asymmetric pattern was complex in that one row consisted of a line of single vortices, whereas the other row consisted of a line of oppositely rotating vortex pairs. The vortex lock-on at three times the Strouhal frequency resulted in the formation of a symmetric street of vortices. In the above cases, the basic patterns persist downstream over a large number of oscillation cycles. When the oscillation frequency is four times the Strouhal frequency, a symmetric pattern is formed but rapidly loses its coherence in the early wake. Filler et al. [14] investigated the response of the shear layers separating from circular cylinder to small amplitude oscillations. They reported that at lower frequencies near the usual Karman shedding frequency, a large resonant peak occurred, whereas at higher imposed frequencies a secondary broad peak in the range of the shear layer

instability frequencies occurred. Also, they reported that in the Karman frequency range of vortex shedding, the wake behaved like a nonlinear oscillator near resonance. These results were explored by numerous investigations for the cases of cross-flow and in-line oscillations [34-37]. More recently, Tokumaru et al. [15] showed that lock-on may be caused by rotational oscillations. They claimed that active control of the near wake vortex formation and flow physics by rotational oscillations of the cylinder can reduce the drag on the cylinder by a factor of six.

The introduction of the absolute convective theory of fluid dynamic stability has opened the road for a new promising approach to understand the physics of vortex formation and near-wake flow development [38-44]. Extensive stability calculations based upon computed and measured mean velocities in the wakes of stationary circular cylinders suggest that the vortex formation region is absolutely unstable while the fully-formed vortex street is convectively unstable. The vortex formation region is thought to be a complex global region that is characterized by the interaction between the model and the flow upstream and downstream propagating vorticity waves [45-47].

In recent years a number of important theoretical advances describing the absolute instabilities of shear flows have been introduced [48-52]. Chomaz et al. [53] introduced the concept of global instability as opposed to absolute instability. Their investigations showed that in order for globally unstable oscillations of a shear flow to occur both the flow must be absolutely unstable and the region of instability must reach a sufficiently large size. As a consequence of the global instability of a bluff body wake is the generation of a highly coherent and nonlinear oscillation, in the absence of external excitation. Therefore, perturbation of this global instability, at a frequency other than its self-excited one, can give rise to a number of interesting phenomena. Williamson et al. [26] as well as

Ongoren et al. [54,55] studied various locked-in and quasi-periodic status of response attainable by forced excitation of a cylinder. The production of a large number of spectral components and the onset of spectral broadening in the near wake due to instabilities from a stationary cylinder, from a cylinder under aeroelastic excitation in one of its spanwise modes or from external excitation of a two dimensional rigid cylinder is extensively described by Olinger et al. [56], and Karaniadakis et al. [57]. They have demonstrated numerically the occurrence of period-doubling in the secondary instability from a circular, stationary cylinder at low Reynolds number. Three-dimensionality of the flow structure is a necessary part of this period doubling process.

Nuzzi et al. [58] investigated the inducement of period-doubled vortex formation from a non-uniform cylinder subjected to forced excitation. They showed that detuning of the highly coherent vortex formation in the spanwise direction, arising from the gradual variation of the cylinder diameter, would promote the occurrence of nonperiodic and period-doubled states. They emphasized that globally locked-in, three dimensional vortex formation can occur along the entire span of the flow. Moreover, if the excitation frequency was properly tuned, regions of period-doubled and locally locked-in vortex formation could exist along various parts of the span. Also, the occurrence of period-doubled vortex formation did not feature vortex coalescence, instead the flow structure bifurcated between two different states. This is obviously different than the classical subharmonic instability in free shear flows.

Form another important view, Baker et al. [59] discussed the transition process and the horseshoe vortex phenomena by implementing the nonlinear dynamics and the chaos theory. They found that as the Reynolds number increases, the number of horseshoe vortices increase from 2 to 4 to

6, respectively. Two distinct sorts of oscillations were reported; period doubling and later on chaos when reaching turbulence flow.

Shirakashi et al. [60] conducted an experimental study on the oscillation behavior of an elastically supported cylinder whose rotational-mode natural frequency $f_{n\theta}$ is several times higher than that for translational-mode f_{nz} . They reported the occurrence of a subharmonic resonance at $f_v/f_n = 3$ in addition to normal one at $f_v/f_n = 1$, where f_v is the Karman vortex shedding frequency and f_n is the natural frequency of the cylinder. They explained these peaks as follows, when the free stream flow velocity U_∞ is low, a translational-mode oscillation occurs at a frequency f_{nz} . As U_∞ increases, its amplitude attains a maximum peak when f_v is equal to f_n , after that a second maximum amplitude occurs at $f_v/f_n = 3$ and the motion is purely translational. As U_∞ becomes even higher, a third maximum amplitude peak around $f_v/f_n = 3$ appears and a rotational-mode dominates the flow process.

It is to be noted that in the case of a cylinder without endplates, and the wall of the test cylinder at a point near to the side-wall, additional peak was found at a frequency about 1/3 the Karman vortex-shedding frequency [60]. They attributed this additional peak to the effect of open slots on the vortex-shedding and not induced by the cylinder oscillation, and there confirmation was that this peak disappeared when using the blocking plates. The effects of the blocking plates on the oscillating behavior of a cylinder can be introduced as follows. In translational-mode oscillation without blocking plates, two peaks appeared in the power spectrum at $f_v/f_{nz} = 1$ and $f_v/f_{nz} = 3$. The second peak is assumed to be caused by the side wall effect. But, when attaching the blocking plates, the higher frequency peaks were completely removed from the power spectrum, whereas the lower frequency peaks became sharper.

Using a good technique to establish the onset of fluid elastic instability, Marn et al. [61] introduced a vorticity formulation of the instability problem using the perturbation techniques then these equations were solved numerically. Moreover, the evolved fluid forces were obtained by integrating the pressures around the cylinder surface in order to predict the threshold for of the dynamic instability. The occurrence of instabilities were investigated and a parametric optimization study was conducted by altering the parametric vector which contained the Reynolds number, the geometry, the disturbance pattern, and the pitch-diameter ratio.

More recently, Higuchi et al. [62] used wavelet analysis to study the unsteady and asymmetric vortex shedding in the wake of two flat plates placed side by side normal to the water flow. The spacing between the two plates was varied over the range of one to two plate widths with $Re=1500$ based on an individual plate width. They found that for a small plate spacing, the deflection of the jet passing through the gap resulted in a larger wake with mostly symmetric vortex shedding on one side and a smaller wake with asymmetric shedding on the other. The intermediate wake presented for small plate spacing resembled that of a single bluff body, whereas a major intermittent structure was observed at the wider spacing. A flow visualization study was conducted. The Fourier spectra of the velocity data at certain position was used and more than one dominant frequency was showed. Wavelet transform (WT) was implemented to map the intermittent near-periodic structures, and quantified their mean energy spectrum. They used the Mexican hat wavelet as a basic wavelet, and the three-dimensional array of numbers was plotted as an energy map by utilizing the Parseval's theorem. The obvious results were that the concentration of energy is nearly periodic in a narrow range of durations and the occasional surging of the flow at long durations, simple counting of the structures reveals a difference in frequency between the two sides of

the wake, and the overall regularity and the some intermittency in the vortex shedding. Thus based on the WT, the structure maps isolate individual events irrespective of the intermittency or modulation of irregular sequences.

In his experimental investigations of the flow around a circular cylinder, Norberg [63] recently studied the influence of aspect ratio on the flow, and the main parameters altered were the Strouhal number and the mean base suction coefficient, both measured at mid-span position of the cylinder. Various aspect ratios L/D , at low blockage ratios were achieved by changing the distance between circular end plates. The Re range was from about 50 to 4×10^4 and the end plate-diameter ratios were from 10 to 30. A parallel shedding, at around mid-span towards both ends of the cylinder, was observed throughout the laminar shedding regime when there was a small but symmetrical free stream velocity increment. At high Re , the parameters at different aspect ratios were compared with those of a quasi-infinite cylinder and the required aspect ratio to which conditions independent of those parameters were reported. A bi-stable flow switching between regular vortex shedding and irregular flow was reported at $Re \approx 2 \times 10^3$ in the subcritical regime with the smallest relative endplate diameter and for aspect ratios less than 7.

By both visualization and force measurements, Gopalkrishnan et al. [64] investigated experimentally the feasibility of free shear flow control and energy extraction from the large eddies in a free shear flow. A D-section Cylinder oscillating transversely as it is forced to move forward at constant speed, and a heaving and pitching foil, situated behind the cylinder are used to demonstrate the feasibility of changing the flow through vorticity control. It was shown experimentally that free shear flows can be partially altered through direct control of the large coherent vortices presented on the flow. It should be noted that the foil was placed in the wake of the D-

section cylinder, sufficiently far behind the cylinder in order to avoid interference with the vortex formation process. The heaving and pitching oscillation of the foil was at a frequency close to the Strouhal frequency of the cylinder, where the cylinder and the foil also moved forward at constant speed. The flow-visualization experiments were conducted in Kalliroscope fluid at Re of 550, whereas force and torque measurements were conducted at Re of 2×10^4 , thus assessing the impact of flow control on the efficiency of the oscillating foil and hence investigating the possibility of energy extraction.

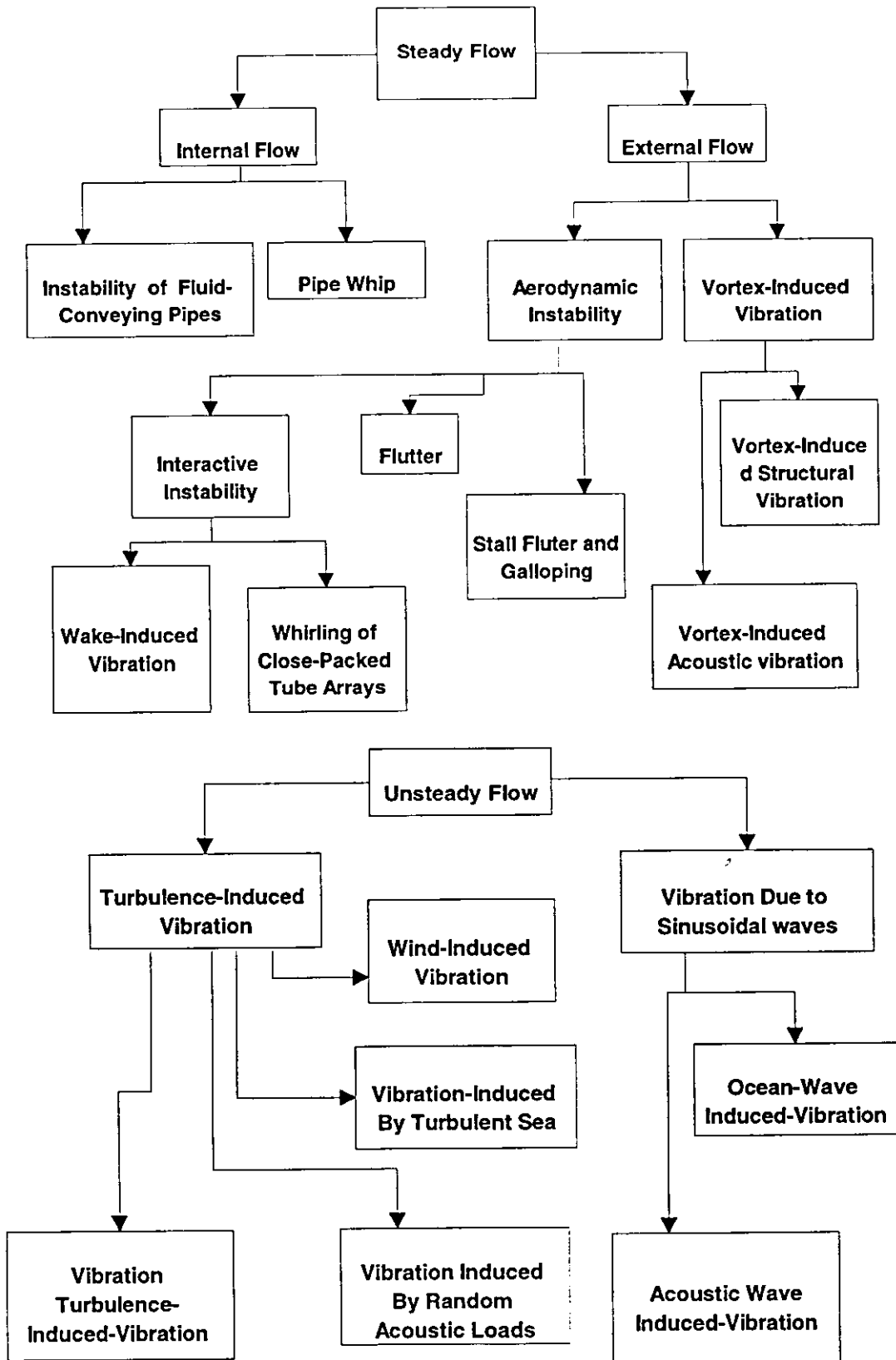


Figure (2.1) : A Classification of Flow Induced-Vibrations [1].

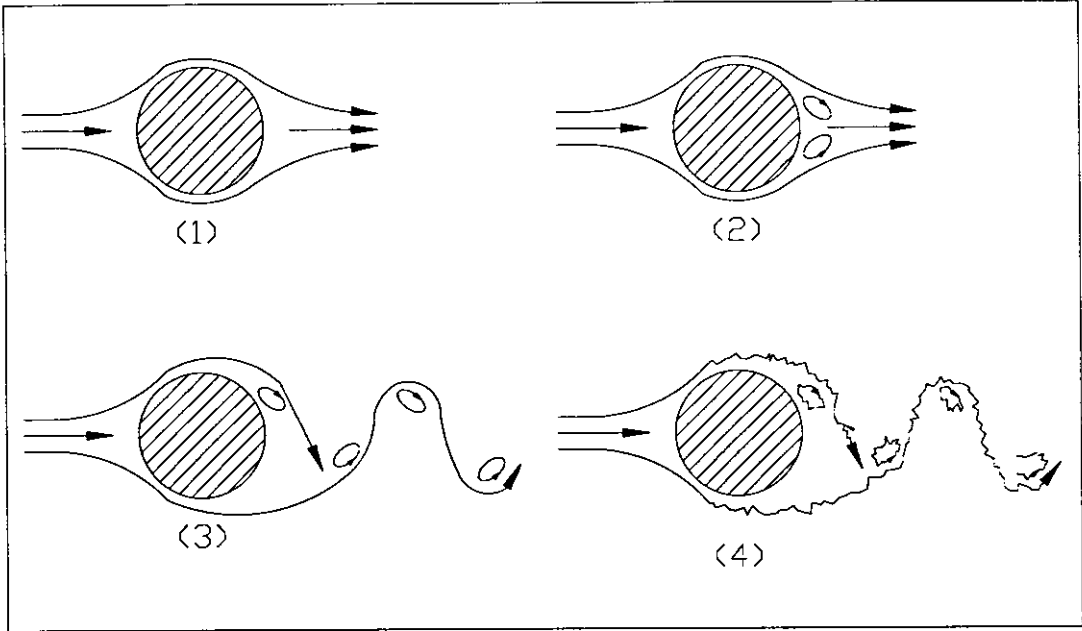


Figure (2.2) : Illustration of the Vortex Shedding Mechanism [1].

CHAPTER 3

SIGNAL PROCESSING

3.1 INTRODUCTION :

New joint time-frequency analysis methods (JTFA) are rapidly finding applications as powerful tools for the analysis of nonstationary signals. Among others, wavelet transform (JTFA method) appears to have the most reliable and adequate representation of the various activities of signals whether transients or stationary.

In this chapter classical methods used to analyze the signals of the flow-induced vibration process are briefly reviewed in the following section, whereas JTFA are outlined in the subsequent section. A separate literature review of JTFA is provided in the last section.

3.2 CLASSICAL METHODS

Signals can be classified into two main categories; deterministic and random (stochastic) signals. The deterministic signals can be completely described as a function of time. However, random signals are those which can not be expressed explicitly as functions of time and are generally classified into stationary and nonstationary. If the statistical parameters, namely, the autocorrelation, or equivalently the power spectrum, and the mean value are time invariant, the signal is said to be stationary; otherwise it is nonstationary.

It is to be pointed out that a stationary signal can exhibit unexpected events, but we know in advance the possibilities of these events, i.e., they are statistically predictable.

Most experimental measurements of random processes are carried out digitally, thus digital computer signal processing (DSP) algorithms have been introduced. For example, any signal analyzed via a personal computer must use DSP. Two main DSP algorithms, namely; digital filtering or Fast Fourier Transform (FFT), are commonly employed to obtain a description of the frequency content of a random signal. In the following subsections, the classical methods, such as, the autocorrelation and the power spectrum methods, are outlined.

3.2.1 THE AUTOCORRELATION

The autocorrelation function provides information about the dependence of a random variable value at one time on the variable value at another time; it is given by

$$R_x(\tau) = \lim_{T \rightarrow \infty} \frac{1}{T} \int_{-T/2}^{T/2} x(t)x(t+\tau)dt = E[x(t)x(t+\tau)] \quad (3.1)$$

where $E[x(t)]$ is the expectation operator.

In its discretized form, the elements of the autocorrelation series can be written as

$$R_x(i) = \sum_{j=0}^{n-1} x(j)x(i+j), \quad i = -(n-1), \dots, -1, 0, 1, \dots, (n-1) \quad (3.2)$$

where n is an integer representing the variable elements (time), and $x(j) = 0$ if $j < 0$ or $j \geq n$. Also, the autocorrelation is an even function of τ , while its maximum is obtained at $\tau = 0$.

3.2.2 THE POWER SPECTRUM

Used for simplicity, the Fourier Transform (FT) and the power spectrum density arise as powerful classical methods to study the frequency content of periodic or stationary random signals.

If the continuous transformation $x(t)$ to $X(f)$ represents a FT pair, see Appendix A, then the discrete Fourier transform (DFT) of the discretized signal $x(n)$, is termed the amplitude spectrum and it is given by

$$X(k) = \sum_{n=0}^{N-1} x(n) e^{-j2\pi kn/N}, \quad k = 0, 1, \dots, N-1 \quad (3.3)$$

and its inverse is thus

$$x(n) = \frac{1}{N} \sum_{k=0}^{N-1} X(k) e^{j2\pi nk/N}, \quad n = 0, 1, \dots, N-1 \quad (3.4)$$

where N is the number of data points.

Although the FT of the signal itself has several interesting properties, listed in Appendix A, it is not often used for random signals, while, Fourier transform of the autocorrelation function is often used to study these random signals and it is termed the power spectrum density. In addition to its representation of the power distribution with respect to frequency, power spectrum density measures the average rate of fluctuation of the random signals. The power spectrum density can be derived from the autocorrelation function as follows; assuming the integral of the autocorrelation function $R_x(\tau)$ from $-\infty$ to ∞ is finite, then the power spectral density function (the power spectrum) is given by

$$X(f) = \int_{-\infty}^{\infty} R_x(\tau) e^{-j2\pi f \tau} d\tau \quad (3.5)$$

where f is the frequency. Moreover, the inverse FT gives the inversion formula of Eq.(3.5) as

$$R_x(\tau) = \int_{-\infty}^{\infty} X(f) e^{j2\pi \tau f} df \quad (3.6)$$

On the other hand, the DFT of Eq.(3.5) is given by

$$S_x(f) = \sum_{n=-\infty}^{\infty} R_x(n) e^{-j2\pi f n} \quad (3.7)$$

Since direct implementation of DFT requires approximately 2^N complex operations for an N points record, a computational technique, the Fast Fourier Transform (FFT), was developed to minimize the number of operations needed to compute the DFT approximately $N \log_2 N$, such that N is a power integer of two. The advantages of the FFT include its speed and memory efficiency; however, the size of the signal array must be a power of two.

In order to adequately represent a stationary process the time record should be longer than the basic cyclic time of the process. If the length of the time record is comparable with the transform size of the analyzing system, then the full power spectrum of the data record is calculated in one pass.

3.3 JOINT TIME-FREQUENCY ANALYSIS

It should be noted that the FT decomposes the analyzed signal canonically into sines and cosines assuming the signal to be periodic and stationary. Since a sinusoidal function is highly localized in frequency domain and infinitely distributed in time domain, the FT does not provide information about time localization of high frequency transients which may exist in a random nonstationary process. Thus, new methods which can provide both time and frequency localization are introduced, and generally called joint time-frequency analysis methods (JTFA). JTFA are classified into linear and quadratic. Linear JTFA, which satisfies the linearity principle given in Appendix A, can be further distinguished as the short-time Fourier transform (STFT), the Gabor transform (GT) and the wavelet transform (WT).

aliasing, time window effect, picket fence effect, and bandwidth-localization tradeoff. For example, for a large analysis window, low frequencies can be calculated, while high frequencies are poorly localized. On the other hand, the STFT in time and frequency domains can not be arbitrarily small because their product is lower banded [66] so that

$$\text{Time - Bandwidth Product} = \Delta t \Delta f \geq 1/4 \pi \quad (3.10)$$

Thus, for impulsive and nonstationary signals which requires good time-frequency resolution, traditional STFT ceases to be productive, since STFT can either provide good frequency-resolution or good time-resolution.

3.3.2 GABOR TRANSFORM & ZAK TRANSFORM

Another technique which overcomes some pitfalls of the STFT is the Gabor transform (GT). Gabor's model, put forward in 1946 [66] is one of the known mutually nonorthogonal representations originally proposed for description of temporal signals in a combined time-frequency space in communications; and it is given by

$$f(t) = \sum_{m=-\infty}^{\infty} \sum_{n=-\infty}^{\infty} a_{mn} g_{mn}(t) \quad (3.11)$$

where $g_{mn}(t) = g(t-n)e^{j2\pi mt}$, with $g(t) = e^{-\pi t^2}$ as a basic window, the expansion coefficients a_{mn} , called Gabor coefficients, are related to the complex spectrogram of the sampled signal on a Gabor lattice [66], or to a sampled cross-ambiguity functions. The interest in the Gabor expansion stems from the fact that the Gabor bases (g_{mn}) are well localized in both time and frequency as well as they are easily generated through a simple time-frequency shifts. However, important issues which may arise when dealing with GT are the completeness, the linear independence and orthogonality of the Gabor bases [67-69].

If completeness of the Gabor bases $g_{mn}(t)$ is assumed, then the biorthogonality condition [70]

$$\int_t f(t) g^*(t - n\tau) e^{-j2\pi m f_o t} dt = \delta[n] \delta[m] \quad (3.12)$$

is sufficient for the perfect reconstruction condition, where

$$\delta[k] = \begin{cases} 1, & k = 0 \\ 0, & k \neq 0 \end{cases} \quad (3.13)$$

It is to be noted that Eq.(3.12) is related to a function called the cross-ambiguity function (or the complex spectrogram), see Appendix A, and it is given by

$$a(\tau, \omega) = \int_{-\infty}^{\infty} f(t) \cdot g^*(t; \tau, \omega) dt \quad (3.14)$$

where $g^*(t; \tau, \omega)$ is a shifted analysis window, given by

$$g^*(t; \tau, \omega) = g^*(t - \tau) e^{-j\omega t} \quad (3.15)$$

Thus the expansion equation of Eq.(3.14) can be written as

$$f(t) = \frac{1}{2\pi} \int_{-\infty}^{\infty} \int_{-\infty}^{\infty} a(\tau, \omega) \cdot g(t; \tau, \omega) d\tau d\omega \quad (3.16)$$

The major tool in getting a discrete version of Eq.(3.16) is the so-called Zak transform [67], which is given by

$$Z(f)(x, y) = \sum_{n=-\infty}^{\infty} f(y - n) e^{-2\pi i n x} \quad (3.17)$$

Daubechies et al. [71] have shown that frames (Appendix A) $\left\{ \langle f, g_{ma, nb} \rangle : m, n \in \mathbb{Z} \right\}$ exist if and only if $a, b \leq 1$, and tight frames in such a case exist with $A = (1/ab) \cdot \|g\|_2^2$, where $\|g\|_2$ is the second order norm of the function g (consult Appendix A). The critical value, $a \cdot b = 1$, by Balian's theorem [72], requires that a reference signal g neither should be very smooth nor should decay very fast. Thus, normalizing and choosing $a = b = 1$ in this investigation and considering only integer lattice and lattices containing this integer lattice as sublattices, the Zak transform of Eq.(3.11) yields

$$Z(f)(x, y) = Z(g)(x, y) \sum_{m=-\infty}^{\infty} \sum_{n=-\infty}^{\infty} a_{mn} e^{j2\pi(nx+my)} \quad (3.18)$$

where the Gabor coefficients can be rewritten as

$$a_{mn} = \int_0^1 \int_0^1 \frac{Z(f)(x, y)}{Z(g)(x, y)} e^{-2\pi i(mx+ny)} dx dy \quad (3.19)$$

Auslander and Tolimieri [73] have shown that $Z(g)(x, y)$ has a zero in the unit square. Hence, in general, there is no way to relate the finite signal energy to the sum of the squares of a_{mn} which may be infinite, i.e.

$$\int_{-\infty}^{\infty} |f(t)|^2 dt \neq \sum_{m=-\infty}^{\infty} \sum_{n=-\infty}^{\infty} |a_{mn}|^2 \quad (3.20)$$

However, Jensen et al. [72] discussed a double series representation of a bounded signal. A new regularized algorithm to compute the coefficients a_{mn} , which avoids the zero problem without affecting the resolution of the reconstructed signal, has been developed [70]. The mathematical formulation and the algorithm can be represented as follows. For a finite duration function f which vanishes outside the interval $[0, N]$, the two dimensional expansion of $M \times N$ array is given by

$$f(m, r) = f\left(\frac{m}{M} + r\right), \quad 0 \leq m < M, \quad 0 \leq r < N \quad (3.21)$$

Thus, the corresponding Zak transform is

$$Z(f)\left(\frac{n}{N}, \frac{m}{M}\right) = \sum_{r=0}^{N-1} f(m, r) e^{-j2\pi(rn/N)} \quad (3.22)$$

where $0 \leq n < N$; $0 \leq m < M$.

The above transform can be formed by utilizing the two-dimensional Fourier transform. Bearing in mind that since g (the basic window) generates a tight frame, then the following equation is set forward as a consequence

$$|Z(g)(x, y)|^2 = A > 0 \quad (3.23)$$

and also the Gabor coefficients are

$$a_{mn} = A^{-1} \langle f, g_{mn} \rangle \quad (3.24)$$

On the other hand, expanding the periodic function $|Z(g)(x, y)|^2$ as a double Fourier series yields

$$|Z(g)(x, y)|^2 = \sum_{m=-\infty}^{\infty} \sum_{n=-\infty}^{\infty} c_{mn} e^{[j2\pi(nx+my)]} \quad (3.25)$$

where

$$c_{mn} = \langle g, g_{mn} \rangle \quad (3.26)$$

Thus, Eq.(3.26) becomes

$$\langle f, g_{mn} \rangle = \sum_{r=-\infty}^{\infty} \sum_{s=-\infty}^{\infty} c_{m-r, n-s} \cdot a_{rs} \quad (3.27)$$

which represents a double convolution and, in general, not an easy task to perform. For digital computation, while assuming f is of finite duration, Eq.(3.11) can be represented as

$$f(t) = \sum_{m=0}^{M-1} \sum_{n=0}^{N-1} a_{mn} g_{mn}(t), \quad M > 0, \quad N > 0 \quad (3.28)$$

Taking the Zak transform of the above equation, while sampling at $x = \frac{r}{4N}$, $y = \frac{s}{M}$, $0 \leq r < N$, $0 \leq s < M$ yields

$$Z(f)\left(\frac{r}{4N}, \frac{s}{M}\right) = Z(g)\left(\frac{r}{4N}, \frac{s}{M}\right) \sum_{m=0}^{M-1} \sum_{n=0}^{N-1} a_{mn} e^{-j2\pi\left(\frac{nr}{4N} + \frac{ms}{M}\right)} \quad (3.29)$$

Upon deconvolution, the above equation yields

$$\sum_{m=0}^{M-1} \sum_{n=0}^{N-1} \langle f, g_{mn} \rangle e^{-j2\pi(nx+my)} = |Z(g)(x, y)|^2 \sum_{m=0}^{M-1} \sum_{n=0}^{N-1} a_{mn} e^{-j2\pi(nx+my)} \quad (3.30)$$

Letting

$$Z_{r,s} = \frac{Z(f)\left(\frac{r}{4N}, \frac{s}{M}\right)}{Z(g)\left(\frac{r}{4N}, \frac{s}{M}\right)} \quad (3.31)$$

Then, Eq.(3.29) becomes

$$Z_{r,s} = \sum_{m=0}^{M-1} \sum_{n=0}^{N-1} a_{mn} e^{-j2\pi\left(\frac{nr}{4N} + \frac{ms}{M}\right)} \quad (3.32)$$

Finally, Gabor coefficients are computed from the above equation by inverting a Vandermonde matrix.

Fig.(3.1) shows a flow chart for the algorithm used to compute the Gabor coefficients after Auslander [70]. This algorithm is implemented via a FORTRAN program, Appendix B, to compute the GT for the signals under consideration.

It is to be pointed out that the Gabor coefficients a_{mn} are a smeared version of the actual time-frequency representation. Hence, to increase the frequency resolution, a wider window $g^*(t)$ is needed, i.e. transient effects occurring during this window will be smeared out in time and frequency as well. Thus, the length of the window is again a compromise between frequency resolution and time resolution.

3.3.3 THE WAVELET TRANSFORM

An alternative JTFA method which overcomes the many pitfalls of both STFT and GT, is the wavelet transform (WT). The WT can be interpreted as a tool that cuts up data or functions into different frequency components, and then studies each component with a resolution matched to its scale [6]. Two major WT methods, which are of practical interest to study nonstationarity signals, include wavelets of the time-frequency type and wavelets of the time-scale type. Time-frequency wavelets are suited, most specifically, to the analysis of quasi-stationary signals, while time-scale wavelets are adapted to signals having a fractal structure, and they are of special interest in the multiresolution analysis where a vast range of scales for signal analysis is used [5]. Another broad classification of WT was given by Daubechies [6]; the continuous wavelet transform (CWT) and the discrete wavelet transform (DWT), which can be further classified into redundant discrete systems (frames) and orthonormal basis of wavelets.

The continuous WT, firstly given by Grossman and Morlet [74], assumes that any time signal can be decomposed canonically into a combination of time-shifted and dilated or compressed basic wavelets; accordingly WT is given by

$$WT_{a,b} = \frac{1}{a^{-0.5}} \int_{-\infty}^{\infty} x(t) h\left(\frac{t-b}{a}\right) dt \quad (3.33)$$

where the wavelet function $h(t)$ is an appropriate window (called basic or mother wavelet) like the modulated Gaussian. Hence, the WT can be defined as the convolution of a signal $x(t)$ with an analysis window $h(t)$ shifted in time by b and dilated by a scale parameter a . The scale parameter a can be chosen such that it is inversely proportional to the frequency. The factor $|a|^{-0.5}$, according to the theory of frames, is used to ensure energy preservations and it is called the normalizing factor [75,76]. In structural dynamics, the normalizing factor, which is obtained by correlating the signal with a sine function and equating the correlation to 1.0, is usually chosen to be $1/a$. The purpose of WT is to extract the localized conditions of the signal labeled by the two parameters a and b and then the signal can be computed by expanding it into a family of functions (tight frames), i.e. into a set of frequency channels of equal bandwidth on a logarithmic scale [75,76].

In comparing Eqs.(3.8) and (3.11) with Eq.(3.33) it is obvious that, whereas the STFT and the GT use a window of constant width and envelope, the WT uses an analyzing window (the basic wavelet) scaled in time and magnitude to have a fixed number of oscillations inside the envelope. Thus, for high frequencies, the basic wavelet is compressed in time, while for low frequencies it is dilated in time. This notion results in good time and frequency resolution of the WT up to theoretical Nyquist frequency. The time-frequency resolution are shown in Fig.(3.2) for comparison [77]. In addition, it is to be noted that whereas the analysis

window in the STFT works as a lowpass filter, it is a bandpass filter in the WT [77].

In general, the mother wavelet may be taken as any waveform; however, the best JTFA resolution is obtained if the mother wavelet is optimally localized in both time and frequency.

The discrete version of Eq.(3.33) (DWT) according to Daubechies [6] is given by

$$WT_{m,n} = a_0^{-m/2} \int_{-\infty}^{\infty} x(t) h(a_0^{-m} t - nb_0) dt \quad (3.34)$$

where $a = a_0^m$ and $b = nb_0 a_0^m$, from Eq.(3.33) with $m, n \in \mathbf{Z}$. Thus, the family of the generated wavelets can be written as

$$h_{m,n}(t) = a_0^{-m/2} h(a_0^{-m} t - nb_0). \quad (3.35)$$

On the other hand, good time-frequency properties can be achieved if discrete values for a and b are chosen such that, the parameter a is chosen to be equal to 2^i where i is termed the octave of the transform [78-81], and the parameter b is taken to be a multiple of a , in particular, ($b = n 2^i$). This choice, provides among others, the availability of zooming while moving from one scale to another in the sense of halving or doubling the scale as well as providing orthonormality of the frames (wavelets family) on $L^2(\mathbf{R})$ when combined to the nature of the wavelet window (mother wavelet) itself. It is to be noted that when the frame (family of wavelets) constitutes an orthonormal basis for $L^2(\mathbf{R})$ (where $L^2(\mathbf{R})$ is the Hilbert space of the square integrable functions), then they are typically appropriate for multiresolution analysis [5].

In our investigation, the flow induced vibration signals are analyzed using the above discretization with $a_0 = 2$ and $b_0 = 1$, respectively. It is to be noted that the Grossman-Morlet wavelets of the form

$$h_{a,b}(t) = \frac{1}{\sqrt{a}} h\left(\frac{t-b}{a}\right), \quad a > 0, \quad b \in \mathbf{R} \quad (3.36)$$

and the wavelets of Daubechies that have the form

$$h_{i,j}(t) = 2^{i/2} h(2^i t - j), \quad i, j \in \mathbf{Z} \quad (3.37)$$

are two cases of time-scale algorithms. However, Gabor-Malvar wavelets of the form

$$h_{k,l}(t) = \omega(t-l) \cos[\pi(k+1/2)(t-l)], \quad k \in \mathbf{N}, l \in \mathbf{Z} \quad (3.38)$$

is considered as time-frequency algorithm. In general, mixing the two points of view and subjecting the Gabor-Malvar wavelets to dyadic dilation leads to the construction of the Daubechies wavelets.

Moreover, it should be emphasized that the selection of a suitable window (wavelet) for the application under consideration is not a trivial matter. The selection of an appropriate wavelet is intensively discussed by Rioul and Tewfik et al. [82,83]. However, some mother wavelets of interesting features, which are frequently used, are introduced in the sequel.

(1) One cycle of the sine-function wavelet, which have the form

$$h(t) = \begin{cases} \frac{1}{\sqrt{\pi}} \sin t, & \text{if } |t| \leq \pi \\ 0, & \text{otherwise} \end{cases} \quad (3.39)$$

The Fourier transform H of h is given by

$$H(\omega) = \frac{\sqrt{2}}{\pi} j \frac{\sin \pi \omega}{1 - \omega^2} \quad (3.40)$$

(2) Mallat wavelet [5], which is developed originally to be used in computer vision applications, is defined as

$$H(\omega) = \frac{e^{-j\omega/2}}{\omega^4} \left(\frac{F(\omega/2) + T}{F(\omega)F(\omega/2)} \right) \quad (3.41)$$

where T is a delay factor, and

$$F(\omega) = \frac{N_1(\omega) + N_2(\omega)}{105 \sin(\omega/2)} \quad (3.42)$$

$$N_1(\omega) = 5 + 30 \cos^2(\omega/2) + 30(\cos^2(\omega/2))(\sin^2(\omega/2))$$

$$N_2(\omega) = 2(\cos^2(\omega/2))(\sin^4(\omega/2)) + 70 \cos^4(\omega/2) + \frac{2}{3} \sin^6(\omega/2)$$

(3) Daubechies [6,84] constructed the following tight frame wavelet, consulting Appendix A for tight frames,

$$H(\omega) = (\log a_0)^{-1/2} \begin{cases} 0 & \omega < l \\ \sin \left[\frac{\pi}{2} v \left(\frac{\omega - l}{l(a_0 - l)} \right) \right] & l \leq \omega \leq a_0 l \\ \cos \left[\frac{\pi}{2} v \left(\frac{\omega - l}{la_0(a_0 - l)} \right) \right] & a_0 l \leq \omega \leq a_0^2 l \\ 0 & \omega \geq a_0^2 l \end{cases} \quad (3.43)$$

where,

$$l = \frac{2\pi}{b_0 a_0^2 - 1} \quad (3.44)$$

and, v is a C^k (or C^∞) function from \mathbf{R} to \mathbf{R} that satisfies,

$$v(x) = \begin{cases} 0 & \text{if } x \leq 0 \\ 1 & \text{if } x \geq 1 \end{cases} \quad (3.45)$$

as an example of a (C^1) function v is

$$v(x) = \begin{cases} 0 & x \leq 0 \\ \sin^2(x \pi/2) & 0 \leq x \leq 1 \\ 1 & x \geq 1 \end{cases} \quad (3.46)$$

and this construction leads to a family of tight wavelet frames with no restrictions on the choice of the parameters a_0, b_0 other than $a_0 > 1$ and $b_0 \neq 0$.

(4) Meyer [85] used Daubechies' wavelet and constructed another one which is appropriate for multirescale analysis and it is given by

$$H_1(\omega) = \frac{1}{\sqrt{2\pi}} e^{j\omega/2} (H(\omega) + H(-\omega)) \quad (3.47)$$

where, $H(\omega)$ is Daubechies' wavelet.

(5) The modulated Gaussian wavelet, which was most often used by Morlet [74] in analyzing seismic data and in his numerical computations, is given by

$$\begin{aligned} h(t) &= \pi^{-1/4} (e^{-j\omega_0 t} - e^{-\omega_0^2/2}) e^{-t^2/2} \\ H(\omega) &= \pi^{-1/4} (e^{-(\omega-\omega_0)^2/2} - e^{-\omega_0^2/2} e^{-\omega^2/2}) \end{aligned} \quad (3.48)$$

The subtraction term in the definition of h , H ensures that $H(0) = 0$; for the value of ω_0 chosen here, this term is negligible in practice. The value of ω_0 has been fixed so that ratio between the highest and the second highest local maxima of $\text{Re}[h]$ is approximately 1/2.

Kadambe and Boudreaux [86,87] used the modulated Gaussian wavelet with

$$\omega_0 = \pi(2 / \ln 2)^{1/2} \quad (3.49)$$

(6) The Mexican-hat wavelet, which is the second derivative of the Gaussian $e^{-t^2/2}$ [84]. If we normalize it so that its L^2 -norm is 1, we obtain

$$\begin{aligned} h(t) &= \frac{2}{\sqrt{3}} \pi^{-1/4} (1 - t^2) e^{-t^2/2} \\ H(\omega) &= \frac{2}{\sqrt{3}} \pi^{-1/4} \omega^2 e^{-\omega^2/2} \end{aligned} \quad (3.50)$$

and if this function is plotted and rotated around its symmetrical axis, then one obtains a shape similar to a Mexican hat.

(7) The eighth derivative of the Gaussian wavelet, which functions like the Mexican hat [84], is appropriate in applications of the wavelet transform to edge detection; and is given by

$$h(t) = \left(\frac{2^{157}!}{15!} \right)^{1/2} \pi^{-1/4} (t^8 - 28t^6 + 210t^4 - 450t^2 + 90) e^{-t^2/2}$$

$$H(\omega) = \left(\frac{2^{157}!}{15!} \right)^{1/2} \pi^{-1/4} \omega^8 e^{-\omega^2/2} \quad (3.51)$$

(8) The harmonic wavelet, which was recently introduced by Newland [4,9], is given by

$$h(t) = \frac{e^{j4\pi t} - e^{j2\pi t}}{j2\pi t}$$

$$H(\omega) = \begin{cases} 1/2\pi, & 2\pi \leq \omega < 4\pi \\ 0, & \text{elsewhere} \end{cases} \quad (3.52)$$

In this case, the basic wavelet is complex and only the real part should be used for the analysis of real signals.

When any of these different basic wavelets is employed, the DWT Eq.(3.34) in the frequency domain takes the form

$$WT_{m,n} = \sum_m \sum_n a_0^m \int_{\omega} e^{j\omega n b_0 a_0^m} H(a_0^m \omega) X(\omega) d\omega \quad (3.53)$$

where $m, n \in \mathbf{Z}$; F and H are the Fourier representation of the analyzed signal and the chosen wavelet, respectively.

Moreover, for the harmonic wavelet, Eq.(3.52), the discretized version in the frequency domain is simply

$$H_{m,n}(\omega) = \begin{cases} 1/(2\pi(n-m)), & m2\pi \leq \omega < n2\pi \\ 0 & \text{elsewhere} \end{cases} \quad (3.54)$$

where $n, m \in \mathbf{R}^+$. However, the DWT, Eq.(3.34) in the time domain cascades into two sets of coefficients, one is real ($WT_{m,n,k}$) while the other is complex ($WT_{m,n,k}^*$), and they are given by

$$WT_{m,n,k} = (n-m) \int_t x(t) h_{m,n}^* \left(t - \frac{k}{n-m} \right) dt \quad (3.55)$$

$$WT_{m,n,k}^* = (n-m) \int x(t) h_{m,n} \left(t - \frac{k}{n-m} \right) dt \quad (3.56)$$

where $n, m \in \mathbf{R}^+$, $k \in \mathbf{Z}$, and $WT_{m,n,k}^*$ is the complex conjugate of $WT_{m,n,k}$ if $x(t)$ is real [4].

A FORTRAN program (shown in Appendix B) was written to find the WT after Abu-Samak [13], the algorithm used is shown in Fig.(3.3).

3.4 LITERATURE SURVEY

Far away from Gabor's classical algorithm [66], Genssar et al. [88] developed an iterative algorithm, called Gabor's iterative algorithm, to calculate numerically Gabor's coefficients. This iterative algorithm was examined for convergence via a method developed according to the theory of digital signal filtering. It had been shown that the algorithm convergence was conditional on the selected type of the window function. For example, when using the Gaussian window (as proposed by Gabor), the algorithm converged only for specific signals. Thus, convergence conditions for the algorithm were formulated, permitting the examination of alternative windows.

In there investigation using the continuous wavelet and Gabor coefficients in the asymptotic limit and under some additional assumptions, Delprat et al. [89] had shown that it was possible to extract some important characteristics of nonstationary signals, like for example instantaneous frequencies and amplitude modulation. However, they also reported that it was difficult to isolate components that strongly interact in the time-frequency plane.

While examining the acceleration of the frame algorithms, Gröchenig [90] had developed a polynomial acceleration technique which improve and accelerate the frame algorithms. This technique was used with frame

algorithm to analyze and reconstruct signals from wavelet theory and from Gabor theory.

For generalizing the Walter sampling theorem (a new version of the classical Shannon sampling theorem), Janssen [91] used the Zak transform for wavelet subspaces. He considered a cardinal series based on signal samples $f(a+n)$, $n \in \mathbf{Z}$ with a possibly not equal to zero (Walter's sampling). Also, he had shown that the stability of the results depends critically on a .

Moreover, Grossman et al. [10] had indicated that the 3D-wavelet phase plot (m, n and $P_{m,n}$), which is given by

$$P_{m,n} = \tan^{-1} \left[\frac{\text{Im} \langle x, h_{m,n} \rangle}{\text{Re} \langle x, h_{m,n} \rangle} \right], \quad (3.57)$$

is particularly suited to singularity detections.

More recently, Newland [4,9] introduced the so-called harmonic wavelets, which he proposed to be a useful tool for the analysis of nonstationary signals especially in the field of vibration measurement and analysis. This wavelet was implemented to analyze some practical examples, and similarities between the wavelet time-frequency maps and the sonograms was deduced.

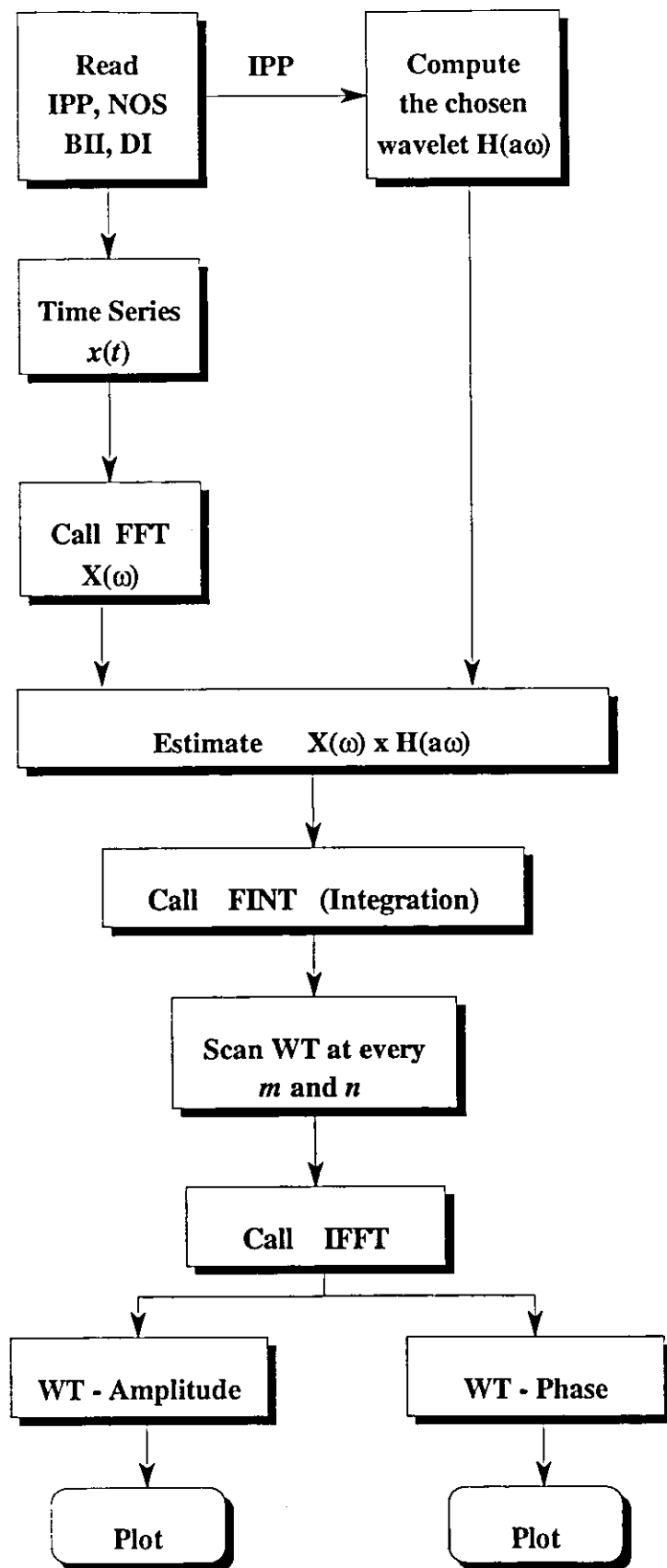


Figure (3.3) : The Wavelet Transform Algorithm [13].

CHAPTER 4

CHAOS

4.1 INTRODUCTION

Any system that is inherently unpredictable may show chaotic behavior. The word "chaos" is derived from the Greek word "χάος" which originally means, according to the Encyclopedia Britannica, the infinite empty space which existed before all things [92].

When considering physical systems, which show random response, chaos may be evolved. However, even linear time dependent processes may show chaotic behavior for certain system parameters, when exposed to random forces [93]. Also, solutions obtained for deterministic differential equations, through simulation, have shown random like properties for linear as well as nonlinear systems in many research fields. However, random responses for several systems which look chaotic are found to be deterministic [94,95].

Thus, random responses of nonlinear systems may indicate chaotic behavior [94,95]. Even for a nonlinear dynamic system whose response is described by a deterministic equation, chaos may exist, since the response becomes unpredictable because of the nonlinearity amplifications of the initial conditions [93]. Also, of special importance is the emergence of chaos in deterministic strongly nonlinear dynamical systems.

In order to study nonlinear differential equations both qualitative and quantitative techniques can be employed [96,97]. Qualitative techniques such as phase space, Poincaré map and stability analysis are mainly concerned with the general stability characteristics of a system near a known solution, rather than with the explicit time history of the motion. However, quantitative techniques such as perturbation methods, numerical

integrations and averaging methods can yield reliable results provided that the system exhibits only weak non-linearities. For strong non-linearities several algorithms have been developed, among them the Fast Galerkin method (FG) which utilizes the FFT [98], the incremental harmonic balance [99] and the alternating frequency/time method [100].

4.2 CHAOS DESCRIPTORS

Chaotic behavior may be identified by a qualitative change using one or more of the following criteria [93,101,102] :

1. Time History : For typical dissipative systems, a start-up transient appears after which the motion settles down to a long-term recurrent behavior. When the motion is periodic, it is repeated at regular intervals. However, when it is chaotic, it has a random-like appearance (i.e. the time history looks chaotic).
2. Power Spectrum : Power spectrum can be used to distinguish between periodic and chaotic responses. It is well known that for a periodic motion, discrete frequencies dominate the power spectrum, while for a chaotic motion, it is continuous, although peaks may be observed in such a process. In general, both periodic and quasi-periodic responses show discrete power spectra, whereas chaotic response show a continuous power spectrum.
3. Autocorrelation : The behavior of the autocorrelation function can be helpful in identifying the presence of chaos. For a periodic motion, the autocorrelation function is periodic, while for a chaotic motion, it decays to zero as the time shift approaches infinity ($\tau \rightarrow \infty$).
4. Phase Plane Portrait : It is a direct implementation of the geometric theory of nonlinear systems and it is useful for second order systems, because the phase space is reduced to a phase plane with trajectories

projected on it. A trajectory of motion forms a closed orbit when the motion is periodic, while it is very complex for a chaotic motion.

5. Poincaré Map : The Poincaré map in the phase plans, as given by Ueda [103], is the transformation of the (x, \dot{x}) -phase plane into itself according to $P:(x_0, \dot{x}_0) \rightarrow [x(t_0 + \tau), \dot{x}(t_0 + \tau)]$, where τ is an appropriate period (forcing period) and x_0, \dot{x}_0 are the initial displacement and velocity, respectively, at $t = t_0$. For autonomous systems, a more general Poincaré map is given by Dowell [101]. In general, Poincaré map is defined by the intersection points of the orbit with a hyperplane in the phase space. The Poincaré map strobed points indicate the periodicity of the response if it is existed. Thus, for a harmonic motion, a single point is presented in the Poincaré map, whereas for N-subharmonic motion, N-points are presented. However, for a chaotic motion, the map has a complex fractal structure. In general, the stroboscopic phase points are restricted to a well defined regions, which is sometimes called the strange attractors of the system.

4.3 PROPERTIES OF CHAOS

To investigate chaotic motion in a proper way several concepts and procedures should be pointed out.

4.3.1 CHAOTIC ATTRACTORS

For a dynamic system an attractor is a point (or object) towards which all nearby solutions move as time evolves. An important parameter for studying chaos is chaotic attractors (strange attractors) which are simply the geometric points in state space to which chaotic trajectories are

attracted. More precisely, a chaotic attractor can be identified as a stable-structure of long-term trajectories in a bounded region of phase space, which folds the bundle of trajectories back onto itself, resulting in a mixing and divergence of nearby states [93]. Attractors can be classified into three categories; equilibrium (point), periodic (cycle) and chaotic (mixing), which represent the commonly observable attractor in dissipative systems. Multiple attractors are common in nonlinear systems where more than one type of attractors are coexisting. More recently, another type of attractors was reported [104,105]; strange non-chaotic attractors.

The type of attractors to which the motion settle to, depends on the initial conditions. Thus, a closure of the initial conditions for which the system will asymptotically approach a particular attractor is called the basin of attraction of the attractor or its catchment region [106-109].

4.3.2 STRUCTURAL STABILITY AND BIFURCATIONS

Stability can be investigated by two different means, the first is to consider the persistence of the behavior of a motion if the initial conditions are perturbed, while the second is to consider the persistence of the behavior of a system if the dynamical system itself or even its parameters are perturbed (structural stability).

Under the first category, a solution is called stable in the sense of Lyapunov if the solution $\phi_\tau(\bar{x})$, $\tau \geq 0$, depends uniformly and continuously on the N-dimensional matrix \bar{x} ; thus for any $\varepsilon > 0$ ($\varepsilon \in \mathbf{R}$) there exists a $\delta(\varepsilon) > 0$ such that if $d(\bar{x}_1, \bar{x}) < \delta$ and $\tau \geq 0$, then $d(\phi_\tau(\bar{x}_1), \phi_\tau(\bar{x})) < \varepsilon$. Otherwise the solution is unstable. In the case of periodic solutions orbital stability is of more concern. The motion is said to be orbitally stable if the unperturbed solutions are periodic functions of time, showing closed trajectories (limit cycles) \bar{C} in the phase space and

every trajectory in the neighborhood of C tends to reach this closed trajectory (limit cycle). However, if there are trajectories tending to leave the neighborhood of C , the solution is said to be orbitally unstable. Another type of stability is that in the sense of Lagrange; it only requires that the solution to be bounded to acquire stability, and it is unstable otherwise.

Another approach as said previously is the structural stability. Guckenheimer and Holmes [110] defined small perturbation of the dynamical system as follows. If F is a map or a vector field, then G is a (C^1, ε) -perturbation of F if there is a compact set $M_c \subset M$ such that $F = G$ on $M - M_c$ and $d(F, G) < \varepsilon$, $d^*(DF, DG) < \varepsilon$ on M_c , where d and d^* are appropriate distance functions. Also, two C^r -maps are called C^k -conjugate or C^k -equivalent ($0 \leq k \leq r$), if there exists a C^k -homeomorphism h such that $h \circ F = G \circ h$. C^0 -equivalence is termed topological equivalence. Two C^r -vector fields \bar{f} and \bar{g} are said to have C^k -equivalence ($0 \leq k \leq r$) if there exists a C^k -diffeomorphism h which takes orbits $\phi_\tau^f(\bar{x})$ of \bar{f} to orbits $\phi_\tau^g(\bar{x})$ of \bar{g} and preserves senses but not necessarily parametrization by time. If h preserves parametrization by time, then it is called conjugacy. A C^r -map F (or equivalently a C^r -vector field \bar{f}) is called structurally stable if there is an $\varepsilon > 0$ such that all (C^1, ε) -perturbations of F (or \bar{f}) are C^0 -equivalent to F (or \bar{f}).

Also, a bifurcation can be defined as a situation in which a dynamical system is not structurally stable. Bifurcations of stationary and periodic solutions are called local bifurcations if only some neighborhood of these solutions needs to be considered. Bifurcation values are usually termed for the parameters at which bifurcations occur. Moreover, the pair of a bifurcation value and a corresponding stationary solution of a differential equation or fixed point of a Poincaré map is called a bifurcation point.

4.3.3 STABILITY AND LYAPUNOV EXPONENTS

A solution of N-dimensional coordinate dynamical system described by the set of equations $\dot{\bar{\mathbf{x}}} = \bar{\mathbf{v}}(\bar{\mathbf{x}}, t)$ with initial conditions $\bar{\mathbf{x}}(t_0) = \bar{\mathbf{x}}_0$, where $\bar{\mathbf{x}} = [x_1, x_2, \dots, x_N]^T$ represent the variables of the N-dimensional phase space, and $\bar{\mathbf{v}} = [v_1, v_2, \dots, v_N]^T$ gives the coupling between the variables, and is determined by the phase flow,

$$\bar{\mathbf{x}}(t) = \phi_{t,t_0}(\bar{\mathbf{x}}_0) \quad (4.1)$$

where ϕ_{t,t_0} is the evolution operator which maps the state $\bar{\mathbf{x}}_0$ at time t_0 to the state $\bar{\mathbf{x}}$ at time t . Small perturbations on the initial conditions are introduced to study the stability of this solution. Thus, the derivative of ϕ with respect to the initial conditions is obtained as

$$D_{x_0} \phi = D_{x_0} \phi_{t,t_0}(\bar{\mathbf{x}}_0) \quad (4.2)$$

It is to be noted that this derivative maps the elements of the tangent space $T_{x_0}M$ to the tangent space T_xM . This transformation can be obtained by integrating the matrix differential equation

$$\frac{d}{dt} [D_{x_0} \phi_{t,t_0}(\bar{\mathbf{x}}_0)] = D_x \bar{\mathbf{v}}(\bar{\mathbf{x}}, t) D_{x_0} \phi_{t,t_0}(\bar{\mathbf{x}}_0) \quad (4.3)$$

with the initial conditions

$$D_{x_0} \phi_{t_0,t_0}(\bar{\mathbf{x}}_0) = \mathbf{I} \quad (4.4)$$

where \mathbf{I} is the identity matrix. These equations, termed the linearized or variational equations, determine the stability of a solution in typical cases. If $D_{x_0} \phi$ grows at an exponential rate as $t \rightarrow \infty$, the solution is unstable, since small perturbations will be augmented, whereas if $D_{x_0} \phi$ decays at an exponential rate the solution is stable.

In order to study the stability of stationary solutions of autonomous systems, the above equations can be integrated as

$$D_{x_0} \phi_{t,t_0}(\bar{\mathbf{x}}_0) = e^{D_x \bar{\mathbf{v}}(\bar{\mathbf{x}}_0, t-t_0)} \quad (4.5)$$

It should be emphasized that the eigenvalues of $D_x \bar{v}(\bar{x}_0)$ indicates the stability of the solution. If all the eigenvalues have a negative real part, the solution is stable, while if at least one eigenvalue has a positive real part the solution is unstable. Typically, the stability of periodic solutions depends on the eigenvalues of the amplification matrix (monodromy matrix), $D_{x_0} \phi_{t_0+p, t_0}(\bar{x}_0)$, where p is the period of the periodic solution. In this case, if all eigenvalues of the monodromy matrix have a modulus smaller than one, the solution is stable, whereas if some eigenvalue has a modulus larger than one, the solution is unstable. It is to be noted that in the autonomous case, although the monodromy matrix has an eigenvalue equal to one, this does not affect the stability of the solution but it means only a shift in time.

For systems which have nonstationary or aperiodic responses, average rates of divergence and convergence are investigated by generalizing the idea of the eigenvalues of the linearized equations, and implementing the Lyapunov exponents (characteristic exponents). The Lyapunov exponents can be defined as

$$\lambda(\delta\bar{x}) = \limsup_{t \rightarrow \infty} \frac{1}{(t - t_0)} \ln \frac{\|D_x \phi_{t, t_0}(\bar{x}_0) \delta\bar{x}\|}{\|\delta\bar{x}\|} \quad (4.6)$$

where $\delta\bar{x}$ is a vector in the tangent space $T_{x_0} M$. Noting that, because

$$\lambda(\delta\bar{x}^{(1)}) + \lambda(\delta\bar{x}^{(2)}) \leq \max\{\lambda(\delta\bar{x}^{(1)}) + \lambda(\delta\bar{x}^{(2)})\} \quad (4.7)$$

and

$$\lambda(\alpha\delta\bar{x}) = \lambda(\delta\bar{x}) \quad (4.8)$$

we can define linear subspaces of $T_{x_0} M$,

$$S_\alpha = \{\delta\bar{x} | \lambda(\delta\bar{x}) \leq \alpha\} \quad (4.9)$$

This implies that there are at most N -different Lyapunov exponents, namely the values of α at which S_α changes its dimension. If the flow on the attractor is ergodic (stationary and the ensemble averages are invariant

irrespective of the time history), we can take the ordinary limit in the above definition in a great generality and the values of the Lyapunov exponents are almost independent of initial conditions [111].

Negative Lyapunov exponents correspond to decay of perturbations of initial values, where as positive Lyapunov exponents correspond to amplification of perturbations of initial values. For stationary solutions, the Lyapunov exponents are only the real parts of the eigenvalues of $D_x \bar{v}(\bar{x}_0)$. For periodic solutions the Lyapunov exponents are

$$\lambda_i = \ln \left(\frac{|\mu_i|}{p} \right) \quad (4.10)$$

where the μ_i are the eigenvalues of the monodromy matrix and p is the period. For quasi-periodic solutions, some Lyapunov exponents can be zero, while the other ones are negative. For aperiodic attractors, some Lyapunov exponents may be positive, which points a sensitive dependence on the initial conditions.

It is to be noted that in any chaotic region, the distance between nearby orbits grows approximately as $e^{\lambda t}$ in the phase space, where λ is the Lyapunov exponent. A positive value of the main characteristic exponent may indicate the existence of chaos [112,114].

4.3.4. FRACTAL DIMENSION

The Lyapunov exponent expresses the dynamical nature of the chaotic regime. A quantity related to static properties and describes the geometry of the strange attractor is the fractal dimension [115,116]. The importance of the concept of fractal dimension to the field of chaotic vibrations is that it can predict the number of independent variables that may ultimately be needed to model the observed chaotic motions in physical problems. More than one definition of the attractor dimension are available [117,118].

However, the fractal dimension of the Poincaré map does not reveal the fractal dimension of the dynamics of the process, because the Poincaré map

lies only in two dimensional space, whereas the process may require more than two dimensional space in order to represent the qualitative features of the dynamics of the process. Thus, to describe the fractal dimension properly, the system degrees of freedom should be found. For systems with unknown degrees of freedom a pseudo-phase space (embedding space) should be constructed using delayed measurement of state variables. The choice of the dimension of the embedding space is very important and should be larger than the minimum degrees of freedom that are required to describe the dynamics of the system [93].

4.4 ROUTES TO CHAOS

In many physical systems, as some control parameters in the governing equations of motion vary, several characteristic changes in the motion may occur due to bifurcations that can lead to chaos. The bifurcation types leading to chaos are the infinite period doubling cascades, the intermittencies and the crises.

The period-doubling route to chaos is the most widely known and studied [120]. In this case, a typical controlling parameter leads the dynamical system through a sequence of successive bifurcations in which the period of all solutions at each step of the bifurcation is twice that at the previous step: thus, this process is called a period-doubling cascade. A common feature of a chaos is a succession of bifurcations to higher and higher subharmonics as a parameter is varied. In some systems, chaos occurs as a sequence of period-doubling bifurcations with a limit point beyond which strange attractors occur.

The second type of routes to chaos involves the intermittency. Intermittency bifurcations to chaos are caused by discontinuous or catastrophic disappearance of a periodic attractor inside a phase space

defined as follows. If a dynamical system with a set of equations of motion $\dot{\bar{\mathbf{X}}} = \bar{\mathbf{v}}(\bar{\mathbf{X}}, t)$, where $\bar{\mathbf{X}} = [x_1, x_2, \dots, x_N]^T$ represents the variables of the N-dimensional phase space, and $\bar{\mathbf{v}} = [v_1, v_2, \dots, v_N]^T$ gives the variables coupling, is considered. The system can be described by N-Lyapunov exponents λ_i ($i = 1, 2, \dots, N$), and if $\sum_{i=1}^N \lambda_i > 0$, then the system never reach any attractor, however, if $\sum_{i=1}^N \lambda_i \leq 0$, then the evolution of the system takes place in a limited subspace of the phase space. Thus, the attractor of the system is a specific subspace which is asymptotically reached in time. Any attractor which is bounded by a piecewise smooth closed surface volume and not a finite set of points, a limit cycle, and a piecewise smooth surface (such as torus), is called a strange attractor. A chaotic attractor is an attractor with at least one positive Lyapunov exponent, whereas a strange non-chaotic attractor is one for which the geometrical structure is strange as well as no positive Lyapunov exponents is encountered [103].

Levitas et al. [132] proposed the simple cell mapping method (SCM) for global analysis of nonlinear dynamical systems. SCM introduces a spatial Poincaré sections in the state space of the dynamical system, subdivision of these sections into cells and construction of a cell-to-cell mapping. The ultimate advantage of this method is its reduction of the cell array size needed in calculations, and thus it is especially appropriate for studying multi-dimensional dynamical systems. This method was tested in R^2 and R^4 state spaces and it showed accordance with previous methods with the advantage of considerable saving in computer time as well as computer memory in addition to improvement in the accuracy of the calculations.

Healey [133] claimed the discovering of a mechanism for generating chaos in boundary layer transition through investigating a laminar flat plate boundary layer undergoing transition to turbulence. Disturbances were introduced via a loudspeaker embedded at some upstream location and the

hot wire anemometry technique was used for velocity measurements. A new technique was used to estimate the number of nonlinearly independent modes in the reconstructed phase portraits, and nonlinear maps were then fitted in order to model the spatial evolution of disturbances.

Sekar and Narayanan [11] investigated by the Fast Galerkin (FG) method and numerical integrations the response of a square prism modeled as a Duffing oscillator subjected to harmonic and flow induced excitations. The system was found to undergo a symmetry-breaking bifurcation followed by a cascade of period-doubling bifurcations which set the system to chaos. The initial period-doubling as well as the symmetry-breaking points were obtained by studying the movements of the eigenvalues of the monodromy matrix. The FG solutions were found to match exactly the numerical integration solutions, because of the sufficiently high number of harmonics retained. This modification to the FG was firstly introduced by Cameron and Griffin [134]. The chaotic solutions were confirmed by the strange attractors, the continuous power spectrum and the existence of positive Lyapunov exponents. Apart from the period-doubling route to chaos, the system entered the chaotic region through the crisis type instability. The parametric space between the free stream velocity and the dimensionless force coefficient was constructed in which the boundaries of symmetry-breaking, period-doubling bifurcations and chaotic regions were identified.

Li and Paidoussis [12] studied the nonlinear dynamics of a standing cantilevered pipe conveying fluid. Perturbation techniques were used to eliminate inertial non-linearities, and then Galerkin's method were used to discretize the system and reduce it into a four dimensional one. The center manifold, averaging and normal forms techniques were implemented in order to simplify the dynamics form, thus the main behaviors of the dynamic system, in the vicinity of the double degeneracy could be

obtained. It was found that a degenerate point is associated with a subcritical pitchfork bifurcation as the buckled pipe under its own weight regained stability for some critical flow. Another degenerate point was associated with a Hopf bifurcation suggesting the onset of limit cycle motion and flutter. These two bifurcations coincide in a doubly degenerate point. Simulations in the neighborhood of the double degeneracy for both autonomous and nonautonomous systems were carried out, then phase orbits bifurcation diagrams and Lyapunov exponents calculations were used to show consistency with the analytical predictions of periodic, quasi-periodic and chaotic oscillations. It was found that chaotic oscillations of the autonomous version of the system existed when the gravity parameter was sufficiently perturbed off the doubly degenerate point. The harmony between analytical predictions and simulations was not complete; since, despite the analytical predictions of hetroclinic orbits for the reduced system, the actual bifurcation observed in simulations were homoclinic, with associated subharmonic bifurcations which lead the system to chaos.

CHAPTER 5

EXPERIMENTAL SETUP & PROCEDURE

5.1 INTRODUCTION

The experimental work in this investigation is concerned with the study of the time series of the vibration signal (acceleration) of the elastically mounted circular cylinder subjected to cross-flow. In what follows a description of the apparatus and instrumentation used as well as the measurements techniques is presented.

It is to be pointed out that basically the same experimental set-up, as described and studied by Al-Bedoor [135], Hijawi [136] and Abu-Samak [13], has been used in this work with the addition a digital data collection and processing system.

5.2 APPARATUS

The experimental investigation was conducted in an open suction type wind tunnel with a square cross section area of $30\text{cm} \times 30\text{cm}$, and of length equal to 200cm , Fig.(5.1). The flow rate was controlled via a double butterfly valve, and was generated from a fan driven by a 5.6kW , 3 phase motor which rotates at 2900 rpm. With these facilities, it was possible to vary the free stream velocity from 4.5 to 27m/s , with the free stream turbulence intensity level below 0.35%.

5.3 THE TEST MODEL

The test cylinder was placed at 1.3m from the inlet of the test section where the flow was found to be fully developed. The range of Reynolds numbers used was approximately $6.12 \times 10^3 < Re < 3.78 \times 10^4$, based on

the outside diameter of the vibrating cylinder. In this range, the Strouhal number for a circular cylinder is 0.2. The test cylinder was of an aluminum tube with cross section of outer diameter $D=21.5mm$, wall thickness $t=0.5mm$ and length $L=440mm$. This combination yields an aspect ratio L/D of 20.5 and mass per unit length \bar{m} of $0.1662kg/m$.

The cylinder mountings used in this experiment are similar to those used by Shirakashi et al. [60]. The cylinder was suspended by two similar clamped plates at its ends, Fig.(5.1). The end plates were placed outside the test section of the wind tunnel to avoid interference with the flow. By adopting this sort of mounting one would minimize the mode coupling effects which may arise from the streamwise and the rotational motions. Motion in the horizontal direction for this mounting is difficult to excite since the plate axial rigidity is much higher than its rigidity in the vertical direction, i.e. the horizontal vibration natural frequency of the cylinder for this mounting is much higher than its natural frequency of the vertical vibration. The cylinder passed through two slots of $28mm \times 28mm$ of the wind tunnel. Note that careful considerations were taken to ensure the two dimensionally of the vortex wake. This was achieved by making the height of the slots at the two sides of the wind tunnel to be much less than nearly four times the diameter of the test cylinder, as was recommended by Graham [137]. This was confirmed by preliminary tests. In order to eliminate the influence of the flow through the slots, blocking plates were attached to the cylinder at both ends. This technique relies upon the isolation of interference effects that arise as a result of the interaction of the tunnel boundary layer with the cylinder [138,139]. Fox [140] reported that the rectangular plates should have an upstream dimension (distance of leading edge from the cylinders axis) sufficiently large to isolate the horseshoes vortex generated at the wall-cylinder interaction, but small enough to avoid substantial boundary layer growth on the plate itself, and

tail dimensions adequate to prevent any wake interference. Using this concept the end plates were squared in design with an area of $7d \times 7d$ with the hole to accommodate the cylinder is at $2.5d$ from the leading edge of the plate as shown in Fig.(5.2). On the other hand, Fig.(5.3) shows a photo for the end plates arrangement.

5.4 INSTRUMENTATION

An accelerometer type (B&K 4370) was attached to the left side of the test cylinder as shown in Fig.(5.1). The output signal from the accelerometer was simultaneously fed to a portable conditional amplifier type (B&K 2626) to reduce aliasing effect, the signal from the conditioning amplifier was fed to a lowpass filter with cutoff frequency equals to two times the sampling frequency. The output of the conditional amplifier was in turn fed to a (Gateway-2000, 8MB-RAM) computer via an interface card type (NI Lab PC+). The free stream velocity was measured by an inclined alcoholic Pitot tube at the fully developed flow region of the wind tunnel. This instrumentation scheme is shown in Figures (5.3-5.4). A digitizing oscilloscope type (HP 54501A) was used to check the results on the PC. A schematic diagram for the test cylinder is shown in Fig.(5.5). In addition, Fig.(5.6) shows schematically a flow chart of the instrumentation setup used in this work.

5.5 EXPERIMENTAL PROCEDURE

The natural frequency f_n and the logarithmic decrement δ of the test cylinder were determined by impulsive test, wherein the cylinder was set into vibration by slightly tapping its center.

The free stream velocity was measured using an inclined Pitot tube placed at 1D in the horizontal direction and 2D in the vertical direction from the static equilibrium position at the mid point of the oscillating cylinder. Various time series were chosen for different free stream velocities. The digitization of the time series by the computer program was carried out at a sampling rate that obeys the Nyquist formula, given by

$$f_s \geq 2f_n \quad (5.1)$$

where f_s is the sampling frequency. Noting that the natural frequency f_n of the cylinder in the transverse direction is about 120Hz, the sampling frequency f_s was chosen to be 4000Hz. This sampling rate was found to be satisfactory for the type of signals considered in this work. A time record of 2050 data points was taken in each experimental run.

A LabView program using the G-language was constructed to acquire the data (time record), to analyze the data by the classical methods, i.e. compute numerically both the autocorrelation function and the power spectrum from the acquired signal, and finally to save the results and the time record on separate files. Several time records have been acquired over range of free stream velocities from 4.00 to 27.00 m/s.

5.6 INSTRUMENTATION AND WT PROGRAM TESTING

The measurement setup was checked for reliability by conducting a vibration test via an exciter with the following instruments, big table head type (B&K 4813), exciter body type (B&K 4801), exciter control type (B&K 1047) and power amplifier type (B&K 2707). Also, the measurement setup was tested by monitoring the vibrations of a vertically mounted beam which was fastened to the previous exciter and the accompanied instruments.

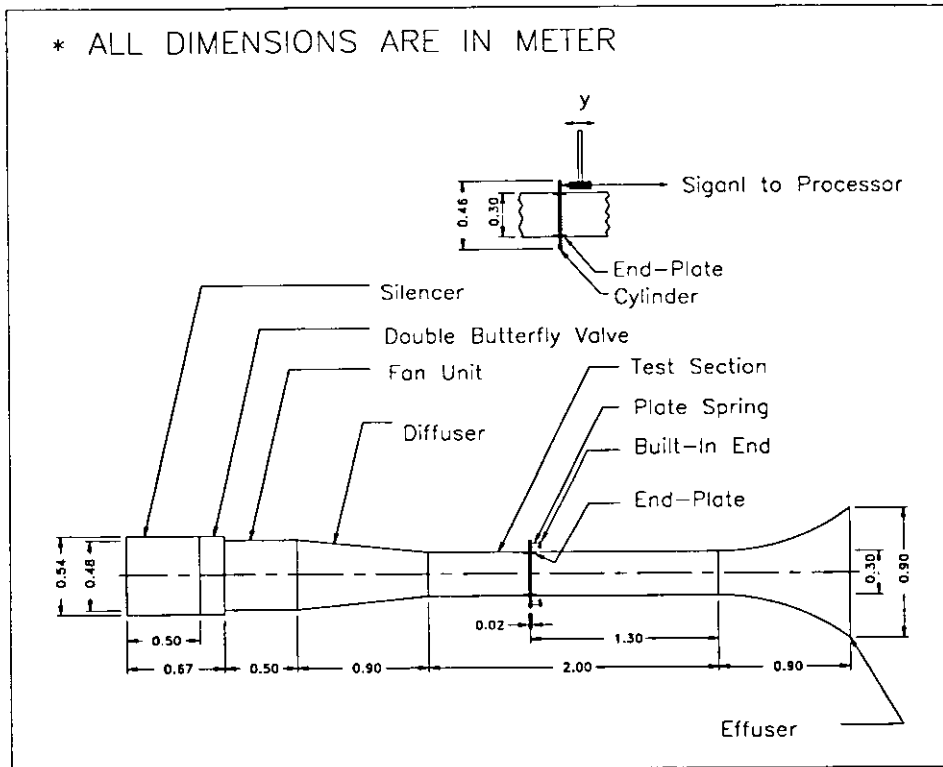


Figure (5.1) : Experimental Setup.

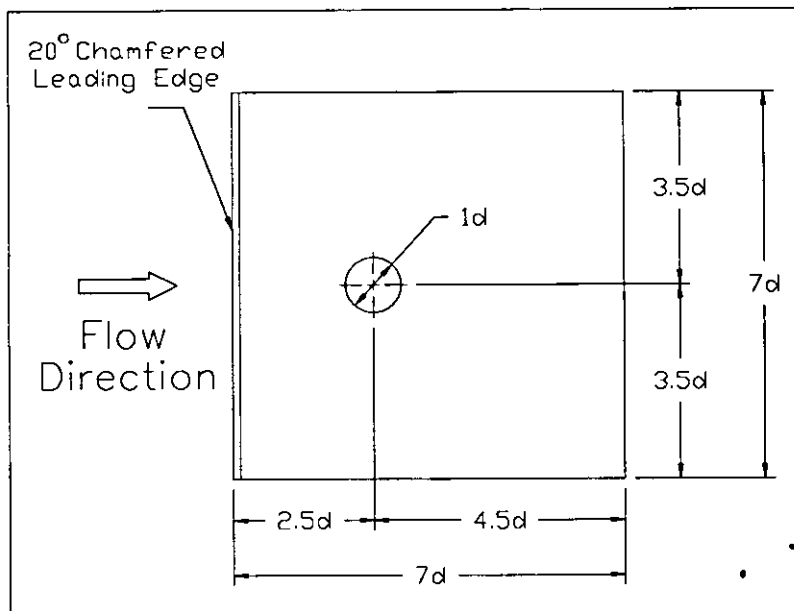


Figure (5.2) : End plates detail [60].

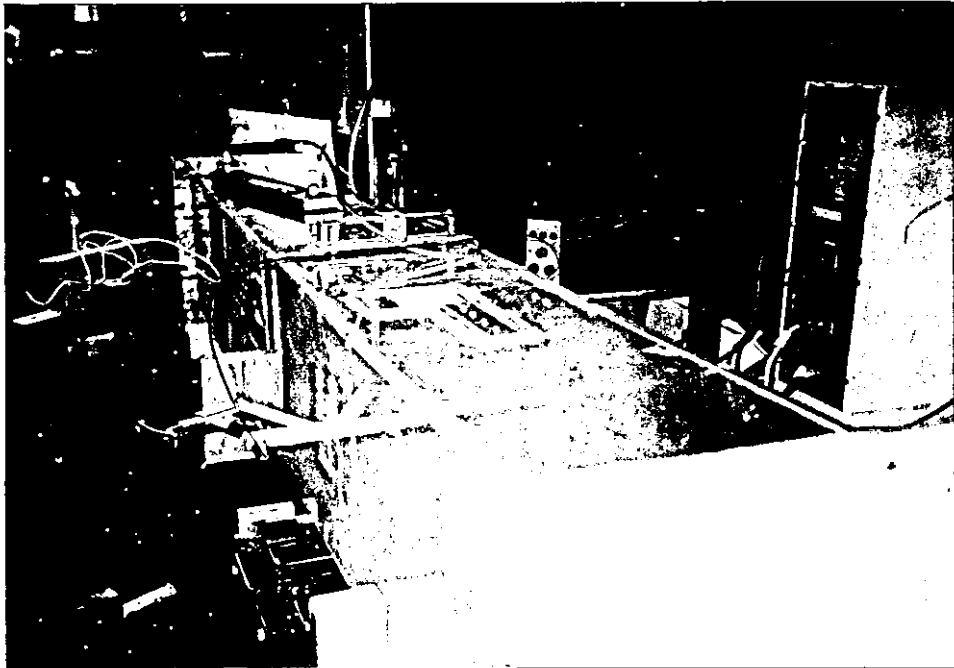


Figure (5.3) : The end plates and the circular cylinder used.



Figure (5.4) : The instruments used in the experimental investigations.

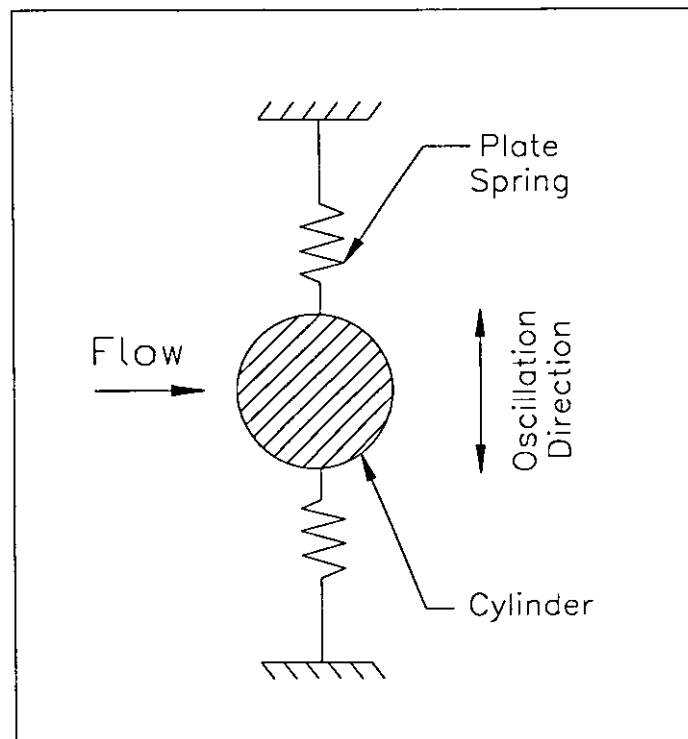


Figure (5.5) : A schematic diagram for the test cylinder used in this work.

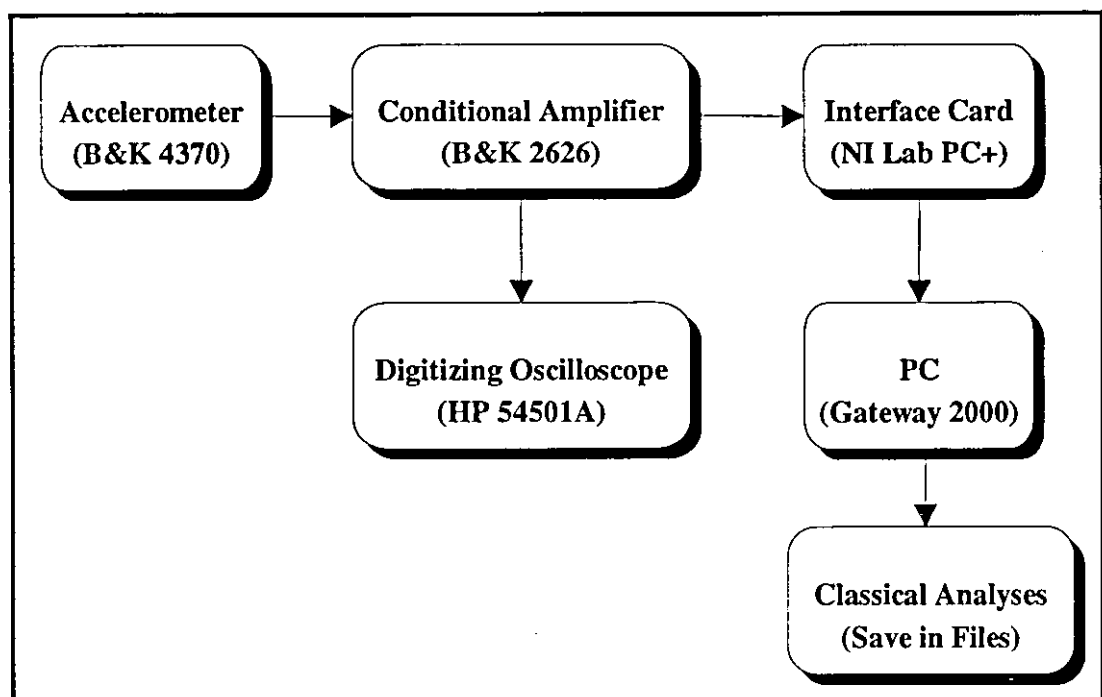


Figure (5.6) : A flow chart of the instrumentation setup used in this work.

CHAPTER 6

RESULTS AND DISCUSSION

6.1 INTRODUCTION

The test cylinder was mounted as discussed in the last chapter, and the natural frequency f_n and the damping ratio of that system were found to be 120 Hz and 0.02, respectively, after a simple impulse test.

The flow velocity was varied gradually in the range of free stream velocities (4.00-27.00 m/s). The recorded time-series (acceleration signals) have been analyzed via several methods to study the dynamic behavior of the flow-induced vibration of an elastically mounted single cylinder in a cross flow.

In the next section, the results of various methods of signal processing, which have been used, are introduced and discussed, whereas chaotic investigations including phase-space portraits, Poincaré-maps and fractal dimensions (correlation factors) of some signals are introduced and discussed in what follows.

6.2 SIGNAL PROCESSING RESULTS

Several analysis methods (autocorrelation, power spectrum, GT and WTs) have been applied to the time series at a free stream velocity of 19.00m/s. Fig.(6.1) shows the time series, the corresponding auto-correlation and power spectrum. On the other hand, Fig.(6.2) shows the corresponding Gabor transform, whereas Fig.(6.3) shows the corresponding WT using the modulated Gaussian wavelet. In this case, the autocorrelation function, Fig.(6.1), indicates that the process is narrow-banded (i.e., the autocorrelation decays slowly with time shift). The

corresponding power spectrum, Fig.(6.1), indicates that there are four dominant frequencies; subharmonic ($f = 1/3 f_n$), fundamental ($f = f_n = 120 Hz$), super-harmonics ($f = 3f_n$ and $f \approx 5f_n$). The third order superharmonic ($f = 3f_n$) appears to have the dominant contribution, while the contributions form the fundamental and the fifth superharmonics are nearly equal, however the subharmonic ($f = 1/3 f_n$) contribution is lower than that of the other three harmonics. This suggests that the process in this case is nonlinear, and probably of cubic type.

It is to be noted that the time-scale used for the wavelet transforms 3D representations replaces the time series and frequency distribution with scale parameters related to time and frequency but not equal to them. The frequency scale obeys the Nyquist frequency, i.e. $1 < a_0^m < f_s$, where f_s is the sampling frequency, $2Tf_s \leq 1$, also the value of the frequency scale (m) on the 3D wavelet plot is related to the actual frequency (f) of the time series waveform by the relation

$$a_0^m = \sqrt{f_o/f} \quad (6.1)$$

where a_0^m is the scale parameter as discussed in chapter three, and f_o is an arbitrary constant which depends on the type of wavelet used, i.e. $f_o = 5.336$ for modulated Gaussian, $f_o = 1.42$ for Mexican hat, $f_o = 2.83$ for eighth derivative of the Gaussian, $f_o = 4.188$ for Daubechie's tight frame. Thus, for the modulated Gaussian shown in Fig.(6.3), for example, $m = -3.04$ corresponds to actual frequency $f = 360 Hz$. On the other hand, the time scale for all the time series, the autocorrelation, the 3D Gabor plot and the 3D wavelet plots for all types of wavelets corresponds to the real time (t) by the relation

$$t = \frac{\text{Time Scale}}{f_s} \quad (6.2)$$

where f_s is the sampling frequency equals to $4 kHz$.

From Fig.(6.2), the Gabor transform shows that energy is mostly concentrated at the fundamental frequency and the third subharmonic ($f = 1/3 f_n$); however other subharmonics, such as $f = 1/4 f_n$, and $f = 3/4 f_n$, appear to have minor contribution with low energy content. The higher frequencies (i.e. including the superharmonics) are not considered due to the long CPU time needed to compute the GT. For example, the CPU time needed for a 128 data-points time record is about 36 hours, whereas for the WT using the modulated Gaussian wavelet it is about 1/4 hour on a VAX machine.

Considering Fig.(6.3), the wavelet transform shows that energy is concentrated at specific frequencies and times. It shows the process to be dominated by the above four harmonic components $f = 1/3 f_n$, $f = f_n$, $f = 3f_n$ and $f = 5f_n$; however, the fifth harmonic has a lower contribution than that of the first, while as in the frequency spectrum results, the third harmonic has the dominant contribution, and the third subharmonic has the least contribution. Also, the wavelet results, Fig.(6.3) indicate that while the third subharmonic and the fundamental persist (continuous with time), the third and the fifth harmonic show intermittent behavior with time (bifurcations from third to fifth superharmonics), where for certain time intervals only one of these two harmonics ($f = 3f_n$, $f = 5f_n$) is present in the response. This may suggest the existence of transient disturbances in the flow or chaotic behavior or some nonlinear modal coupling in the response of the cylinder, which requires further investigations.

Figures (6.4-6.6) show the 3D wavelet plots of the time series in Fig.(6.1) obtained using as mother wavelets, Mexican hat, eighth derivative of the Gaussian and Daubechies tight frame, respectively.

The Mexican hat wavelet, Fig.(6.4), indicates that the process is dominated by the third superharmonic ($f = 3f_n$) of variable magnitude,

and continuous with time, while the fundamental harmonic has a relatively small contribution and is discontinuous with time. The subharmonic ($f = 1/3 f_n$) and superharmonics ($f \geq 3 f_n$) contributions shown in Fig.(6.3) using the modulated Gaussian are not clearly identified in Fig.(6.4), whereas another time discontinuous contribution at ($f = 12 f_n$) appears.

The eighth derivative of the Gaussian wavelet Fig.(6.5) shows that the process is totally dominated by a time continuous tenth subharmonic ($f = 0.1 f_n$) of nearly constant magnitude and does not show any significant contribution from other harmonics except from a very high continuous superharmonic at ($f \approx 24 f_n$) which is of very small magnitude.

The Daubechie's tight frame wavelet Fig.(6.6) shows a time changing frequency content from low frequencies of about $4 Hz$ to higher ones of about $17 \times 10^3 Hz$ of changing magnitudes with maximum peaks occurring at lower frequency $f \approx 4 Hz$. It is difficult in this case to make a precise judgments on the frequency content of the process.

Based on the above results, in comparing Fig.(6.3) with Figures (6.4-6.6) and Fig.(6.1), it was decided that the modulated Gaussian is the most adequate wavelet to be used for the frequency analysis of the process under consideration. This conclusion was adopted depending on our knowledge of the actual process and the instrumentaion setup used, for example if the natural frequency f_n is as obtained before (i.e. 120 Hz), then it is nonresonable that a frequency at $f \approx 24 f_n$ has a contribution of the results within the above selected wavelet (the eighth derivative of the Gaussian). For this reason only the results using the modulated Gaussian are presented at different free stream velocities in the sequel.

Further interpretation of the singularities, if existed, and the phase modulations can be grasped by utilizing the 3D-phase-shift plot of the WT.

Figures (6.7-6.8) show the 3D phase plots of the WT using the modulated Gaussian at a free stream velocity of 19.00m/s; Fig.(6.7) shows the range of $(0-180^0)$, whereas Fig.(6.8) shows the range of $(-180-0^0)$. It can be seen from these two figures that even though the third superharmonic persists, it changes phase with the elapse of time (i.e. singularities). However, the fundamental harmonic shows a constant phase with time. In addition, many phase changes are encountered for high superharmonics.

The results shown from the 3D-phase plots, Figures (6.7-6.8), the topology of the Mexican hat wavelet transform plot, Fig.(6.4), and the bifurcations of harmonics as shown by the modulated Gaussian wavelet transform plot, Fig.(6.3), may indicate the process to be nonstationary.

Fig.(6.9) shows the time series waveform, and the corresponding autocorrelation and the power spectrum for a free stream velocity of 4.98m/s. Fig.(6.10) shows the corresponding 3D modulated Gaussian wavelet plot, Fig.(6.11) is another view of Fig.(6.10) using shorter time scale. In this case, the autocorrelation indicates that the process is broad-banded and the power spectrum shows the process to be dominated by the fundamental harmonic ($f = f_n$), a subharmonic ($f = 1/3 f_n$) and a superharmonic ($f = 2 f_n$) as well as the existence of other superharmonics up to $f = 10 f_n$. The wavelet transform Figures (6.10-6.11) shows the existence of a dominant time continuous superharmonic ($f = 3 f_n$) of variable magnitude, a time continuous fundamental harmonic of smaller and nearly constant magnitude and intermittent superharmonics ($f > 3 f_n$) up to ($f = 10 f_n$) of variable magnitudes and no superharmonic ($f = 2 f_n$). The fact that the process is broad-banded suggests that the process may be chaotic which requires further investigations.

Fig.(6.12) shows the time series, the corresponding autocorrelation and power spectrum, whereas Fig.(6.13) shows the corresponding modulated

Gaussian 3D wavelet plot at a free stream velocity of 5.50m/s. The autocorrelation and the power spectrum indicate that the process is broad-banded with the existence of low subharmonic ($f = 1/3 f_n$), fundamental ($f = f_n$) and superharmonics up to $f = 7 f_n$ all of appreciable magnitude. On the other hand, wavelet results indicate that the process is dominated by a time continuous fundamental harmonic of nearly equal magnitudes, a higher magnitude time continuous third subharmonic ($f = 1/3 f_n$), and a smaller magnitude time discontinuous superharmonic ($f = 3 f_n$). Very low and intermittent contributions are also observed from high superharmonics up to $f = 9 f_n$.

Fig.(6.14) shows the time series, the corresponding autocorrelation and power spectrum, whereas Fig.(6.15) shows the corresponding modulated Gaussian 3D wavelet plot at a free stream velocity of 24.08m/s. The autocorrelation and the power spectrum indicate that the process is broad-banded with the existence of low subharmonic ($f = 1/3 f_n$), fundamental ($f = f_n$) and superharmonics up to $f = 8 f_n$ all of appreciable magnitude. However, wavelet results indicate that the process is dominated by a time continuous superharmonic ($f = 3 f_n$) of variable magnitude, a smaller magnitude time continuous fundamental harmonic and very small intermittent sub- and superharmonic components.

In this case, the power spectra do not well correlate with the wavelet transform as the process in this case may be nonstationary and thus the power spectrum alone is not adequate to supply enough information concerning the frequency content of the process.

Figures (6.16-6.17) show two different time series, the corresponding autocorrelation and power spectrum for each time series at a free stream velocity of 26.00m/s, whereas Figures (6.18-6.19) show the corresponding modulated Gaussian 3D wavelet plot, for the time series of Fig.(6.16) and Fig.(6.17), respectively. Here, the autocorrelation for both time series

indicates that the process is narrow-banded; however, the power spectrum of the first time series presented in Fig.(6.16) indicates that the process is dominated by the low subharmonic ($f = 1/3 f_n$), the fundamental ($f = f_n$) and superharmonics up to $f = 8 f_n$, whereas the power spectrum of the second time series Fig.(6.17) shows a larger contribution of the lower subharmonic ($f = 1/3 f_n$) in addition to the other harmonics in the first time series. Figures (6.18-6.19) show the wavelet 3D plot of the first time series and the second time series, respectively, using the modulated Gaussian window. Here again the WT contradicts the FT results, and show that for both time series, Figures (6.16-6.17), the main contribution comes from the persisting variable magnitude third superharmonic ($f = 3 f_n$) for both time series under consideration; however, other harmonics such as the fundamental and high harmonics are observed but with low magnitude in both Figures (6.18-6.19). On the other hand, the WT of both time series show almost the same topology of the 3D-wavelet maps, i.e. they carry the same information, which means the WT gives almost a complete description of the time and frequency content of the signals such that if the time record is big enough to carry all the information of the dynamic behavior of the system, it will be revealed in just one wavelet transform run.

It is to be noted that the peak at $f = 1/3 f_n$ observed in the power spectra at the above stream velocities ($U_\infty = 4.98$, $U_\infty = 5.50$, $U_\infty = 19.00$, $U_\infty = 24.08$ and $U_\infty = 26.00$ m/s) does not appear in the wavelet transform, whereas it appears only at one low velocity of ($U_\infty = 5.50$ m/s); however it appears with very small component compared to other harmonic at $U_\infty = 19.00$. Although, as indicated above, this peak appeared in power spectrum for the above free stream velocities, it vanishes in the wavelet transforms; this agree with Shirakashi's assumption [60], which states that this peak vanishes when introducing endplates.

Whereas the frequency spectrum indicates constant, with time, frequency content of the vibration signal, the wavelet transform indicates that some of the harmonic components of the signal are intermittent with time and exhibit a bifurcation schemes which suggests that the process undergoes nonlinear dynamics which may lead the system to chaotic behavior; it may also suggest that some transient (intermittent) perturbations occur in the flow which may be due to the fan dynamics.

In general, from the WT representations of the various free stream velocities discussed, one can deduce that the fundamental frequency indicates the translational mode, whereas the third superharmonic may indicate the rotational mode. The bifurcation of harmonics (especially super ones), as seen in most of the WT representations, is a strong indication of the chaotic behavior of the system.

6.3 CHAOTIC BEHAVIOR INVESTIGATIONS

The above results lead naturally to the analysis of the possible chaotic responses of the several time series obtained. Thus, for every time series discussed above, the phase plane, the Poincaré map, the correlation function and the D_2 correlation dimension factor are obtained. Three FORTRAN programs, Appendix C, have been developed to give the phase-plane data, the Poincaré map data, and the correlation factor data, respectively.

Fig.(6.20) shows the phase-plane portrait, the corresponding Poincaré map, and the corresponding correlation function for a stream velocity of 4.98m/s. The Poincaré maps were carefully constructed by choosing a sampling rate (t_n) of 4 for our work by considering the phase-plane plots [95]. The phase plane suggests the possibility of chaotic behavior since no certain pattern is found, while the Poincaré map shows a lot of scattered

points which again indicates powerfully the existence of chaos. However, the slope of the correlation function (the D_2 correlation dimension factor) presented in Fig.(6.20.c) is found to be 1.65872 which is greater than one, thus the system at the stated parameters is chaotic.

Fig.(6.21) shows the phase-plane portrait, the corresponding Poincaré map, and the corresponding correlation function for a free stream velocity of 5.50m/s. The phase plane and the Poincaré map suggest the possibility of chaotic behavior. However, the D_2 correlation dimension factor presented in Fig.(6.21.c) is found to be 1.88259 which is greater than one, thus the system at the stated parameters is chaotic.

Figures (6.22-6.24) show the phase planes, the Poincaré maps and the correlation functions at free stream velocities of 19.00, 24.08, and 26.00m/s, respectively; the D_2 correlation dimension factors are found to be 1.67353, 1.92052, and 1.80941, respectively. Thus all these signals are chaotic and the system under consideration undergoes strong nonlinearity which led the system into chaos.

The velocity versus the D_2 correlation dimension factor is shown in Fig.(6.25); here one can deduce that the degree of chaos (the power of divergence of nearby orbits) trends to increase with velocity, but with fluctuating behavior at high velocities, and minimum peaks at 4.50 and 19.00m/s free stream velocities.

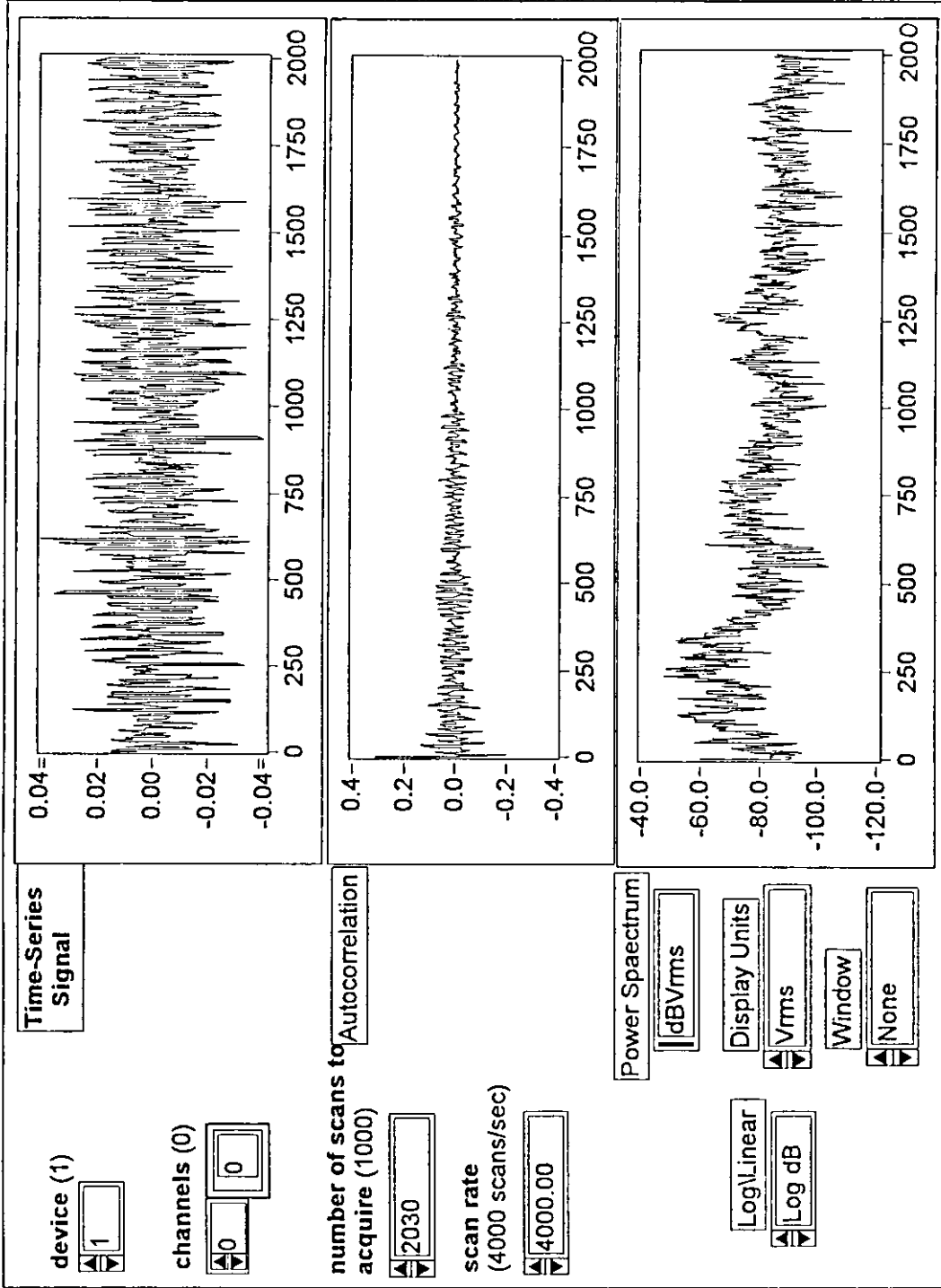


Figure (6.1) : The time series, the corresponding autocorrelation, and the corresponding power spectrum at a free stream velocity of 19.00m/s.

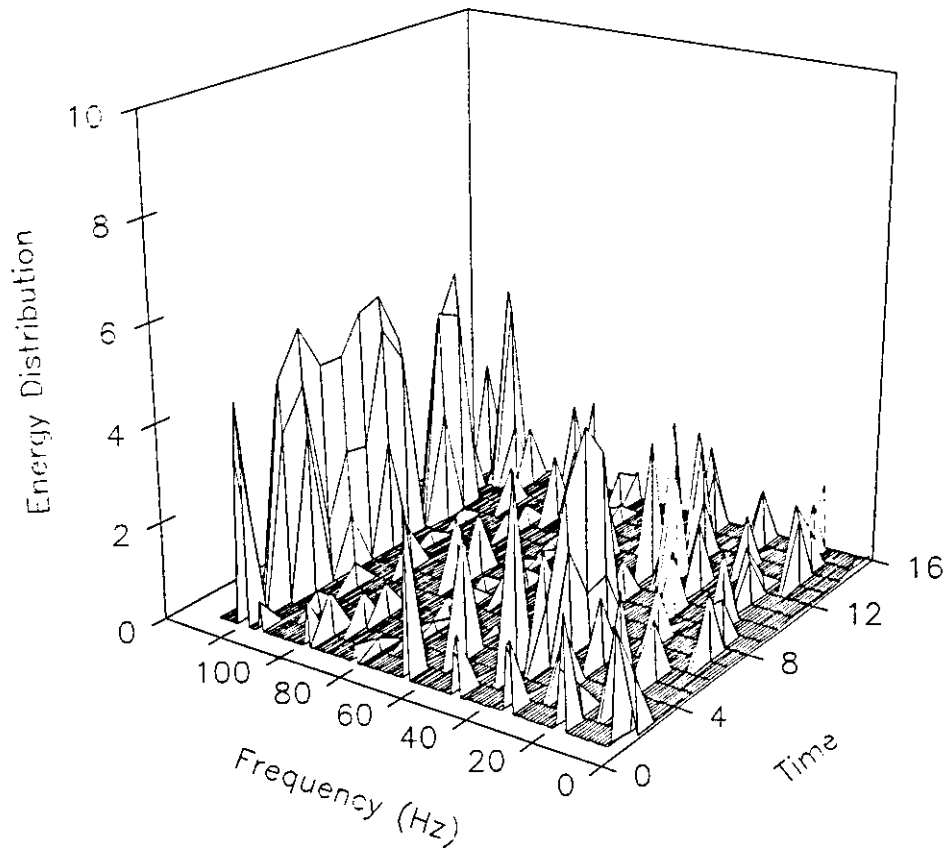


Figure (6.2) : The 3D-Gabor plot at a free stream velocity of 19.00m/s.

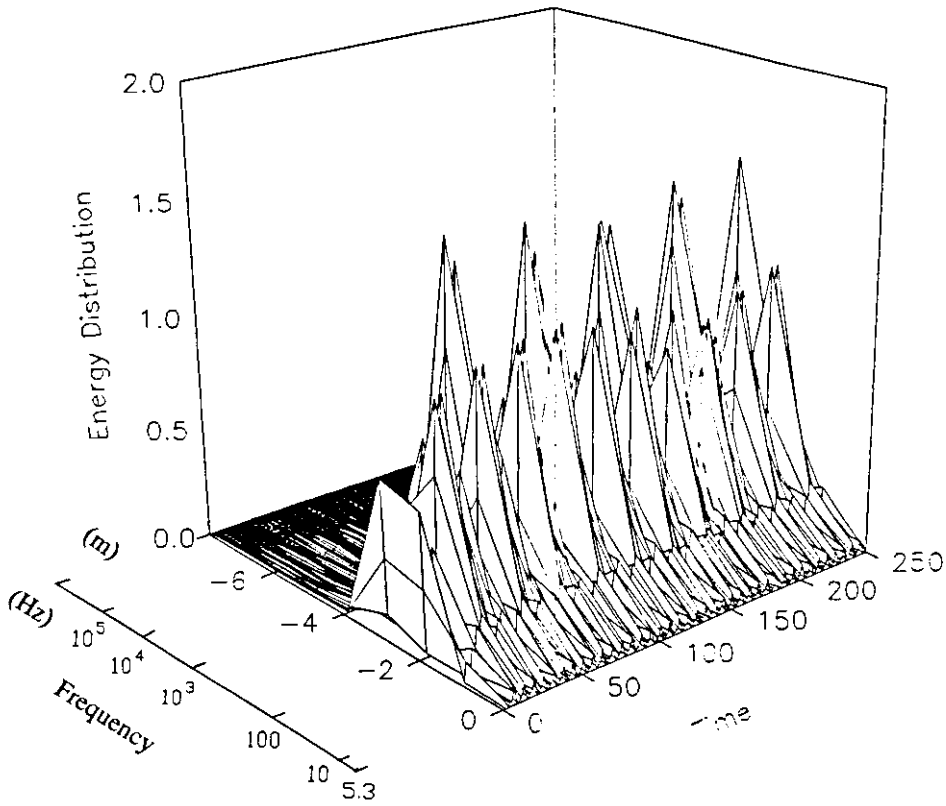


Figure (6.3) : The 3D-wavelet plot using the modulated Gaussian as a mother wavelet at a free stream velocity of 19.00m/s.

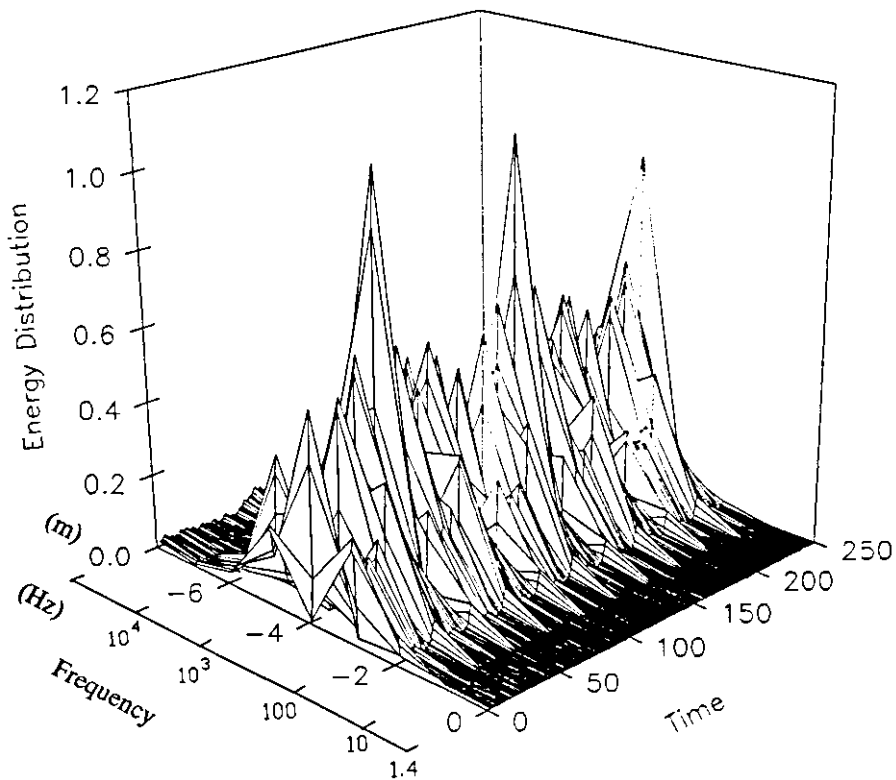


Figure (6.4) : The 3D-wavelet plot using the Mexican hat as a mother wavelet at a free stream velocity of 19.00m/s.

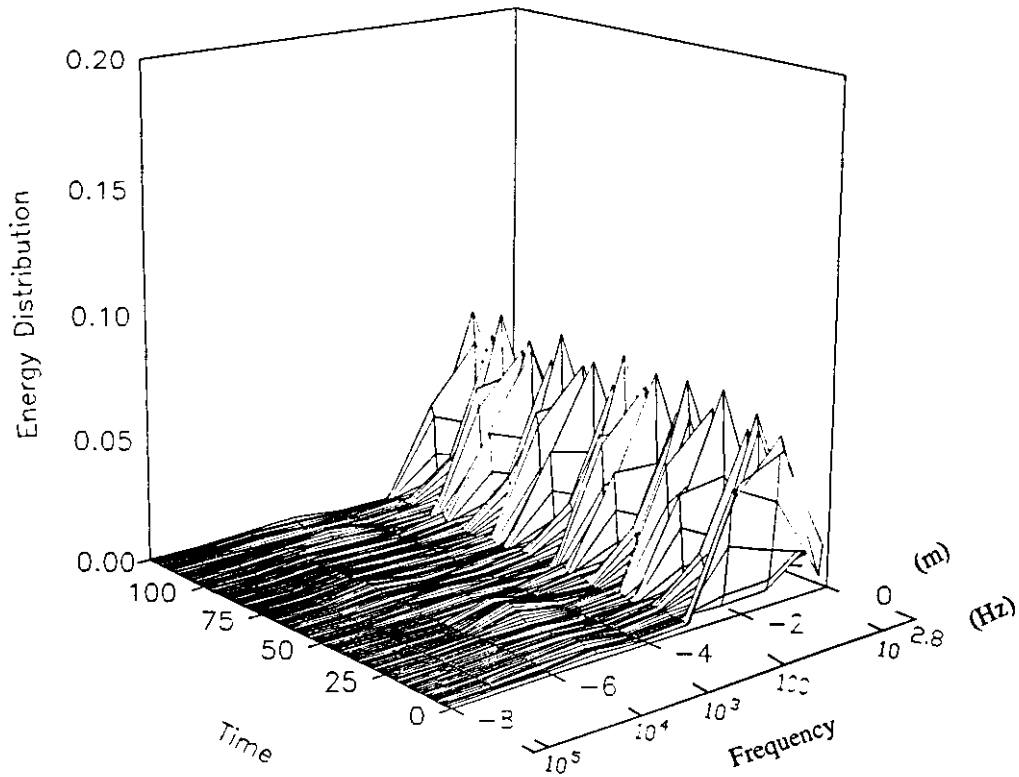


Figure (6.5) : The 3D-wavelet plot using the eighth derivative of the Gaussian as a mother wavelet at a free stream velocity of 19.00m/s.

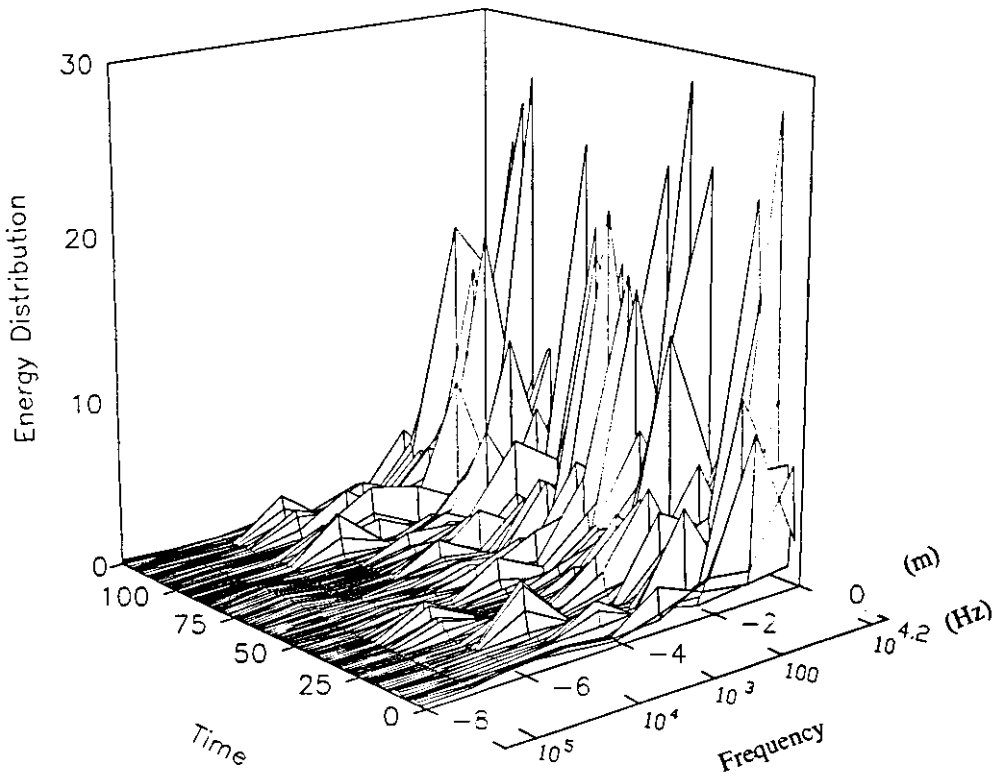


Figure (6.6) : The 3D-wavelet plot using Daubechies' tight frame as a mother wavelet at a free stream velocity of 19.00m/s.

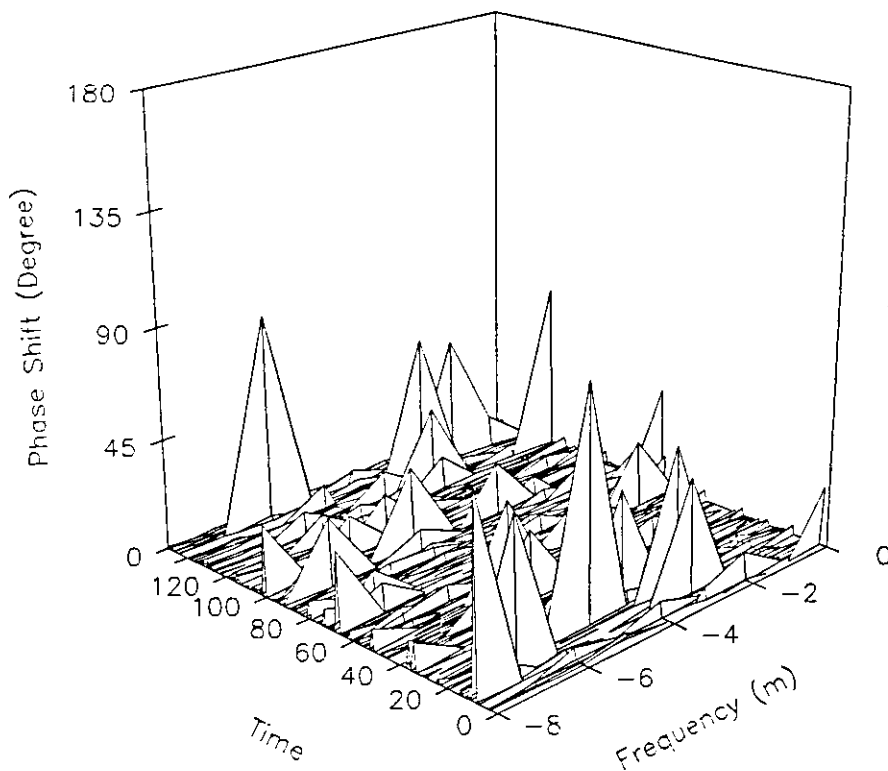


Figure (6.7) : The 3D-phase-plot of the wavelet on the range $(0-180^\circ)$ using the modulated Gaussian as a mother wavelet at a free stream velocity of 19.00m/s.

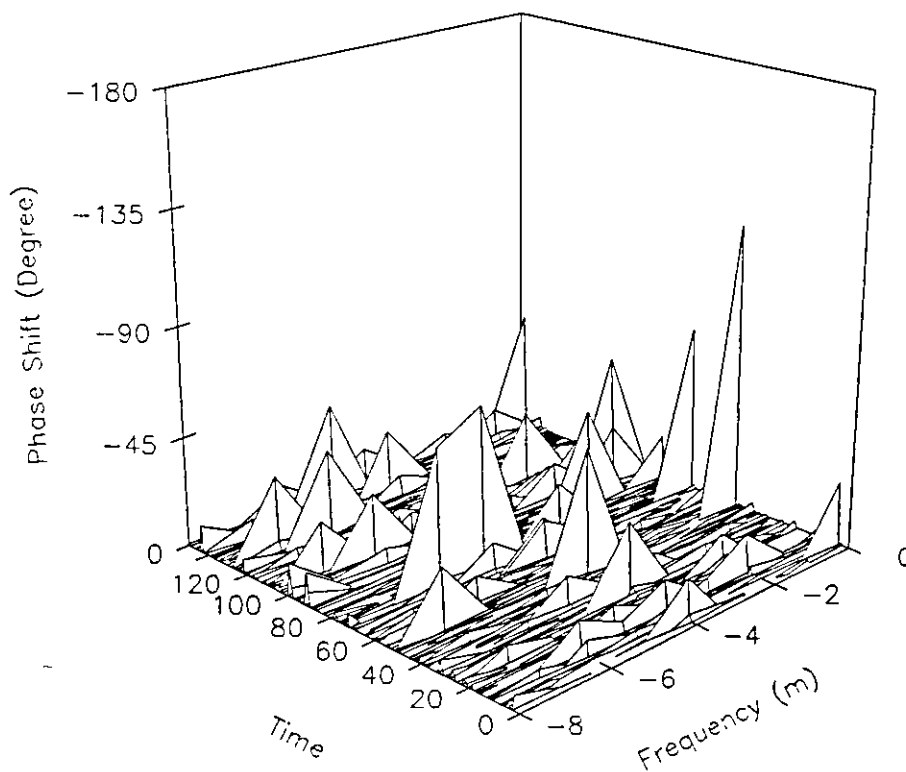


Figure (6.8) : The 3D-phase-plot of the wavelet on the range $(-180^\circ-0)$ using the modulated Gaussian as a mother wavelet at a free stream velocity of 19.00m/s.

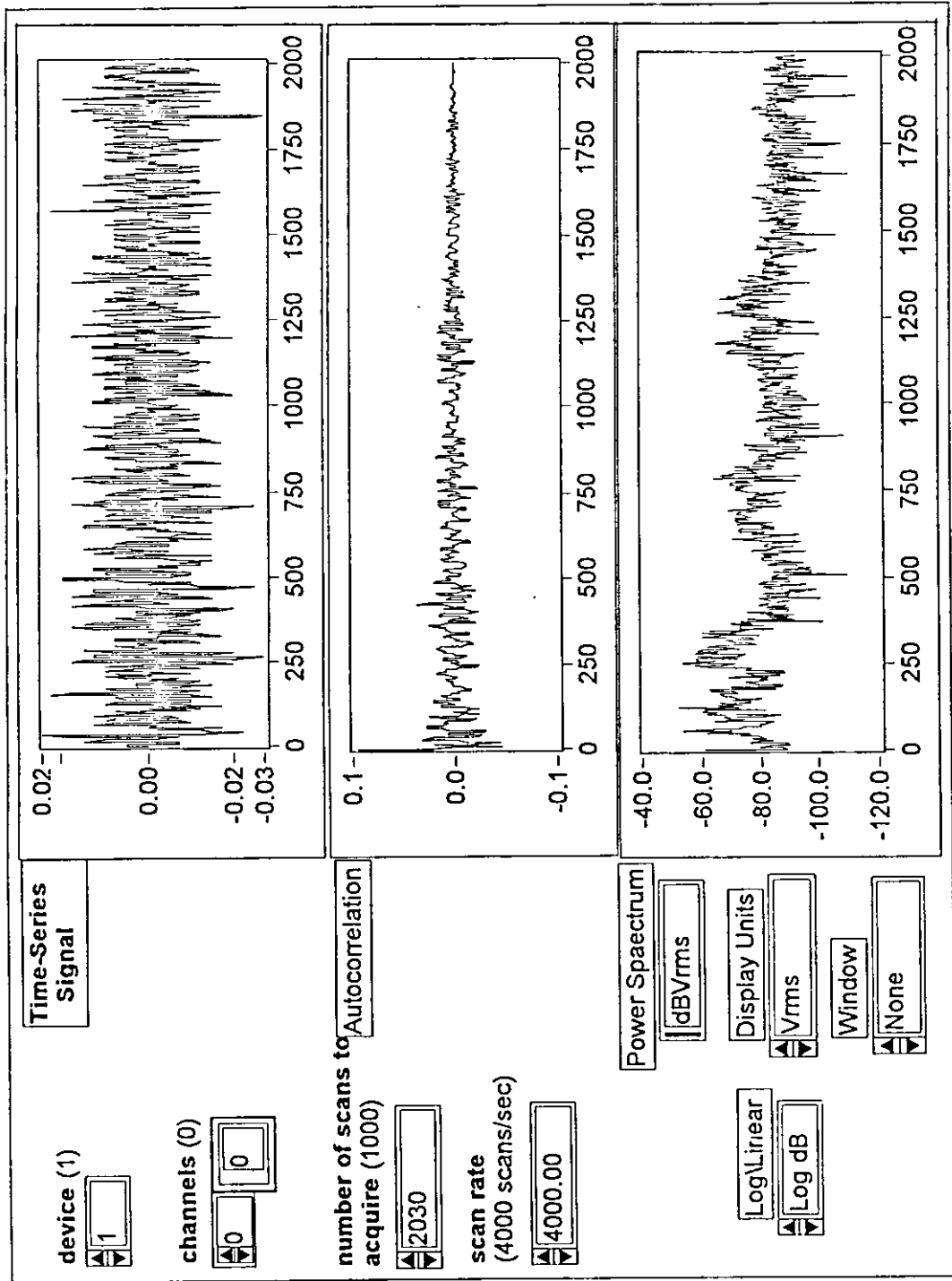


Figure (6.9) : The time series, the corresponding autocorrelation, and the corresponding power spectrum at a free stream velocity of 4.98m/s.

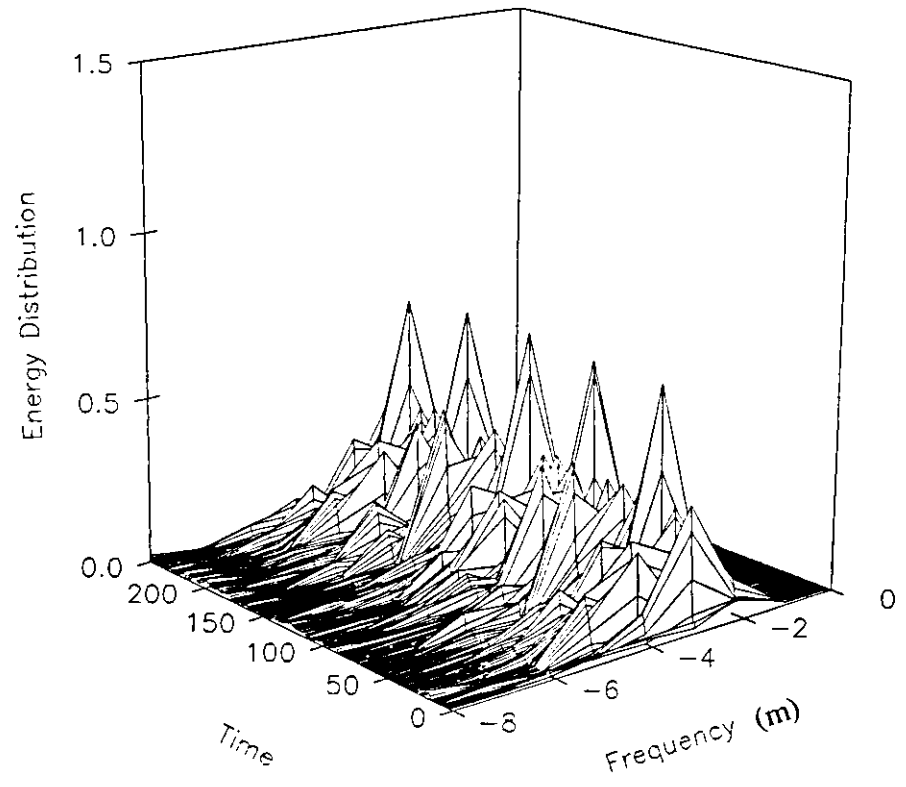


Figure (6.10) : The 3D-wavelet plot using the modulated Gaussian as a mother wavelet at a free stream velocity of 4.98m/s.

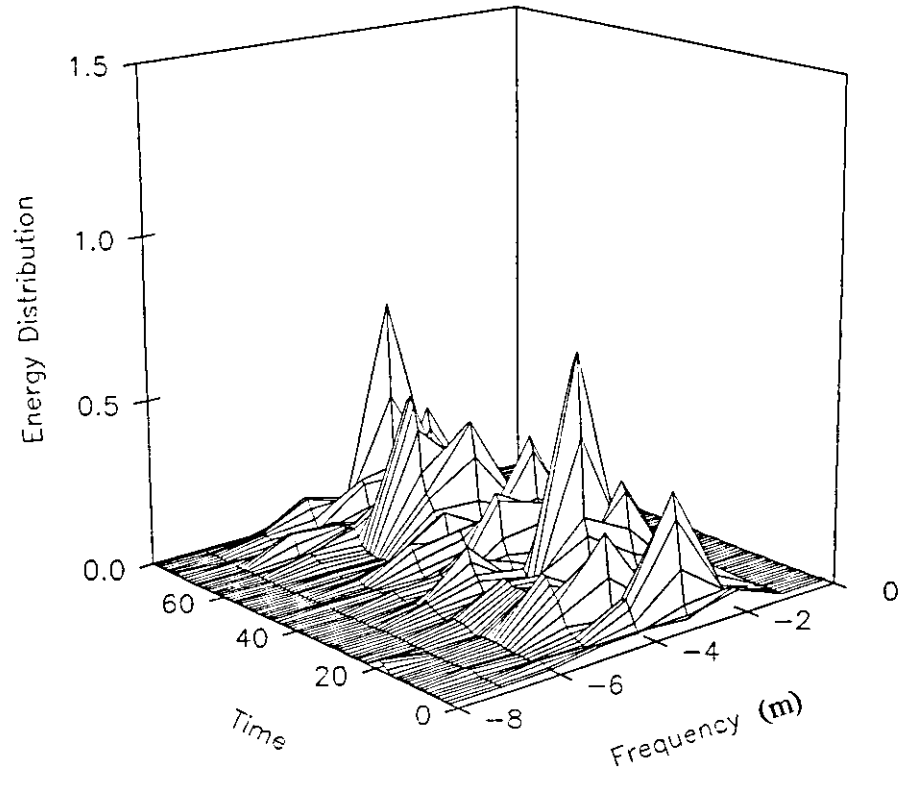


Figure (6.11) : Another view of Figure (6.10) using a shorter time scale.

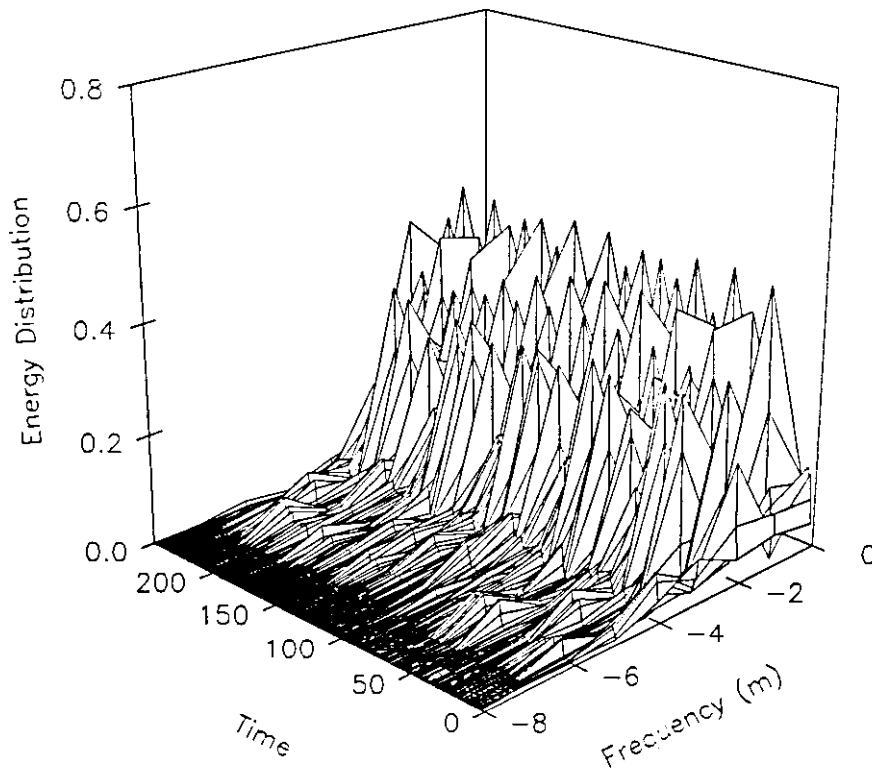


Figure (6.13) : The 3D-wavelet plot using the modulated Gaussian as a mother wavelet at a free stream velocity of 5.50m/s.

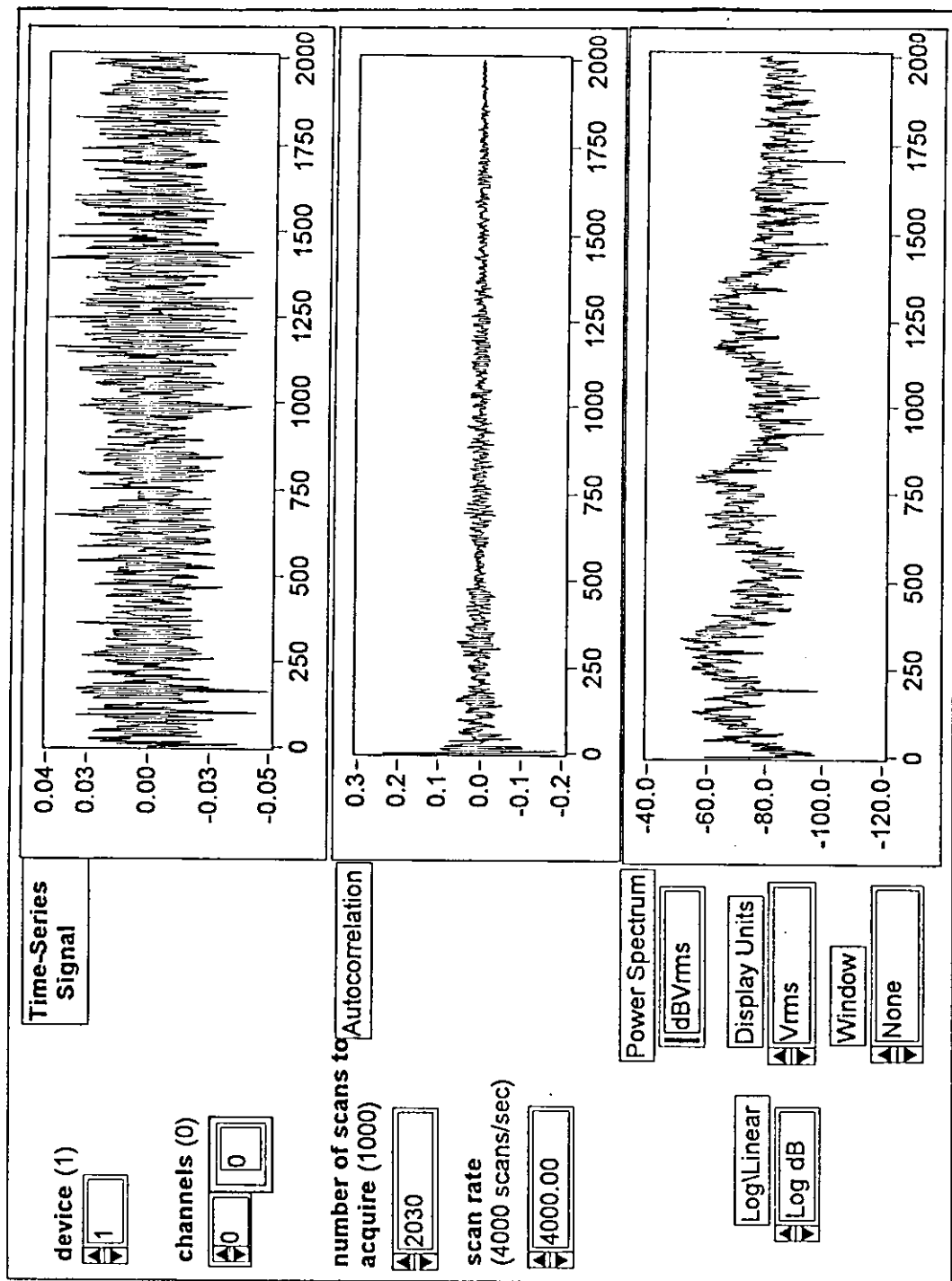


Figure (6.14) : The time series, the corresponding autocorrelation, and the corresponding power spectrum at a free stream velocity of 24.08m/s.

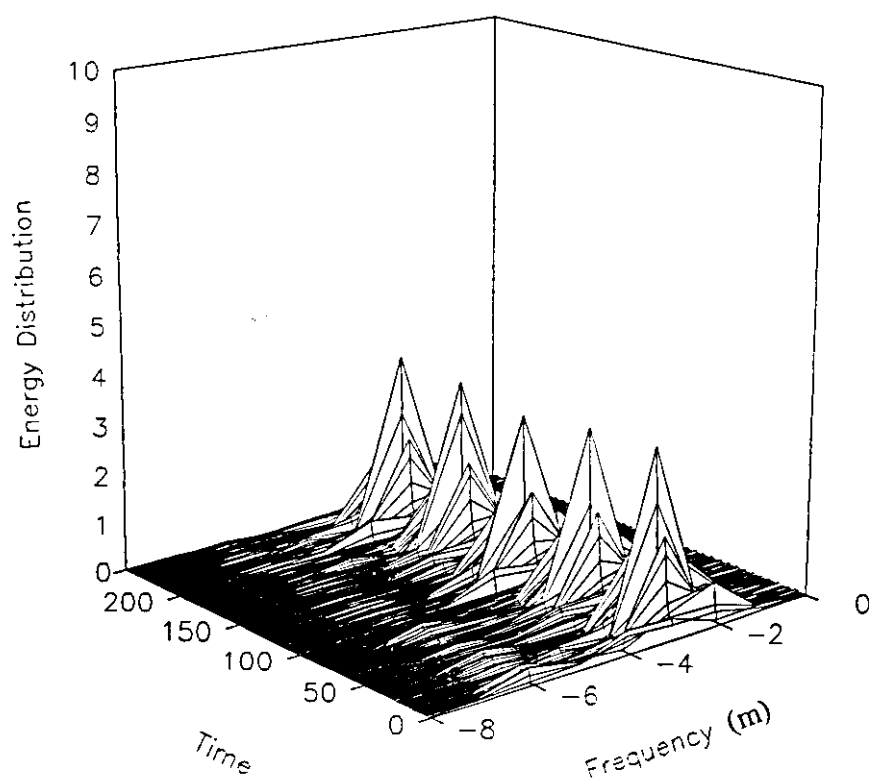


Figure (6.15) : The 3D-wavelet plot using the modulated Gaussian as a mother wavelet at a free stream velocity of 24.08m/s.

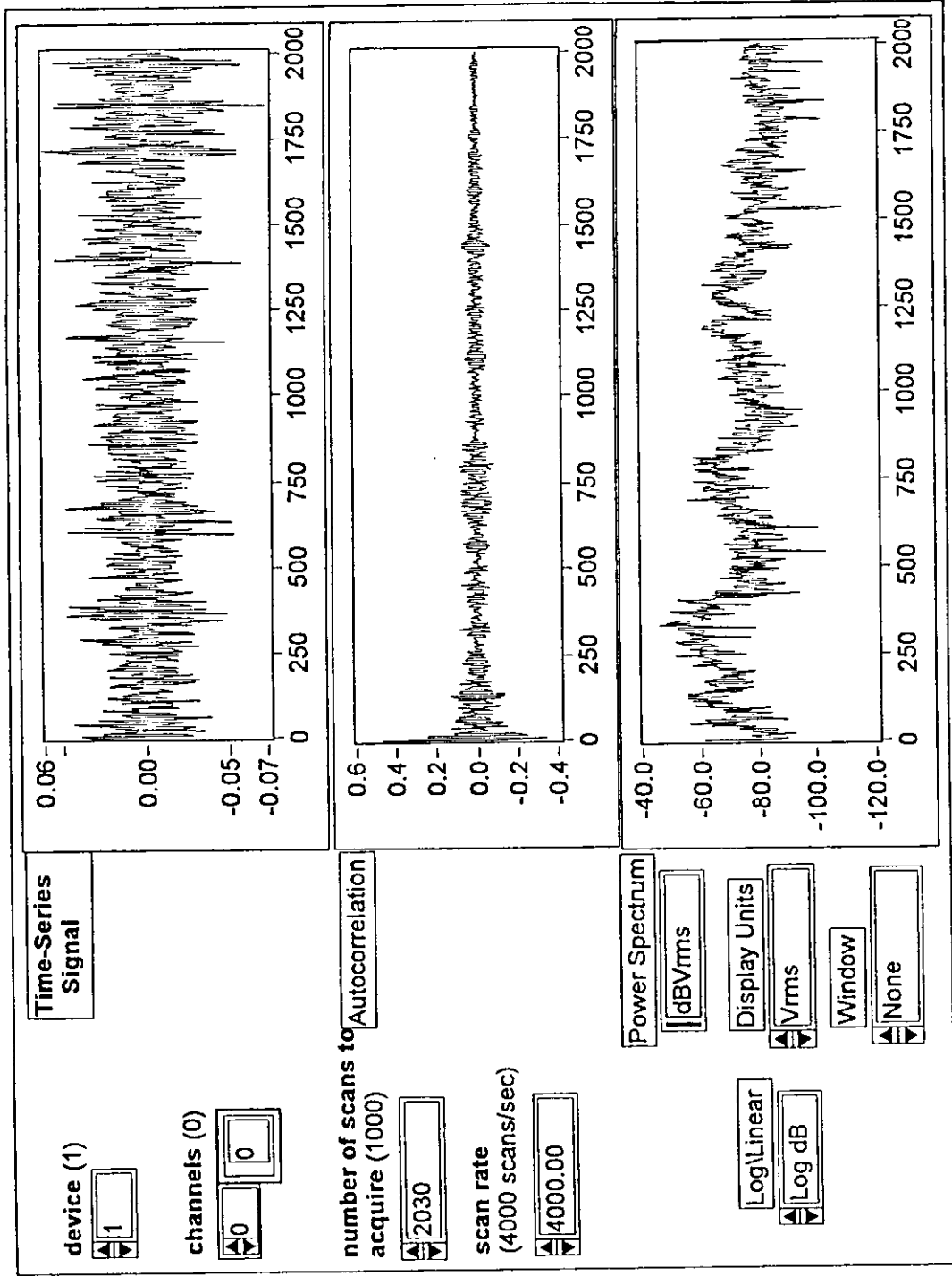


Figure (6.16) : The first time series, the corresponding autocorrelation, and the corresponding power spectrum at a free stream velocity of 26.00m/s.

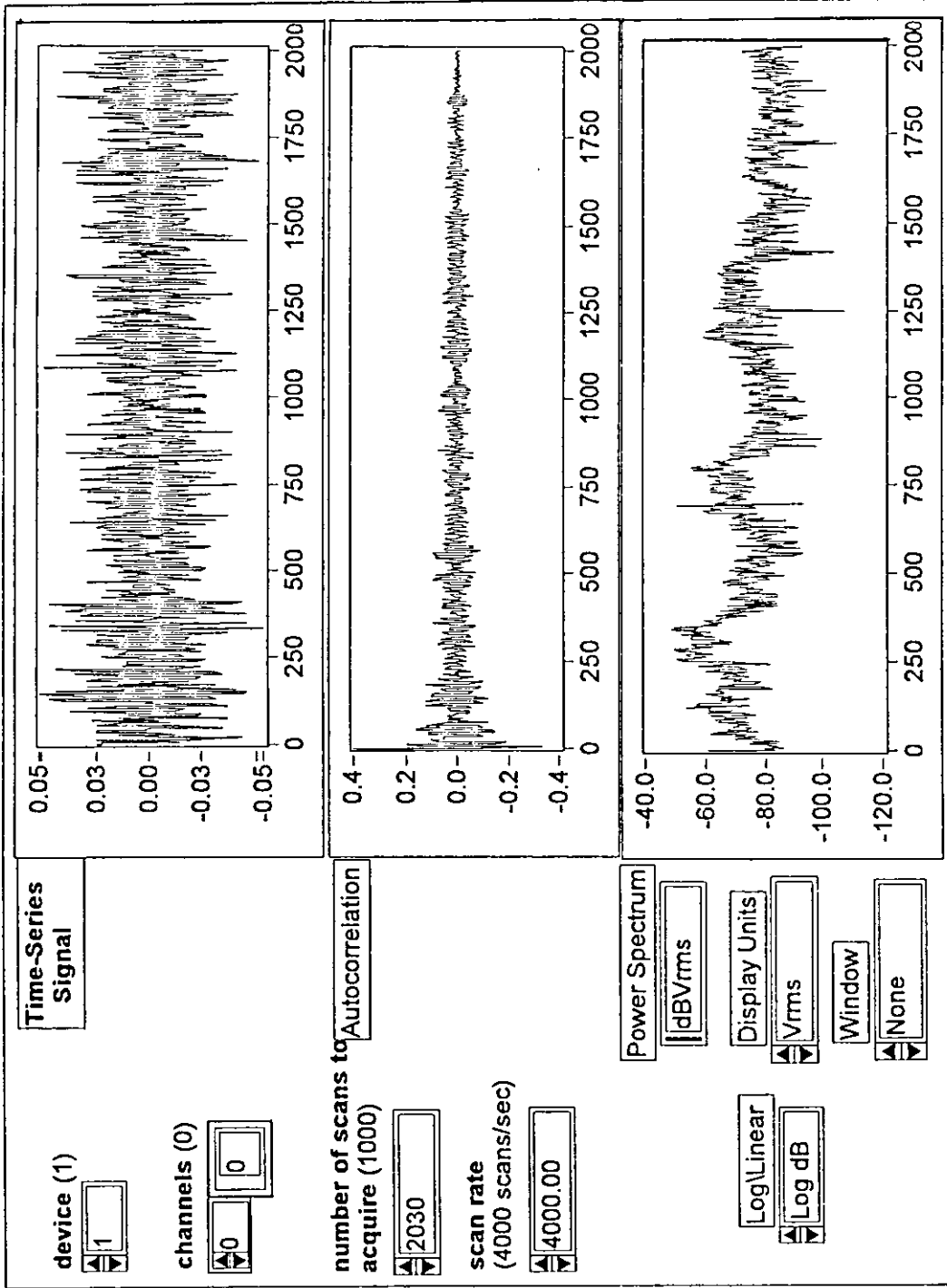


Figure (6.17) : The second time series, the corresponding autocorrelation, and the corresponding power spectrum at a free stream velocity of 26.00m/s.

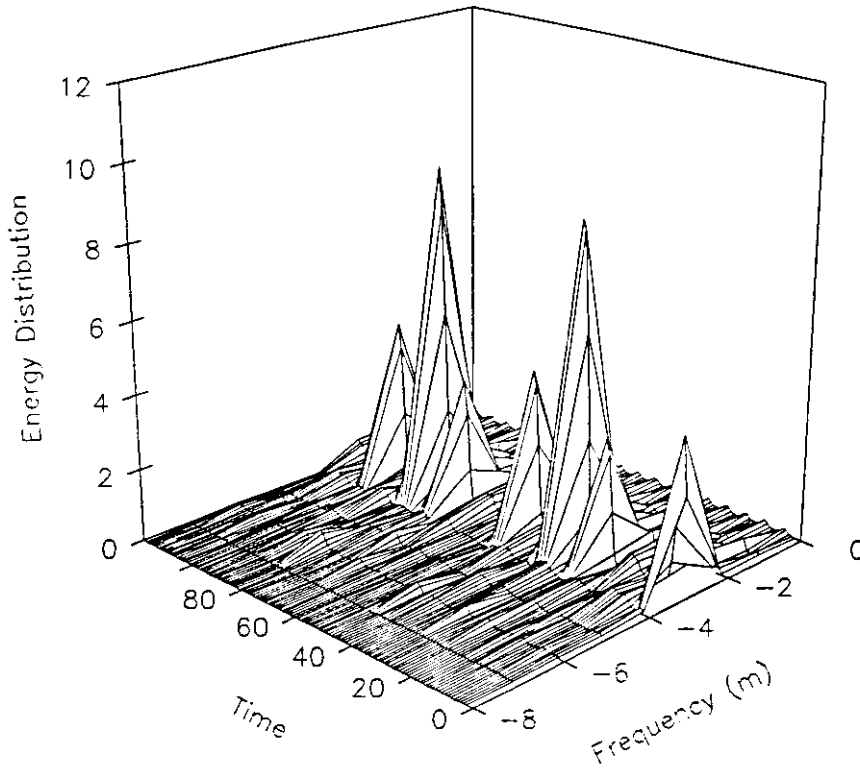


Figure (6.18) : The 3D-wavelet plot of the first time series using the modulated Gaussian as a mother wavelet at a free stream velocity of 26.00m/s.

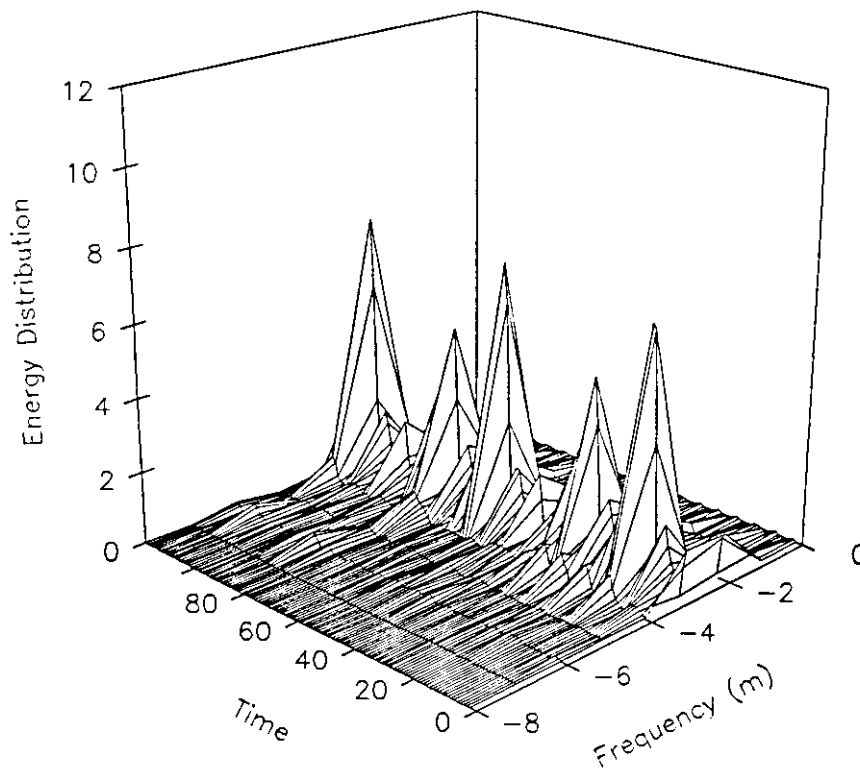


Figure (6.19) : The 3D-wavelet plot of the second time series using the modulated Gaussian as a mother wavelet at a free stream velocity of 26.00m/s.

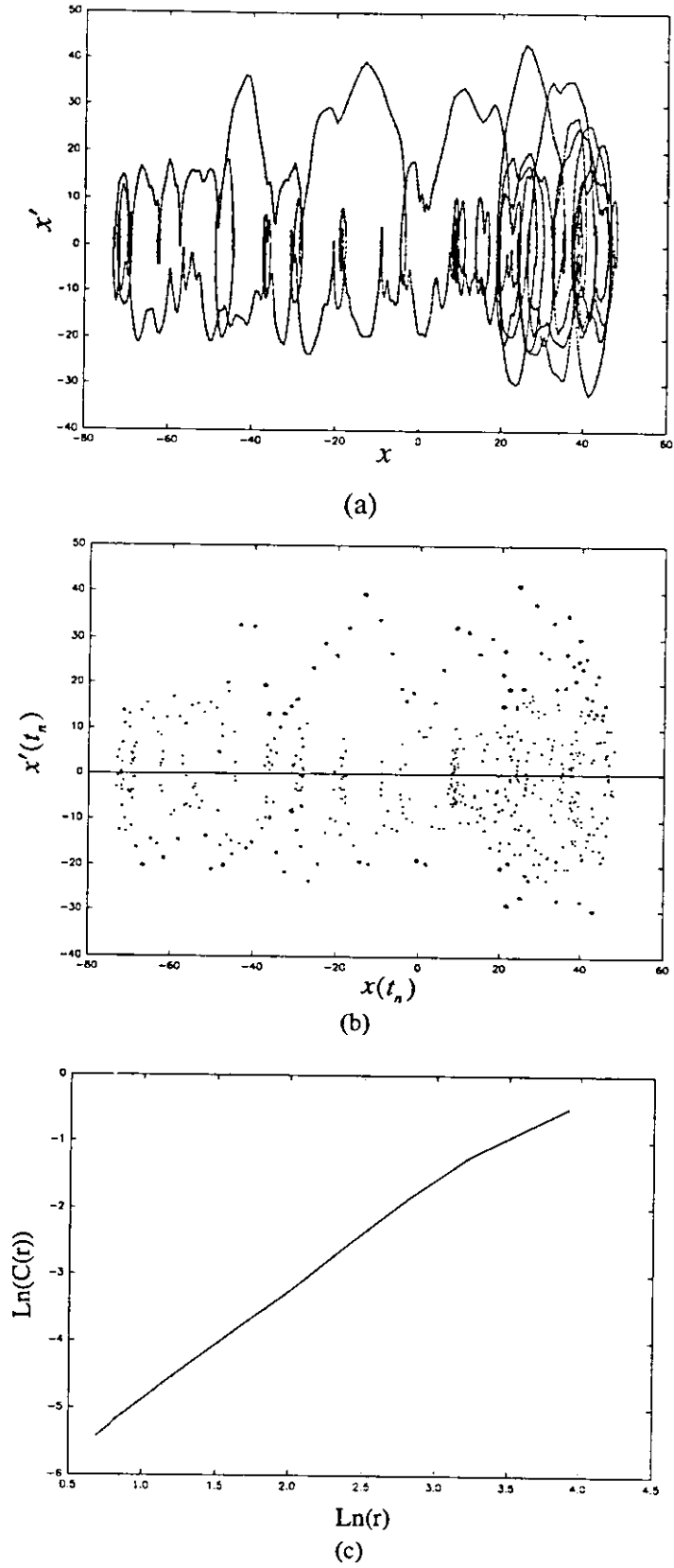


Figure (6.20) : (a) Phase plot, (b) Poincaré map, and (c) the D_2 correlation dimension factor at a free stream velocity of 4.98m/s.

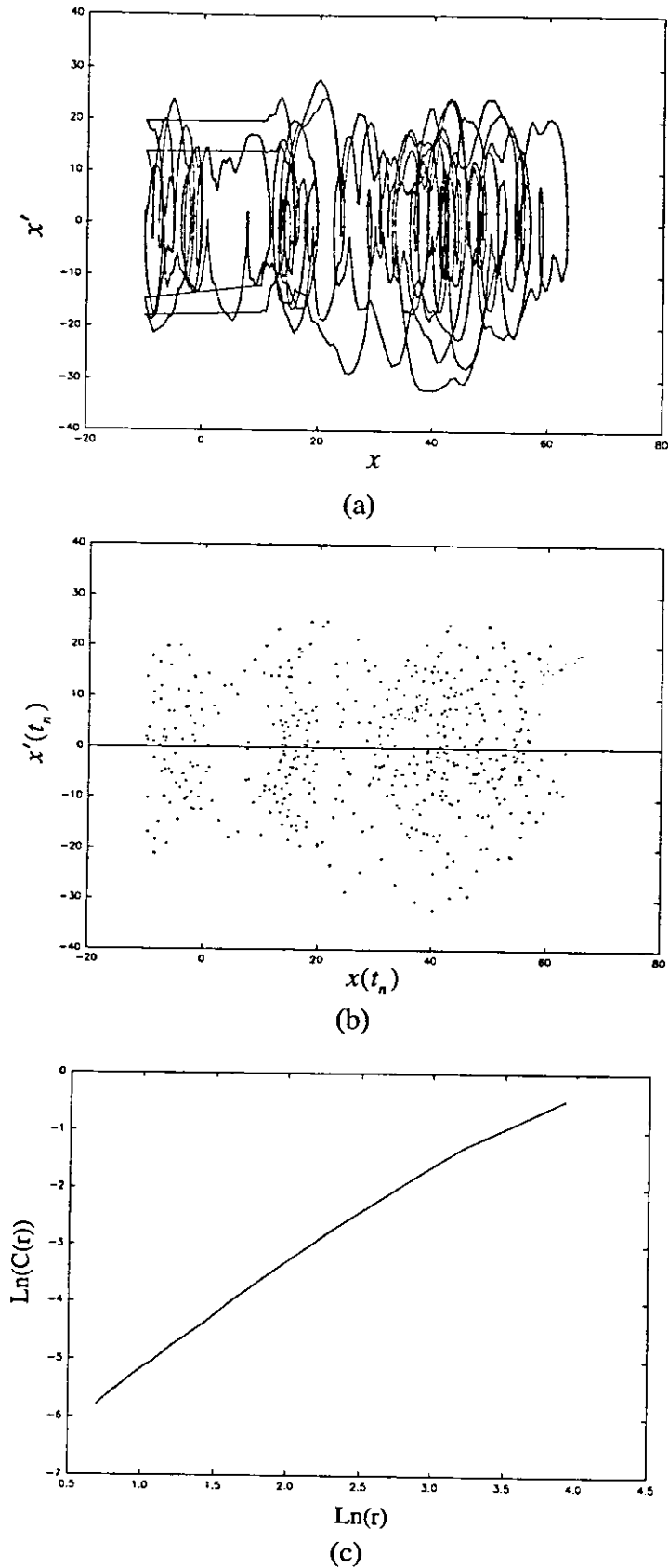


Figure (6.21) : (a) Phase plot, (b) Poincaré map, and (c) the D_2 correlation dimension factor at a free stream velocity of 5.50m/s.

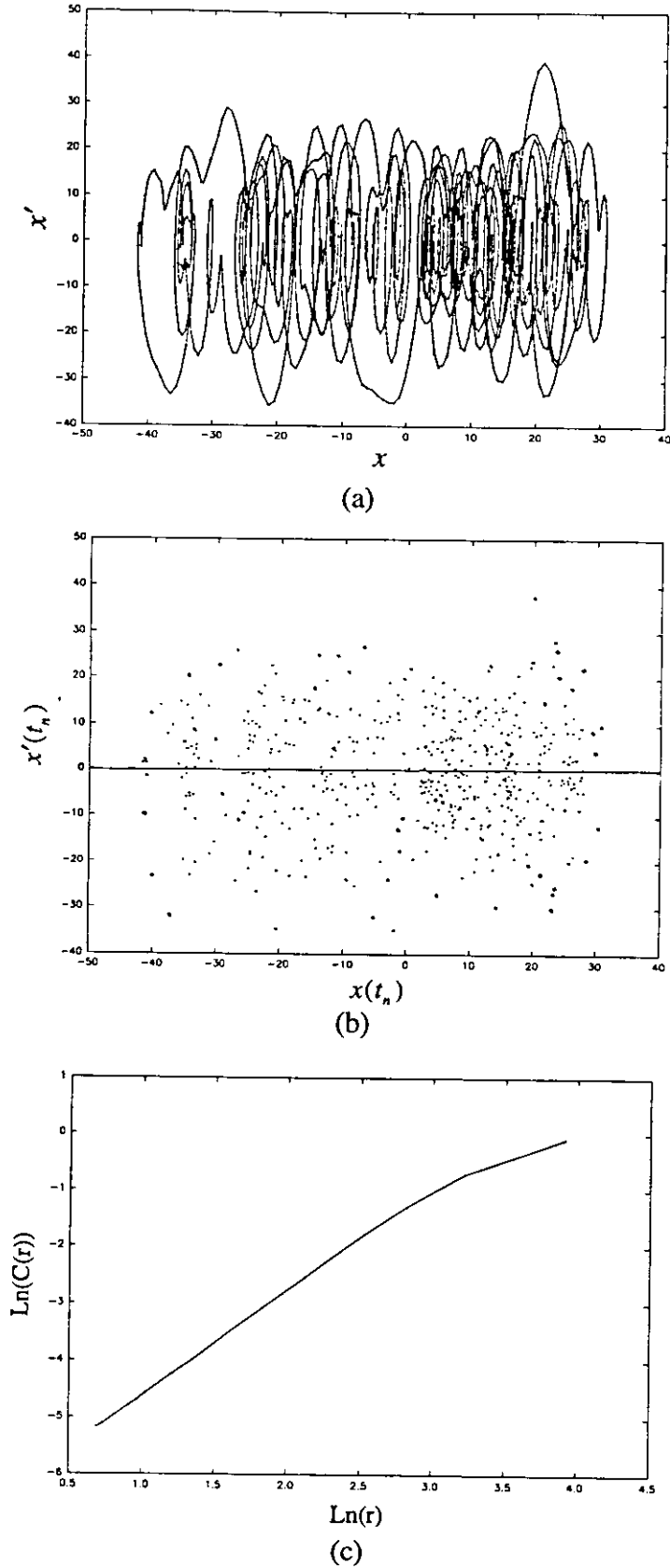


Figure (6.22) : (a) Phase plot, (b) Poincaré map, and (c) the D_2 correlation dimension factor at a free stream velocity of 19.00m/s.

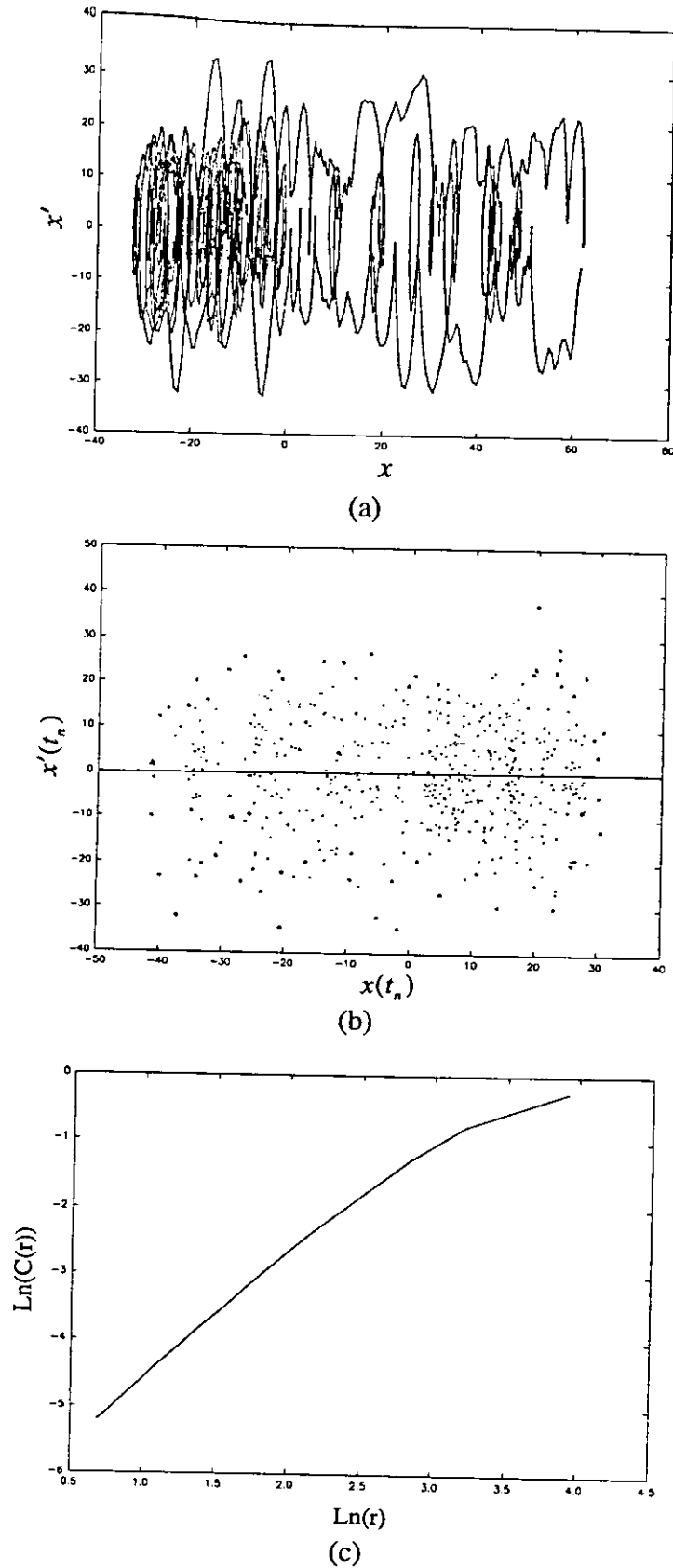


Figure (6.23) : (a) Phase plot, (b) Poincaré map, and (c) the D_2 correlation dimension factor at a free stream velocity of 24.08m/s.

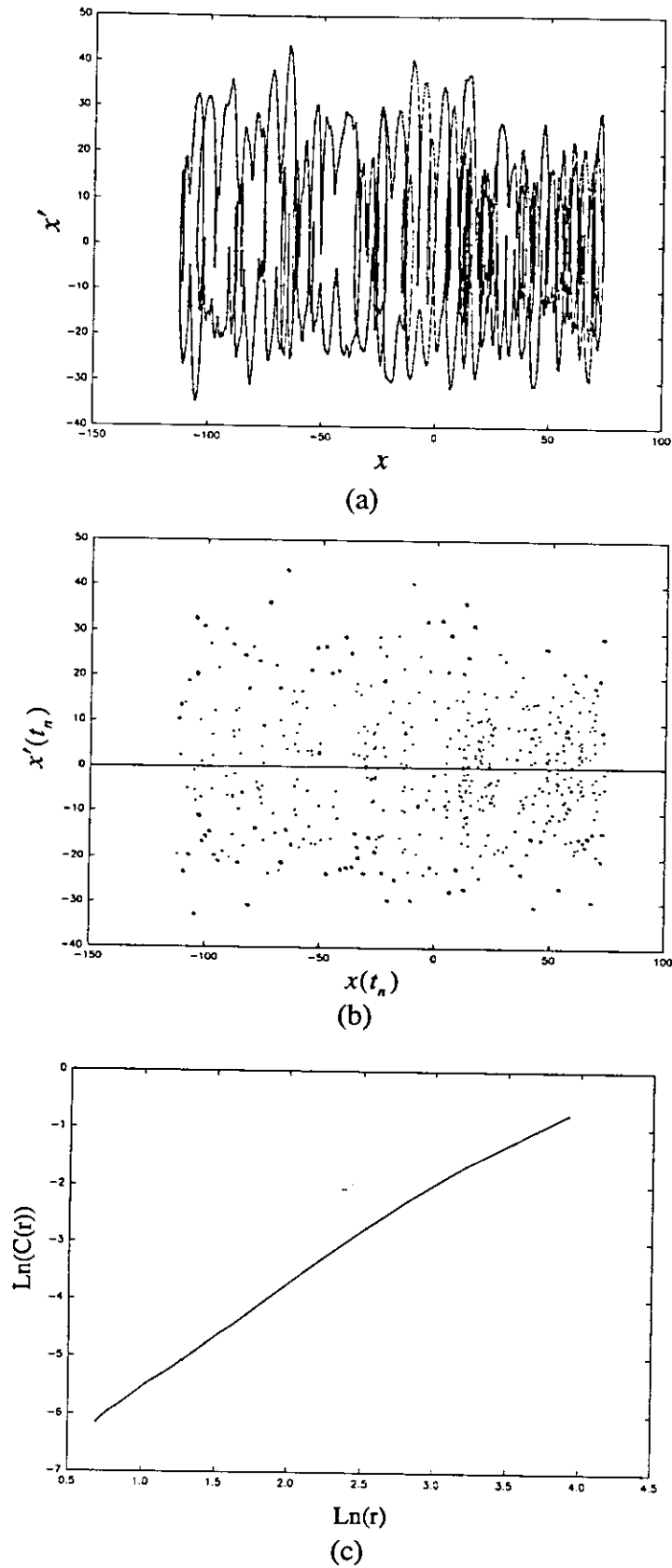


Figure (6.24) : (a) Phase plot, (b) Poincaré map, and (c) the D_2 correlation dimension factor at a free stream velocity of 26.00m/s.

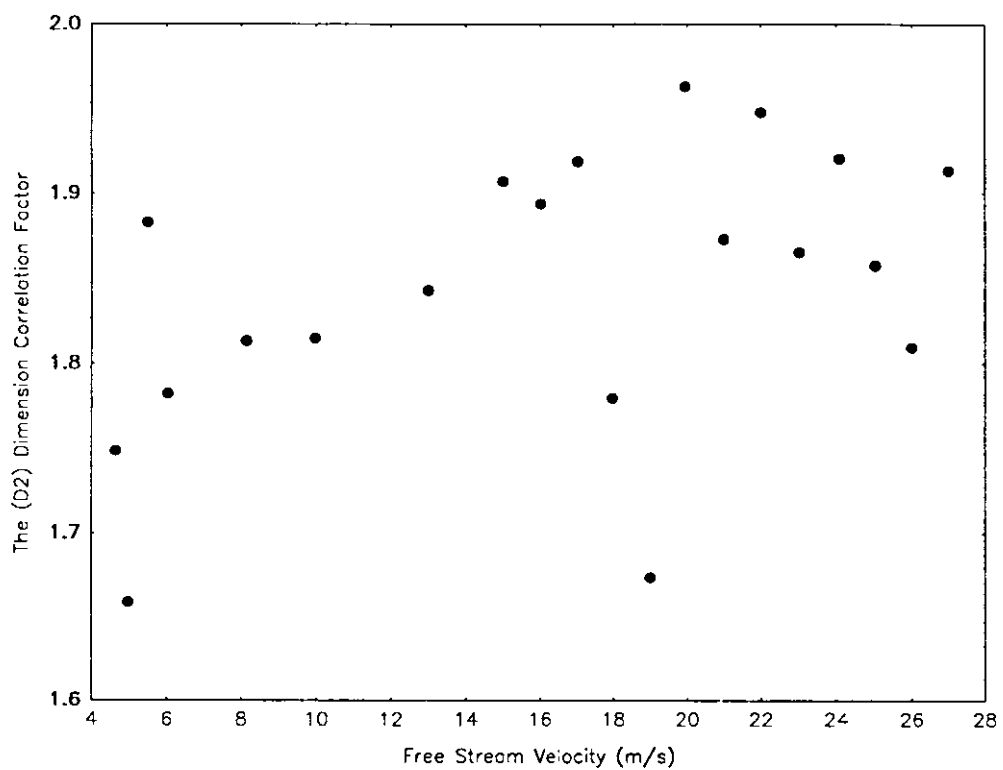


Figure (6.25) : The D_2 correlation dimension factor versus the free stream velocity.

CHAPTER 7

CONCLUSIONS & RECOMMENDATIONS

7.1 INTRODUCTION

This chapter summarizes the important points which have emerged from the present investigation, and outline areas which need further investigation.

7.2 CONCLUSIONS

Several points have emerged from the various techniques used to represent and analyze the flow induced vibration signals. These points can be outlined as follows.

1. As expected, the time series of the vibration (acceleration) of the elastically mounted circular cylinder in a cross flow viewed at different velocities appear completely random, with the possibility of being nonstationary.
2. The results of frequency analysis show that, in general, most of the energy is concentrated at three definite peaks, the fundamental, the third sub- and the third super-harmonics.
3. The classical methods are insufficient for a thorough investigation of the dynamic process under consideration and can lead to erroneous conclusions about the dynamic activities of the process.
4. The WT can be a powerful and efficient technique for joint time-frequency analysis if properly used, i.e. one should be aware of the properties of the particular wavelet used in a certain application.

5. Of the several wavelet tested in this work, the modulated Gaussian is found to give the most realistic results, when compared to those available in the literature using different signal analysis techniques.
6. A representation of only the amplitude of a complex wavelet is not enough to thoroughly investigate the singularities of the process, thus, one should also examine the phase which corresponds to the imaginary part of the complex wavelet function.
7. The Gabor transform, in addition of requiring a large computational facility than the WT for the same data record, does not seem to be adequate for the present relatively low frequency process.
8. For the particular free stream velocity values considered in this work, they are found mostly to be chaotic.
9. The order of harmonics excited in the results of the various frequency analyses suggests that the nonlinearity in the process is of the third type. This may be used in the formulation of a theoretical model for this process.
10. The WT is an efficient method in the analysis of chaotic signals as it can reveal more clearly than the classical methods the possible route to chaos and the way the various harmonics bifurcates to others as the process undergoes transitional chaotic behavior.
11. Among the classical chaotic techniques used, the phase-plans portraits and the Poincaré maps suggest the possibility of chaotic behavior. However, the fractal dimensions indicate the emergence of chaos, thus supporting the results obtained using the WT.

7.3 RECOMMENDATIONS

1. Other wavelet techniques, such as wavelet packets should be investigated for the capability of extracting information about the

- flow induced vibration phenomena. Also, the newly developed complex wavelet techniques such as, the harmonic wavelets, should be investigated.
2. The fractal dimension of the Poincaré map does not represent the fractal dimension of the dynamics of the process, because the Poincaré map represents only a two dimensional space, and the process under consideration may require more than two dimensional space to capture the qualitative features of the dynamics of the process. Thus, to describe the system properly one should take into account the number of degrees of freedom required to describe the system.
 3. A more realistic study requires consideration of longer time records, and thus requires much larger storage and computational capability of system used in this work.

REFERENCES

- [1] BLEVINS, R. D.: FLOW-INDUCED VIBRATION, VON-NOSTRAND REINHOLD, NEW YORK, 1977.
- [2] BISHOP, R. E. D. AND HASSAN, A. Y.: "THE LIFT AND DRAG FORCES ON A CIRCULAR CYLINDER," PROC. R. SOC., LONDON, SERIES A, VOL.277, 1964, PP.51-75.
- [3] KOOPMANN, G. H.: "THE VORTEX WAKES OF VIBRATING CYLINDERS AT LOW REYNOLDS NUMBERS," J. FLUID MECH., VOL.28, 1967, PP.501-512.
- [4] NEWLAND, D. E.: "WAVELET ANALYSIS OF VIBRATION, PART 1: THEORY," J. VIB. ACOUS., VOL.116, 1994, PP.409-416.
- [5] MALLAT, S. G.: "A THEORY FOR MULTIREOLUTION SIGNAL DECOMPOSITION: THE WAVELET REPRESENTATION," IEEE. TRANS. ON PATTERN ANALY. AND MACHINE INTELEGENCE., VOL.11, NO.7, 1989.
- [6] DAUBECHIES, I.: TEN LECTURES ON WAVELETS, 3RD ED., SIAM, SOCIETY FOR IND. AND APPL. MATH., 1994.
- [7] ARNEODO, A. AND GRASSEAU, G. : "WAVELET TRANSFORMS OF MULTIFRACTALS," PHYS. REV. LET., VOL.61, NO.20, 1988, PP. 2281-2284.
- [8] DAVID, P. M. AND CHARPON, B. : "UNDERWATER ACOUSTIC SIGNAL ANALYSIS WITH WAVELET PROCESS," J. ACOUST. SOC. AM., VOL.87, NO.5, 1989, PP. 2118-2121.
- [9] NEWLAND D. E.: "WAVELET ANALYSIS OF VIBRATION, PART 2: WAVELET MAPS," J. VIB. ACOUS., VOL.116, 1994, PP.417-425.
- [10] GROSSMAN, R., HOLSCHNEIDER, M., KRONLAND-MARTINENT, R. AND MORLET, J.: "DETECTION OF ABRUPT CHANGES IN THE SOUND SIGNALS WITH THE HELP OF WAVELET TRANSFORMS, IN INVERSE PROBLEMS: AN INTERDISCIPLINARY STUDY," ADVANCES IN ELECTRONICS AND ELECTRON PHYSICS, SUPPLEMENT 19, ACADEMIC PRESS, NEW YORK, 1987, PP.298-306.
- [11] SEKAR, P. AND NARAYANAN, S.: "PERIODIC AND CHAOTIC MOTIONS IF A SQUARE PRISM IN CROSS-FLOW," J. SOUND AND VIB., VOL.170, NO.1, 1994, PP.1-24.
- [12] LI, G. X. AND PAIDOUSSIS, M. P.: "STABILITY, DOUBLE DEGENERACY AND CHAOS IN CANTILEVERED PIPES

- CONVEYING FLUID," INT. J. NON-LINEAR MECH., VOL.29, NO.1,1994, PP.83-107.
- [13]ABU-SAMAK, M.: "THE WAVELET TRANSFORM ANALYSES OF FLOW-INDUCED VIBRATION PHENOMENON," M.SC. THESIS, UNIVERSITY OF JORDAN, AMMAN, JORDAN, 1994.
- [14]FILLER, J. R., MARSTON, P. L. AND MIH, W. C.: "RESPONSE OF THE SHEAR LAYERS SEPARATING FROM A CIRCULAR CYLINDER TO SMALL AMPLITUDE ROTATIONAL OSCILLATION," J. FLUID MECH., VOL. 231, 1991, PP. 481-499.
- [15]TOKUMARU, P. T. AND DIMOTAKIS, P. E.: "ROTARY OSCILLATION CONTROL OF A CYLINDER WAKE," J. FLUID MECH., VOL. 224, 1991, PP. 77-90.
- [16]ANAGNOSTOPOULOS, P. AND BEARMAN, P.: "RESPONSE CHARACTERISTICS OF A VORTEX-EXCITED CYLINDER AT A LOW REYNOLDS NUMBERS," J. FLUID AND STRUCTURE, VOL. 6, 1992, PP. 39-50.
- [17]BOKAIAN, A.: "GALLOPING OF A CIRCULAR IN THE WAKE OF ANOTHER," J. SOUND AND VIBRATION, VOL. 128(1), 1989, PP. 71-85.
- [18]BEARMAN, P. W.: "VORTEX SHEDDING FROM OSCILLATING BLUFF BODIES," ANN. REV. FLUID MECH., VOL. 6, 1984, PP. 195-222.
- [19]ROSHKO, A.: "ON THE DRAG AND SHEDDING FREQUENCY OF TWO-DIMENSIONAL BLUFF BODIES," NAT. ADV. COMM. FOR AERO., WASHINGTON, DC, TECHNICAL NOTE 3169, 1954.
- [20]ROSHKO, A.: "ON THE WAKE AND DRAG OF BLUFF BODIES," J. AERO. SCI., VOL. 22, 1955, PP. 124-132.
- [21]GERRARD, J. H.: "THE MECHANICS OF THE FORMATION REGION OF VORTICES BEHIND BLUFF BODIES," J. FLUID MECH., VOL. 25, 1966, PP. 401-413.
- [22]BEARMAN, P. W.: "INVESTIGATION OF THE FLOW BEHIND A TWO DIMENSIONAL MODEL WITH A BLUNT TRAILING EDGE AND FITTED WITH SPLITTER PLATES," J. FLUID MECH., VOL. 21, PP. 241-255, 1965.
- [23]BEARMAN, P. W.: "ON VORTEX STREET WAKES," J. FLUID MECH., VOL. 28, 1967, PP. 625-641.

- [24]UNAL, M. F. AND ROCKWELL, D.: "ON VORTEX FORMATION FROM A CYLINDER. PART 1. THE INITIAL INSTABILITY," J. FLUID MECH., VOL. 190, 1988, PP. 491-512.
- [25]UNAL, M. F. AND ROCKWELL, D.: "ON VORTEX FORMATION FROM A CYLINDER. PART 2. CONTROL BY SPLITTER PLATE INTERFERENCE," J. FLUID MECH., VOL. 190, 1988, PP.513-529.
- [26]WILLIAMSON, C. H. K. AND ROSHKO, A.: "VORTEX FORMATION IN THE WAKE OF AN OSCILLATING CYLINDER," J. FLUIDS STRUCT., VOL.2, 1988, PP.350-381.
- [27]GRIFFIN, O. M. AND HALL, M. S.: "REVIEW- VORTEX SHEDDING LOCK-ON AND FLOW CONTROL IN BLUFF BODY WAKES," TRANS. OF ASME, J. FLUID ENG., VOL.113, 1991, PP.526-537.
- [28]BAYLAC, G., BAI, D. AND GREGOIRE, J. P.: "STUDY OF ACOUSTIC PHENOMENA IN A TUBE BANK," PROC. OF THE INTER. SYMPOSIUM ON VIB. PROBLEMS IN INDUSTRY, KESWICK, ENGLAND, U.K. ATOMIC ENERGY AUTHORITY, NO. 219, 1973.
- [29]U.S. SENATE COMMITTEE ON ARMED SERVICES PREPAREDNESS INVESTIGATING SUBCOMMITTEE: "INQUIRY INTO THE COLLAPSE OF TEXAS TOWER NO. 4," 87TH CONGRESS CONF., FIRST SESSION, MAY 1961.
- [30]SARPKAYA, T.: "VORTEX INDUCED OSCILLATIONS: A SELECTIVE REVIEW," ASME J. APPLIED MECH., VOL.46, 1979, PP.241-258.
- [31]GRIFFIN, O. M.: "FLOW SIMILITUDE AND VORTEX LOCK-ON IN BLUFF BODY NEAR-WAKES," PHYS. FLUID A., VOL.1 1989, PP.697-703,.
- [32]GRIFFIN, O. M. AND RAMBERG, S. E.: "THE VORTEX-STREET WAKES OF VIBRATING CYLINDER," J. FLUID MECH., VOL.66, 1974, PP.553-576.
- [33]GRIFFIN, O. M., SKOP, R. A. AND KOOPMAN, G. H.: "THE VORTEX-EXCITED RESONANT VIBRATIONS OF CIRCULAR CYLINDER," J. SOUND AND VIB., VOL.31, 1973, PP.235-249.
- [34]BEARMAN, P. W.: "SOME MEASUREMENTS OF THE DISTORTION OF TURBULENCE APPROACHING A TWO-DIMENSIONAL BLUFF BODY," J. FLUID MECHANICS, VOL.53, 1972, PP.451-467.

- [35] BERGER, E.: "ON A MECHANISM OF VORTEX EXCITED CYLINDER," J. WIND ENG. AND IND. AERODYNAMICS, VOL.28, 1988, PP.301-310.
- [36] FARELL, C. AND BLESSMAN, J.: "ON CRITICAL FLOW AROUND SMOOTH CIRCULAR CYLINDERS," J. FLUID MECH., VOL.136, 1983, PP.375-391.
- [37] BISHOP, R. D. AND HASSAN, A. Y.: "THE LIFT AND DRAG FORCES ON A CIRCULAR CYLINDER IN FLOWING FLUID," PROCEEDINGS OF THE ROYAL SOCIETY, LONDON, SERIES A, VOL.277, 1964, PP.32-50.
- [38] TRIANTAFYLLOU, G., KUPFER, K. AND BERS, A.: "ABSOLUTE INSTABILITIES AND SELF-SUSTAINED OSCILLATIONS IN THE WAKES OF CIRCULAR CYLINDERS," PHYS. REV. LET., VOL.59, 1987, PP.1914-1917.
- [39] OERTEL, A.: "WAKES BEHIND BLUFF BODIES," ANN. REV. FLUID MECH., VOL.22, 1990, PP.539-564.
- [40] HUERRE, P. AND MONKEWITZ, P.: "LOCAL AND GLOBAL INSTABILITIES IN SPATIALLY DEVELOPING FLOWS," ANN. REV. FLUID MECH., VOL.22, 1990, PP.476-537.
- [41] MORKOVIN, M. V.: "FLOW AROUND CIRCULAR CYLINDERS. A KALEIDOSCOPE OF CHALLENGING FLUID PHENOMENA," ASME SYMPOSIUM ON FULLY SEPARATED FLOWS, ASME, NEW YORK, 1964.
- [42] GRIFFIN, O. M.: "A UNIVERSAL STROUHAL NUMBER FOR THE LOCKING-ON OF VORTEX SHEDDING TO THE VIBRATIONS OF BLUFF CYLINDERS," J. FLUID MECH., VOL.85, 1978, PP.591-606.
- [43] GRIFFIN, O. M. AND RAMBERG, S. E.: "VORTEX SHEDDING FROM A CYLINDER VIBRATING IN LINE WITH AN INCIDENT UNIFORM FLOW," J. FLUID MECH., VOL.75, 1976, PP.257-271.
- [44] IWAN, W. D. AND BLEVINS, R. D.: "A MODEL FOR VORTEX INDUCED OSCILLATION OF STRUCTURES," TRANS. OF ASME, J. APPLIED MECH., 1974, PP.581-586.
- [45] HOWELL, J. F. AND NOVEK, M.: "VORTEX SHEDDING CIRCULAR CYLINDERS IN TURBULENT FLOW," WIND ENG. PROCEEDINGS OF THE FIFTH INT. CONF. FOR COLINSE. COLORADO, U.S.A, VOL.2, 1979, PP.619-631.

- [46]ROCKWELL, D.: "ACTIVE CONTROL OF GLOBALLY-UNSTABLE SEPARATED FLOWS," PROC. ASME INT. SYMPOSIUM ON NONSTEADY FLUID DYNAMICS, FED, VOL.92, 1990, PP.379-394.
- [47]NAKAGAWA, T.: "A FORMATION MECHANISM OF ALTERNATING VORTICES BEHIND A CIRCULAR CYLINDER AT HIGH REYNOLDS NUMBER," J. WIND ENG. AND IND. AERODYNAMICS, VOL.25, 1986, PP.113-129.
- [48]HUERRE, P. AND MONKEWITZ, P. A.: "ABSOLUTE AND CONVECTIVE INSTABILITIES IN FREE SHEAR LAYERS," J. FLUID MECH., VOL.159, 1985, PP.151-168.
- [49]KOCH, W.: "LOCAL INSTABILITY CHARACTERISTICS AND FREQUENCY DETERMINATION OF SELF-EXCITED WAKE FLOWS," J. SOUND AND VIB., VOL.99, 1985, PP.53-83.
- [50]MONKEWITZ, P. A. AND NGUYEN, L. N.: "ABSOLUTE INSTABILITY IN THE NEAR WAKE OF THREE DIMENSIONAL BLUFF BODIES," J. FLUID STRUCT., VOL.1, 1987, PP.165-184.
- [51]TRIANTAFYLLOU, G. S., TRIANTAFYLLOU, M. S. AND CHRYSOSTOMODIS, C.: "ON THE FORMATION OF VORTEX STREETS BEHIND CIRCULAR CYLINDERS," J. FLUID MECH., VOL.170, 1986, PP.461-477.
- [52]MONKEWITZ, P. A.: "THE ABSOLUTE AND CONVECTIVE NATURE OF INSTABILITY IN TWO DIMENSIONAL WAKES AT LOW REYNOLDS NUMBER," PHYS. FLUIDS, VOL.31, 1988, PP.999-1006.
- [53]CHOMAZ, J. M., HUERRE, P. AND REDEKOPP, L. T.: "BIFURCATIONS TO LOCAL AND GLOBAL MODES IN SPATIALLY DEVELOPING FLOWS," PHYS. REV. LETT., VOL.60, 1988, PP.25-28.
- [54]ONGOREN, A. AND ROCKWELL, D.: "FLOW STRUCTURE FROM AN OSCILLATING CYLINDER. PART 1. MECHANISMS OF PHASE SHIFT AND RECOVERY OF THE NEAR WAKE," J. FLUID MECH., VOL.191, 1988, PP.197-223.
- [55]ONGOREN, A. AND ROCKWELL, D.: "FLOW STRUCTURE FROM AN OSCILLATING CYLINDER. PART 2. LOAD COMPETITION IN THE NEAR WAKE," J. FLUID MECH., VOL.191, 1988, PP.225-245.

- [56]OLINGER, D. G. AND SREENIVASAN, K. R.: "NONLINEAR DYNAMICS OF THE WAKE OF AN OSCILLATING CYLINDER," PHYS. REV. LETT., VOL.60, 1988, PP.797-800.
- [57]KARANIADAKIS, G. E. AND TRIANTAFYLLOU, G. S.: "PERIOD DOUBLING CASCADE IN THE WAKE OF A CIRCULAR CYLINDER," BULL. AM. PHYS. SOC., VOL.35, 1990, PP.2242.
- [58]NUZZI, F., MAGNESS, C. AND ROCKWELL, D.: "THREE-DIMENSIONAL VORTEX FORMATION FROM AN OSCILLATING, NON-UNIFORM CYLINDER," J. FLUID MECH., VOL.238, 1992, PP.31-54.
- [59]BAKER, C. J.: "THE OSCILLATION OF HORSESHOE VORTEX SYSTEM," TRANS. OF ASME, J. FLUID ENG., VOL.113, 1991, PP.489-494.
- [60]SHIRAKASHI, M., ISHIDA, Y. AND WAKIYA, S.: "HIGHER VELOCITY RESONANCE OF CIRCULAR CYLINDERS IN CROSS-FLOW," TRANS. OF ASME, J. FLUID ENG., VOL.107, SEPT. 1985, PP.392-396.
- [61]MARN, J. AND CATTON, I.: "ANALYSIS OF FLOW INDUCED VIBRATION USING THE VORTICITY TRANSPORT EQUATION," J. FLUID ENG., VOL.115, 1993, PP.485-492.
- [62]HIGUCHI, H., LEWALLE, J. AND CRANE, P.: "ON THE STRUCTURE OF A TWO-DIMENSIONAL WAKE BEHIND A PAIR OF FLAT PLATES," PHYS. FLUIDS, VOL.6, NO.1, 1994, PP.297-305.
- [63]NORBERG, C.: "AN EXPERIMENTAL INVESTIGATION OF THE FLOW AROUND A CIRCULAR CYLINDER: INFLUENCE OF ASPECT RATIO," J. FLUID MECH., VOL.258, 1994, PP.287-316.
- [64]GOPALKRISHNAN, M. S., TRIANTAFYLLOU, M. S., TRIANTAFYLLOU, G. S. AND BARRET, D.: "ACTIVE VORTICITY CONTROL IN A SHEAR FLOW USING A FLAPPING FOIL," J. FLUID MECH., VOL.274, 1994, PP.1-21.
- [65]NAWAB, S. N. AND QUATIERI, T. F.: ADVANCED TOPICS IN SIGNAL PROCESSING, LIM AND OPPENHEIM, PRENTICE HALL, ENGLEWOOD CLIFFS, NJ, 1988.
- [66]GABOR, D.: "THEORY OF COMMUNICATIONS," J. IEEE (LONDON), VOL.93 (III), 1946, PP. 429-457.
- [67]BASTIAANAS, M. J.: "A SAMPLING THEOREM FOR THE COMPLEX SPECTOGRAM AND GABOR'S EXPANSION OF A

- SIGNAL IN GAUSSIAN ELEMENTARY SIGNALS," OPTICAL ENG., VOL.20, NO.4, 1981, PP.594-598.
- [68]JANSSEN, A. J.: "GABOR REPRESENTATION OF GENERALIZED FUNCTIONS," J. MATH. ANAL. APPL., VOL.83, 1981, PP.377-394.
- [69]DAUBECHIES, I., JAFFARD, S. AND JOURNÉ, J. L.: "A SIMPLE WILSON ORTHONORMAL BASIS WITH EXPONENTIAL DECAY," SIAM, J. MATH. ANAL., 1991, PP.554-573.
- [70]AUSLANDER, L. AND GERTNER, I. C.: "THE DISCRETE ZAK TRANSFORM APPLICATION TO TIME-FREQUENCY ANALYSIS AND SYNTHESIS OF NONSTATIONARY SIGNALS," IEEE, TRANS. SIG. PROC., VOL.39, NO.4, 1991, PP.825-835.
- [71]DAUBECHIES, I., GROSSMAN, A. AND MEYER, Y.: "PAINLESS NONORTHOGONAL EXPANSIONS," J. MATH. PHYS., VOL.27, 1986, PP.1271-1283.
- [72]JENSEN, H. E., HOHOLD, T. AND JUSTESEN, J.: "DOUBLE SERIES REPRESENTATION OF BOUNDED SIGNALS," IEEE, TRANS. INFO. THEORY, VOL.34, NO.4, 1988, PP.613-625.
- [73]AUSLANDER, L. AND TOLIMIERI, R.: ABELIAN HARMONIC ANALYSIS, THETA FUNCTIONS AND FUNCTION ALGEBRA ON NILMANIFOLDS, NEW YORK, SPRINGER, 1975.
- [74]GROSSMANN, A. AND MORLET, J.: "TRANSFORM ASSOCIATED WITH SQUARE INTEGRABLE GROUP REPRESENTATION I," J. MATH. A PHYS., VOL.27, 1985.
- [75]DAUBECHIES, I.: "ORTHONORMAL BASIS OF COMPACTLY SUPPORTED WAVELETS I," CON. PURE APPLIED MATH., VOL.XLL, 1988, PP. 909-996.
- [76]DAUBECHIES, I.: "ORTHONORMAL BASIS OF COMPACTLY SUPPORTED WAVELETS II," VARIATIONS ON A THEME, AT AND T PREPRINT, 1988.
- [77]RIOUL, O. AND VETTERLI, M.: "WAVELETS AND SIGNAL PROCESSING," IEEE, SIG. PROC. MAGAZINE, 1991, PP.14-38.
- [78]SHENSA, M.: "THE DISCRETE WAVELET TRANSFORM: WEDDING THE A TROUS AND MALLAT ALGORITHMS," IEEE, TRANS. SIG. PROC., VOL.40, NO.10, 1992, PP. 2464-2484.
- [79]MALLAT, S.: "A THEORY FOR MULTIREOLUTION SIGNAL DECOMPOSITION: THE WAVELET REPRESENTATION," IEEE,

- TRANS. PAT. ANAL., MACHINE INTELL., VOL.11, NO.7, 1989, PP. 674-693.
- [80]MALLAT, S.: "MULTIFREQUENCY CHANNEL DECOMPOSITIONS OF IMAGES AND WAVELET MODELS," IEEE, TRANS. ACOUSTIC, SPEECH, AND SIG. PROC., VOL.37, NO.12, 1989, PP.2091-2110.
- [81]DAUBECHIES, I.: "THE WAVELET TRANSFORM: A METHOD FOR TIME-FREQUENCY LOCALIZATION," ADVANCES IN SPECTRUM ANALYSIS AND ARRAY PROC., CHAPTER 8, VOL.1, S. HAYKIN ED., PRENTICE HALL, ENGLEWOOD CLIFFS, NJ, 1991, PP.366-417.
- [82]RIOUL, O.: "A DISCRETE TIME MULTIREOLUTION THEORY," IEEE, TRANS. SIG. PROC., VOL.41, NO.8, 1993, PP.2591-2606.
- [83]TEWFIK, A., SINHA, D. AND JORGENSEN, P.: "ON THE OPTIMAL CHOICE OF A WAVELET FOR SIGNAL REPRESENTATION," IEEE, TRANS. INFO. THEORY, VOL.38, NO.2, 1992, PP.747-765.
- [84]DAUBECHIES, I.: "THE WAVELET TRANSFORM, TIME-FREQUENCY LOCALIZATION AND SIGNAL ANALYSIS", IEEE, TRANS. INFO. THEORY, VOL.36, NO.5, 1990, PP.961-1005.
- [85]MEYER, Y.: ONDELETES, HERMANN, NEW YORK, 1990.
- [86]KADAMBE, S. AND BOUDREAUX-BARTELS, G. F.: "A COMPARISON OF THE EXISTANCE OF CROSS TERMS IN THE WIGNER DISTRIBUTION AND THE SQUARED MAGNITUDE OF THE WAVELET TRANSFORM AND THE SHORT TIME FOURIER TRANSFORM," IEEE, TRANS. SIG. PROC., VOL.40, NO.10, 1992, PP.2483-2499.
- [87]KADAMBE, S. AND BOUDREAUX-BARTELS, G. F.: "APPLICATION OF THE WAVELET TRANSFORM FOR PITCH DETECTION OF SPEECH SIGNALS," IEEE, TRANS. INFO. THEORY, VOL.38, NO.2, 1992, PP.469-472.
- [88]GENOSSAR, T. AND PORAT, M.: "CAN ONE EVALUATE THE GABOR EXPANSION USING GABOR'S ITERATIVE ALGORITHM," IEEE, TRANS. SIG. PROC., VOL.40, NO.8, 1992.
- [89]DELPRAT, N., ESCUDIÉ, B., GUILLEMAIN, P., KRONLAND-MARTINET, R., TCHAMITCHIAN, P. AND TORRÉSANI, B.: "ASYMPTOTIC WAVELET AND GABOR ANALYSIS:

- EXTRACTION OF INSTANTANEOUS FREQUENCIES," IEEE, TRANS. INFO. THEORY, VOL.38, NO.2, 1992, PP.644-664.
- [90]GRÖCHENIG, K.: "ACCELERATION OF THE FRAME ALGORITHM," IEEE, TRANS. SIG. PROC., VOL.41, NO.12, 1993, PP.3331-3340.
- [91]JANSSEN, A. J.: "THE ZAK TRANSFORM AND SAMPLING THEOREMS FOR WAVELET SUBSPACES," IEEE, TRANS. SIG. PROC., VOL.41, NO.12, 1993, PP.3360-3364.
- [92]THE BRITANNICA ENCYCLOPAEDIA OF AMERICAN ART : ENCYCLOPAEDIA BRITANNICA, CHICAGO, ILL., 1973.
- [93]SHUSTER, H.: DETERMINISTIC CHAOS: AN INTRODUCTION, WEINHEIM, PHYSK-VERLAG, GMBH, 1984.
- [94]HOLMES, P. J. AND MOON, F. C.: "BIFURCATIONS TO DIVERGENCE AND FLUTTER IN FLOW INDUCED OSCILLATIONS: AN INFINITE DIMENSIONAL ANALYSIS," INTER. FEDERATION OF AUTOMATIC CONTROL, VOL.14, 1978, PP.367-384.
- [95]MOON , F. C.: CHAOTIC VIBRATIONS: AN INTRODUCTION FOR APPLIED SCIENTISTS ENGINEERS, NEW YORK, JOHN WILEY & SONS INC., 1987.
- [96]GUCKENHEIMER, J. AND HOLMES, P. J.: NON-LINEAR OSCILLATIONS, DYNAMICAL SYSTEMS AND BIFURCATIONS OF VECTOR FIELDS, APPLIED MATHEMATICAL SCIENCES SERIES, NO.42, NEW YORK: SPRINGER-VERLAG, 2ND. EDITION, 1986.
- [97]NAYFEH, A. H.: INTRODUCTION TO PERTURBATION TECHNIQUES, NEW YORK: JOHN WILEY, 1981.
- [98]LING, F. H. AND WU, X. X.: "FAST GALERKIN METHOD AND ITS APPLICATION TO DETERMINE PERIODIC SOLUTIONS OF NON-LINEAR OSCILLATORS," INTER. J. NON-LINEAR MECH., VOL.22, NO.2, 1987, PP.89-98.
- [99]LAU, S. L., CHEUNG, Y. K. AND WU, S. Y.: "VARIABLE PARAMETER INCREMENTATION METHOD FOR DYNAMIC STABILITY OF LINEAR AND NONLINEAR ELASTIC SYSTEMS," AMSE, J. APPLIED MECH., VOL.49, 1982, PP.849-853.

- [100]LING, F. H.: "AN ALTERNATING FREQUENCY/TIME DOMAIN METHOD FOR CALCULATING THE STEADY STATE RESPONSE OF NONLINEAR DYNAMICAL SYSTEMS: DISCUSSION/AUTHOR'S CLOSURE," ASME, J. APPLIED MECH., VOL.57, 1990, PP.251-252.
- [101]DOWELL, E. H.: "OBSERVATIONS AND EVOLUTION OF CHAOS FOR AN AUTONOMOUS SYSTEM," ASME, J. APPL. MECH., VOL.51, 1984, PP.664-673.
- [102]MAHFOUZ, I. A. AND BADRAKHAN, F.: "CHAOTIC BEHAVIOR OF SOME PIECEWISE-LINEAR SYSTEMS WITH SET-UP SPRING OR WITH UNSYMMETRIC ELASTICITY," J. SOUND AND VIB., VOL.143, NO.2, 1990, PP.255-288.
- [103]UEDA, Y.: "STEADY MOTIONS EXHIBITED BY DUFFING'S EQUATION: A PICTURE BOOK OF REGULAR AND CHAOTIC MOTIONS," NEW APPROACHES TO NONLINEAR PROBLEMS IN DYNAMICS, SIAM, 1980, PP.311-322.
- [104]KAPITANIAK, T. AND WOJEWODA, J.: "STRANGE NON-CHAOTIC ATTRACTORS OF A QUASI-PERIODICALLY FORCED VAN DER POL'S OSCILLATOR," J. SOUND AND VIB., VOL.138, NO.1, 1990, PP.162-169.
- [105]ROMEIREAS, F. J., AND OTT, E.: "STRANGE NON-CHAOTIC ATTRACTORS OF DAMPED PENDULUM WITH QUASIPERIODIC FORCING," PHYS. REV. A, VOL.35, 1987, PP.4404-4413.
- [106]MCDONALD, S. W., GREBOGI, C., OTT, E. AND YORK, J.; "FRACTAL BASIN BOUNDARIES," PHYSICA D, VOL.17, 1985, PP.125-153.
- [107]MCLAUGHLIN, J. B.: "PERIOD-DOUBLING BIFURCATIONS AND CHAOTIC MOTIOAN OF A PARAMETRICALLY FORCED PENDULUM," J. STATISTICAL PHYSICS, VOL.24, 1981, PP.375-388.
- [108]PEZESHKI, C. AND DOWELL, E. H.: "ON CHAOS AND FRACTAL BEHAVIOR IN A GENERALIZED DUFFING'S SYSTEM," PHYSICA D, VOL.32, 1988, PP.194-209.
- [109]ISOMAKI, H. M. AND VON BOEHM, J.: "FRACTAL BASIN BOUNDARIES OF AN IMPACTING PARTICLE," PHYSICS LETTERS, VOL.126(A), 1988, PP.484-490.

- [110]GUCKENHEIMER, J. AND HOLMES, P.: NONLINEAR OSCILLATIONS, DYNAMICAL SYSTEMS AND BIFURCATIONS OF VECTOR FIELDS, SPRINGER-VERLAG, NEW YORK, 1983.
- [111]OSELEDEC, V. I.: "A MULTIPLICATION ERGODIC THEOREM, LYAPUNOV CHARACTERISTIC NUMBERS FOR DYNAMICAL SYSTEMS," TRANS. MOSCOW MATHEMATICAL SOCIETY, VOL.19, 1968, PP.197-231.
- [112]UEDA, Y.; "RANDOMLY TRANSITIONAL PHENOMENA IN THE SYSTEM GOVERNED BY DUFFING'S EQUATION," J. STATISTICAL PHYSICS, VOL.20, 1979, PP.181-196.
- [113]LICHTENBERG, A. J. AND LIEBERMAN, M. A.: REGULAR AND STOCHASTIC MOTION, NEW YORK, SPRINGER-VERLAG, 1982.
- [114]WOLF, A., SWIFT, J. B., SWINNEY, H. L. AND VASTANO, J. A.: "DETERMINING LYAPUNOV EXPONENTS FROM A TIME SERIES," PHYSICA D, VOL.16, 1985, PP.285-317.
- [115]MOON, F. C. AND LI, G. X.: "THE FRACTAL DIMENSION OF THE TWO-WELL POTENTIAL STRANGE ATTRACTOR," PHYSICA D, VOL.17, 1985, PP.99-108.
- [116]YOUNG, L. S.: "DIMENSION, ENTROPY AND LYAPUNOV EXPONENTS IN DIFFERENTIABLE DYNAMICAL SYSTEMS," PHYSICA A, VOL.124, 1984, PP.639-646.
- [117]ABRAHAM, N. B., ALBANO, A. M., DAS, B., DEGUZMAN, G., YONG, S., GIPGGIA, R. S., PUCCIONI, G. P. AND TREDICCA, J. R.: "CALCULATING THE DIMENSION OF ATTRACTORS FROM SMALL DATA SETS," PHYSICS LETTERS, VOL.114(A), 1986., PP.217-221
- [118]FARMER, J. D., OTT, E. AND YORK, J. A.: "THE DIMENSION OF CHAOTIC ATTRACTORS," PHYSICA D, VOL.7, 1983, PP.153-180.
- [119]GRASSBERGER, P. AND PROCCACIA, I.: "CHARACTERIZATION OF STRANGE ATTRACTORS," PHYS. REV. LETT., VOL.50, 1983, PP.346-349.
- [120]FEIGENBAUM, M. J.: "UNIVERSAL BEHAVIOR IN NON-LINEAR SYSTEMS," PHYSICA D, VOL.7, 1983, PP.16-39.
- [121]THOMPSON, J. M. T. AND STEWART, H. B.: NONLINEAR DYNAMICS AND CHAOS, NEW YORK, WILEY, 1986.

- [122]GREBOGI, C., OTT, E. AND YORKE, J. A.: "CHAOTIC ATTRACTORS IN CRISES," PHYS. REV. LETT., VOL. 48, 1982, PP.1507-1510.
- [123]GREBOGI, C., OTT, E. AND YORKE, J. A.: "CRISES, SUDDEN CHANGES IN CHAOTIC ATTRACTORS AND TRANSIENT CHAOS," PHYSICA D, VOL.7, 1983, PP.181-200.
- [124]PARKINSON, G. V. AND SMITH, J. D.: "THE SQUARE PRISM AS A AEROELASTIC OSCILLATOR," QUARTERLY J. APPLIED MATH., VOL.17, NO.2, 1964, PP.225-239.
- [125]DOWELL, E. H.: "NONLINEAR OSCILLATIONS OF A FLUTTERING PLATE," AMERICAN INST. OF AERONAUTICS AND ASTRONAUTICS J., VOL.4, NO.7, 1966, PP.1267-1275.
- [126]HOLMES, P. J. AND MOON, F. C.: "BIFURCATIONS TO DIVERGENCE AND FLUTTER IN FLOW INDUCED OSCILLATIONS: AN INFINITE DIMENSIONAL ANALYSIS," INTER. FEDERATION OF AUTOMATIC CONTROL, VOL.14, 1978, PP.367-384.
- [127]MOON, F. C.: CHAOTIC VIBRATIONS, NEW YORK: WILEY INTERSCIENCE, 1987.
- [128]TONGUE, B. H.: "CHARACTERISTICS OF NUMERICAL SIMULATIONS OF CHAOTIC SYSTEMS," ASME, J. APPL. MECH., VOL.54, 1987, PP.695-699.
- [129]KAPITANIAK, T. AND WOJEWODA, J.: "CHAOS IN A LIMIT CYCLE SYSTEM WITH ALMOST PERIODIC EXCITATION," J. PHYSICS A, VOL.21, 1988, PP.843-847.
- [130]KAPITANIAK, T.: "COMBINED BIFURCATION AND TRANSITION TO CHAOS IN NONLINEAR OSCILLATOR WITH TWO EXTERNAL PERIODIC FORCES," J. SOUND AND VIB., VOL.121, 1988, PP.259-268.
- [131]KAPITANIAK, T., AWREJCEWICZ, J. AND STEEB, W. H.: "CHAOTIC BEHAVIOR OF AN ANHARMONIC OSCILLATOR WITH PERIODIC EXCITATION," J. PHYSICS A, VOL.20, 1987, PP.252-255.
- [132]LEVITAS, J., WELLER, T. AND SINGER, J.: "POINCARÉ-LIKE SIMPLE CELL MAPPING FOR NON-LINEAR DYNAMICAL SYSTEMS," J. SOUND AND VIB., VOL.176, NO.5, 1994, PP.641-662.

- [133]HEALEY, J. J.: "SPATIAL CHAOS IN BOUNDARY LAYER TRANSITION," APPLIED SCIENTIFIC RESEARCH, VOL.51, 1993, PP.49-53.
- [134]CAMERON, T. M. AND GRIFFIN, J. H.: "AN ALTERNATING FREQUENCY/TIME DOMAIN METHOD FOR CALCULATING THE STEADY STATE RESPONSE OF NONLINEAR DYNAMIC SYSTEMS," ASME, J. APPL. MECH., VOL.56, 1989, PP.149-154.
- [135]AL-BEDDOOR, B.: "EFFECT OF FLOW HISTORY ON THE FLOW INDUCED VIBRATIONS OF ROUGH INTERFERING BODIES," M.SC. THESIS, UNIVERSITY OF JORDAN, AMMAN, JORDAN, 1989.
- [136]HIJAWI, M. S.: "INFLUENCE OF INTERFERENCE, TURBULENCE INTENSITY AND SURFACE ROUGHNESS ON THE FLOW-INDUCED VIBRATION OF A CIRCULAR CYLINDER," M.SC. THESIS, UNIVERSITY OF JORDAN, AMMAN, JORDAN, 1991.
- [137]GRAHAM, J. M.: "THE EFFECT OF END PLATES ON THE TWO DIMENSIONALITY OF A VORTEX WAKE," THE AERONAUTICAL QUARTERLY, 1969, PP.237-247.
- [138]ARGOUL, F., ARBEODO, A., GRASSEAU, G., GAGNEY, Y., HOPFINGER, E. F. AND FRISCH, U.: "WAVELET ANALYSIS OF TURBULENCE REVEALS THE MULTIFRACTAL NATURE OF THE RICHARDSON CASCADE," NATURE, VOL.338, 1989, PP. 51-53.
- [139]ZABUSKY, N.: "COMPUTATIONAL SYNERGETICS," PHYSICS TODAY, 1984, PP.2-11.
- [140]FOX, T. A.: "ENDPLATES INTERFERENCE EFFECTS ON THE AERODYNAMICS OF A CIRCULAR CYLINDER IN UNIFORM FLOW," AERONAUTICAL J., 1992, PP.10-14.

APPENDIX A

BASIC MATHEMATICAL EQUATIONS

A.1 THE P-DEGREE NORM

For a Hilbert space of P-degrees R^P , the norm of a function $f = f(t)$ defined as

$$\|f\|_p = \left[\int |f(t)|^p dt \right]^{1/p} \quad (\text{A.1})$$

A.2 LINEARITY PRINCIPLE

If

$$x(t) = a * x_1(t) + b * x_2(t) \quad (\text{A.2})$$

then a function TFR (Time-Frequency Representation) of $x(t)$ is linear if

$$TFR(x(t)) = a * TFR(x_1(t)) + b * TFR(x_2(t)) \quad (\text{A.3})$$

A.3 FOURIER TRANSFORM PROPERTIES

A.3.1 DEFINITION

A periodic discrete sequence $x[n]$ can be represented by a Fourier integral as

$$x[n] = \frac{1}{2\pi} \int_{-\pi}^{\pi} X(\omega) e^{j\omega n} d\omega \quad (\text{A.4})$$

where $X(e^{j\omega})$ is the Fourier transform and is given by

$$X(\omega) = \sum_{n=-\infty}^{\infty} x[n] e^{j\omega n} \quad (\text{A.5})$$

Eq.(A.4) is usually termed the inverse Fourier transform. Moreover, Eqs.(A.4) and (A.5) form a Fourier transform pair which is given the notation

$$x[n] \stackrel{f}{\Leftrightarrow} X(\omega) \quad (\text{A.6})$$

where f denotes the Fourier transform.

A.3.2 LINEARITY OF THE FOURIER TRANSFORM

If

$$x_1[n] \stackrel{f}{\Leftrightarrow} X_1[\omega] \quad (\text{A.7})$$

and

$$x_2[n] \stackrel{f}{\Leftrightarrow} X_2[\omega] \quad (\text{A.8})$$

then

$$a x_1[n] + b x_2[n] \stackrel{f}{\Leftrightarrow} a X_1[\omega] + b X_2[\omega] \quad (\text{A.9})$$

A.3.3 TIME SHIFTING AND FREQUENCY SHIFTING

If

$$x[n] \stackrel{f}{\Leftrightarrow} X(\omega) \quad (\text{A.10})$$

then the n_o time-shifted sequence is

$$x[n - n_o] \stackrel{f}{\Leftrightarrow} e^{-jn_o\omega} X(\omega) \quad (\text{A.11})$$

and the ω_o frequency-shifted Fourier transform is

$$e^{j\omega_o n} x[n] \stackrel{f}{\Leftrightarrow} X(\omega - \omega_o) \quad (\text{A.12})$$

A.3.4 DIFFERENTIATION IN FREQUENCY DOMAIN

If

$$x[n] \stackrel{f}{\Leftrightarrow} X(\omega) \quad (\text{A.13})$$

then

$$nx[n] \stackrel{f}{\Leftrightarrow} j \frac{d}{d\omega} (X(\omega)) \quad (\text{A.14})$$

A.3.5 THE CONVOLUTION THEOREM

If

$$x[n] \stackrel{f}{\Leftrightarrow} X(\omega) \quad (\text{A.15})$$

and

$$h[n] \stackrel{f}{\Leftrightarrow} H(\omega) \quad (\text{A.16})$$

and if

$$y[n] = \sum_{k=-\infty}^{\infty} x[n]h[n-k] = x[n]*h[n] \quad (\text{A.17})$$

then

$$Y(\omega) = X(\omega)H(\omega) \quad (\text{A.18})$$

A.3.6 THE MODULATION OR WINDOWING THEOREM

If

$$X[n] \stackrel{f}{\Leftrightarrow} X(\omega) \quad (\text{A.19})$$

and

$$w[n] \stackrel{f}{\Leftrightarrow} W(\theta) \quad (\text{A.20})$$

and if

$$y[n] = x[n]w[n] \quad (\text{A.21})$$

then

$$Y(\omega) = \frac{1}{2\pi} \int_{-\pi}^{\pi} X(\theta)W(\omega - \theta)d\theta \quad (\text{A.22})$$

A.3.7 PARSEVAL'S THEOREM

If

$$x[n] \stackrel{f}{\Leftrightarrow} X(\omega) \quad (\text{A.23})$$

then

$$E = \sum_{n=-\infty}^{\infty} |x[n]|^2 \quad (\text{A.24})$$

for all $f \in L^2(R)$. The frame condition guarantees that the coefficients

$$\langle f, g_{ma,nb} \rangle, m, n \in Z \quad (\text{A.35})$$

uniquely determine f and that a numerical stable algorithm can be found to compute f from the coefficients.

A.7 ORTHOGONAL BASIS

A frame $\{g_{ma,nb} : m, n \in Z\}$ is orthonormal if the frame condition holds with $B = 1$, i.e.

$$\sum_{m \in Z} \sum_{n \in Z} |\langle f, g_{ma,nb} \rangle|^2 \leq \|f\|_2^2 \quad (\text{A.36})$$

The function f will not be generally determined by the coefficients. If a frame is an orthonormal basis then

$$\sum_{m \in Z} \sum_{n \in Z} |\langle f, g_{ma,nb} \rangle|^2 = \|f\|_2^2 \quad (\text{A.37})$$

and thus

$$f = \sum_{m \in Z} \sum_{n \in Z} \langle f, g_{ma,nb} \rangle g_{ma,nb} \quad (\text{A.38})$$

which gives the proper reconstruction of f .

A.8 TIGHT FRAMES

A frame is called a tight frame if $A = B$ (equal frame bounds), thus

$$\|f\|_2^2 = A^{-1} \sum_{m \in Z} \sum_{n \in Z} |\langle f, g_{ma,nb} \rangle|^2 \quad (\text{A.39})$$

and

$$f = A^{-1} \sum_{m \in Z} \sum_{n \in Z} \langle f, g_{ma,nb} \rangle g_{ma,nb} \quad (\text{A.40})$$

It is to be noted that the computational advantages of orthonormality are retained; i.e. the signal energy, up to the scaling factor A^{-1} , is given by the

energy of the sequence of samples and the signal can be reconstructed from these coefficients.

For any frame, a "dual" reference signal \tilde{g} can be found such that the set of functions

$$\{\tilde{g}_{ma,nb} : m, n \in Z\} \quad (\text{A.41})$$

is a frame with

$$B^{-1}\|f\|_2^2 \leq \sum_{m \in Z} \sum_{n \in Z} |\langle f, \tilde{g}_{ma,nb} \rangle|^2 \leq A^{-1}\|f\|_2^2 \quad (\text{A.42})$$

and

$$f = \sum_{m \in Z} \sum_{n \in Z} \langle f, g_{ma,nb} \rangle \tilde{g}_{ma,nb} \quad (\text{A.43})$$

APPENDIX B

GT AND WT COMPUTER PROGRAMS

```

CCCCCCCCCCCCCCCCCCCCCCCCCCCCCCCCCCCCCCCCCCCCCCCCCCCCCCCC C
C           THE FIRST PROGRAM C
C   THIS FUNCTION COMPUTES THE GABOR COEFFICIENTS C
C           THE GABOR TRANSFORM. C
CCCCCCCCCCCCCCCCCCCCCCCCCCCCCCCCCCCCCCCCCCCCCCCCCCCCCCCC C
      DIMENSION TT(0:1025), XA(0:1025), XG(0:1025)
      COMPLEX*16 XX(0:1025,0:1025),X(0:1025,0:1025),W(0:1025,0:1025)
      COMPLEX*16 HA(0:1025,0:1025),HG(0:1025,0:1025),W1(0:1025,0:1025)
      COMPLEX*16 WW(0:1025,0:1025),G(0:1025,0:1025)
      COMPLEX*16 DA(0:1025,0:1025),DG(0:1025,0:1025)
      DOUBLE PRECISION PHASE(0:1025,0:1025)
      DOUBLE PRECISION A(0:1025,0:1025),AN1R,AN1I
      OPEN(UNIT=1,FILE='V12S1.TXT',STATUS='OLD')
      OPEN(UNIT=4,FILE='V12G1.OUT',STATUS='NEW')
      OPEN(UNIT=12,FILE='V12PHG1.OUT',STATUS='NEW')
      PI=4.*ATAN(1.)
      LI=1
      HH=1.
      NOS = 1024
      MOS = NOS
C   WRITE(*,*)'PLEASE ! ENTER THE NUMBER OF SAMPLES (NOS)?'
C   READ(*,*) NOS

      DO 3 K=1,NOS
      READ(1,*) AIZ
      XA(K)= AIZ
      X(LI,K) = CMPLX(AIZ,0.)
3   CONTINUE

      DO 11 I=1,NOS
      XG(I) = G_FUN( REAL(I) / REAL(NOS) )
11  CONTINUE

      NOSD2 = NOS/2.
      MOSD2 = MOS/2.
      MPM = LOG(REAL(MOSD2)) / LOG(2.)
      NPN = LOG(REAL(NOSD2)) / LOG(2.)
      XZ = N / (4*NOSD2)

```

```

YZ = M / MOSD2

      CALL FN(MOSD2,NOSD2,XA,DA)
DO 99 N = 1,NOSD2
      DO 88 M = 1,MOSD2
          CALL ZT(M,N,MPM,MOSD2,NPN,NOSD2,XZ,YZ,PI,DA,HA)
          CALL FN(MOSD2,NOSD2,XG,DG)
          CALL ZT(M,N,MPM,MOSD2,NPN,NOSD2,XZ,YZ,PI,DG,HG)
88      CONTINUE
99      CONTINUE
          DO 77 I = 1,MOSD2
              DO 66 J = 1,NOSD2
                  RGMAG = REAL(HG(I,J))**2 + DIMAG(HG(I,J))**2
                  IGMAG = CMPLX( RGMAG , 0. )
                  W1(I,J) = HA(I,J)*HG(I,J)
66          CONTINUE
77          CONTINUE

CALL ID2FFT(W1,MPM,MOSD2,NPN,NOSD2,W)
DO 55 M = 1,MOSD2
DO 44 N = 1,NOSD2
    AN1R = REAL(W1(M,N))
    AN1I = DIMAG(W1(M,N))
    A(M,N) = AN1R**2 + AN1I**2
WRITE(*,*)'A=',A(M,N),'W1=',W1(M,N)
    IF (AN1R.NE.0.0) THEN
        PHASE(M,N) = DTAN(AN1I/AN1R)
    ELSE
        PHASE(M,N) = 90.0*PI/180.0
    END IF
    WRITE(12,135) M,N,PHASE(M,N)
135    FORMAT(I3,3X,I5,2X,F56.4)
        WRITE(4,134) M,N,A(M,N)
134    FORMAT(I3,3X,I5,2X,F56.3)
44    CONTINUE
55    CONTINUE
STOP
END

```

```

C      THIS SUBROUTINE PERFORMS THE ZAK TRANSFORM OF A
C      TWO DIMENSIONAL FUNCTION
SUBROUTINE ZT(M,N,MPM,MOSD2,NPN,NOSD2,XZ,YZ,PI,D,H)
COMPLEX*16 D(0:1025,0:1025), H(0:1025,0:1025)
COMPLEX*16 A(0:1025),B(0:1025), TTT
DOUBLE PRECISION AN2I, AN2R
COMPLEX*16 SUM
C      XZ = N / (4*NOSD2)
C      YZ = M / MOSD2
      PI = 4.0*ATAN(1.0)
      CALL D2FFT(A,B,MPM,MOSD2,NPN,NOSD2,D)
      DO 20 J = 1,NOSD2
      TTT = CMPLX( 0. , 2*PI*N*J/(4.*NOSD2) )
      H(M,J) = H(M,J) + D(M,J)*EXP(TTT)
20    CONTINUE
      RETURN
      END

C      THIS SUBROUTINE TRANSFORMS ONE DIMENSIONAL BOUNDED
C      FUNCTION INTO TWO DIMENSIONAL ONE
SUBROUTINE FN(MOSD2,NOSD2,AA,D)
COMPLEX*16 D(0:1025,0:1025)
DIMENSION AA(0:1025)
DO 1 IJ = 1,NOSD2
DO 2 IK = 1,MOSD2
  IF(((IK+IJ).GT.MOSD2*2).OR.((IK+IJ).GT.NOSD2*2)) GOTO 2
  D(IK,IJ) = CMPLX( AA(IK+IJ) , 0.)
2    CONTINUE
1    CONTINUE
      RETURN
      END
COMPLEX FUNCTION PSIG(D,WWI,W)
COMPLEX G,TT1
PI = 4.*ATAN(1.)
      PSI = SQRT(SQRT(2.)/D)*D/(SQRT(2.*PI))
&      *EXP( -W**2 / (4.*SQRT(PI)/D)**2 )
      RETURN
      END

```

```

COMPLEX FUNCTION GG(IIP,D,WWI,W)
COMPLEX G,TT1
PI = 4.*ATAN(1.)
      GG = SQRT(SQRT(2.)/D)*D/(SQRT(2.*PI))
&      *EXP(-W**2/(4.*(SQRT(PI)/D)**2))
RETURN
END

C THIS SUBROUTINE CARRIES OUT 1D FFT
SUBROUTINE FFT(A,N,NB)
COMPLEX A(NB),UD,W,T
DO 11 JI = 1,NB
11  A(JI) = A(JI)/NB
    NBD2 = NB/2
    NBM1 = NB-1
    JI = 1
    DO 40 L = 1,NBM1
    IF(L.GE.JI) GOTO 20
    T = A(JI)
    A(JI) = A(L)
    A(L) = T
20  K = NBD2
30  IF(K.GE.JI) GOTO 40
    JI = JI-K
    K = K/2
    GOTO 30
40  JI = JI+K
    PI = 4.0*ATAN(1.0)
    DO 16 M = 1,N
    UD = (1.0,0.0)
    ME = 2**M
    K = ME/2
    W = CMPLX(COS(PI/K)-SIN(PI/K))
    DO 16 JI = 1,K
    DO 15 L = JI, NB, ME
    LP = L+JI
    T = A(LP)*UD

```



```

6          CONTINUE
RETURN
END

C  THE GAUSSIAN FUNCTION OF GABOR MODEL
DOUBLE PRECISION FUNCTION G_FUN(T)
PI = 4.0*ATAN(1.0)
G_FUN = EXP(-PI*T**2)
RETURN
END

C  THIS SUBROUTINE CARRY OUT THE INVERSE 2D FFT
SUBROUTINE ID2FFT(C,N1,NB1,N2,NB2,W)
COMPLEX*16 C(0:1025,0:1025), W(0:1025,0:1025), TTT, SUM
PI = 4.0*ATAN(1.0)
DO 35 M = 1,NB1
DO 30 N = 1,NB2
SUM = (0.,0.)
DO 25 I = 1,NB1
DO 20 J = 1,NB2
TTT = CMPLX(0., 2*PI*((I-1)*M/NB1 + (J-1)*N/NB2) )
SUM = SUM + C(I,J)*EXP(TTT)
20    CONTINUE
25    CONTINUE
W(M,N) = SUM
30    CONTINUE
35    CONTINUE
RETURN
END

```

```

CCCCCCCCCCCCCCCCCCCCCCCCCCCCCCCCCCCCCCCCCCCCCCCCCCCCCCCC C
C           THE SECOND PROGRAM                                C
C   THIS PROGRAM COMPUTES THE AMPLITUDE AND PHASE OF        C
C   THE WAVELET TRANSFORM USING ONE OF THE FOLLOWING        C
C   WAVELETS g(t) :                                         C
C   1 THE MODULATED GAUSSIAN                                  C
C   2 THE MEXICAN HAT                                        C
C   3 THE 8TH DERIVATIVES OF THE GAUSSIAN                    C
C   4 DAUBECHIES' TIGHT FRAME                                C
C   5 POLYNOMIAL SPLINES OF ORDER 3                          C
C   6 Y MEYERS CONSTRUCTION                                  C
C   7 ONE CYCLE OF THE SINE FUNCTION                          C
CCCCCCCCCCCCCCCCCCCCCCCCCCCCCCCCCCCCCCCCCCCCCCCCCCCCCCCC C
      DIMENSION TT(8900), XA(-525:-525,8900)
      COMPLEX*16 XX(-525:-525,8900),X(-525:-525,8900),W(-525:-525,8900)
      COMPLEX*16 H(-525:-525,8900),W1(-525:-525,8900),W2(-525:-525,8900)
      COMPLEX*16 WW(-525:-525,8900)
      DOUBLE PRECISION PHASE(-525:-525,8900)
      DOUBLE PRECISION A(-525:-525,8900),AN1R,AN1I

      OPEN(UNIT=1,FILE='V19S1.TXT',STATUS='OLD')
      OPEN(UNIT=4,FILE='V19W1.OUT',STATUS='NEW')
      OPEN(UNIT=12,FILE='V19PH1.OUT',STATUS='NEW')

      PI = 4.*ATAN(1.)
C   THE COEFFICIENTS a0 AND b0 ARE DI AND BII, RESPECTIVELY
      DI = 2.
      BII = 1.
C   READ (*,111) IIP
      IIP = 1
C111 FORMAT(I1)
C   WRITE(*,*)'PLEASE ENTER THE NUMBER OF SAMPLES (NOS)?'
C   READ(*,*) NOS
      NOS = 2048

      DO 3 K = 1,NOS
      READ(1,4) AIZ
      XA(LI,K) = AIZ

```



```

4   FORMAT(F10.6)
   X(LI,K) = CMPLX(XA(LI,K),0.)
3   CONTINUE
   CALL FFTC(X,NOS,0)
   INFT = 1024

   DO 99 N = 2,NOS+1
     DO 88 M = -INFT,INFT
       CALL WT(IIP,M,N,PI,DI,BII,NOS,H)
         DO 77 J = 1,NOS
           W1(M,J) = H(M,J)*X(LI,J)
77    CONTINUE
       CALL FINT(W1,NOS,M,HH)
       W(M,N) = (SQRT(2.**M))*W1(M,NOS+1)
       CALL FFTC(W,NOS,1)
       AN1R = REAL(W(M,N))
       AN1I = DIMAG(W(M,N))
       A(M,N) = AN1R**2 + AN1I**2
         IF (AN1R.NE.0.0) THEN
           PHASE(M,N) = DTAN(AN1I/AN1R)
         ELSE
           PHASE(M,N) = 90.0*PI/180.0
         END IF
       WRITE(12,135) M,N,PHASE(M,N)
135  FORMAT(I3,3X,I5,2X,F56.4)
     IF(M.GE.1) GOTO 88
     WRITE(4,134) M,N,A(M,N)
134  FORMAT(I3,3X,I5,2X,F56.3)
88    CONTINUE
99    CONTINUE
   STOP
   END

C   THIS SUBROUTINE COMPUTES THE WT AT CERTAIN M AND N
   SUBROUTINE WT(IIP,M,N,PI,DI,BII,NOS,H)
   COMPLEX*16 XX(-525:-525,8900),H(-525:-525,8900)
   COMPLEX*16 TTT
   DOUBLE PRECISION AN2I,AN2R

```

```

DO 2 J = 2,NOS
  W = REAL(J)
  AA = DBLE((DI**M)*W)
  XX(M,J) = PSI(IIP,DI,BII,AA)
  AN2R = REAL(XX(M,J))
  AN2I = DIMAG(XX(M,J))
  TTT = CMPLX(0.,DI**M*BII*N*J)
  H(M,J) = EXP(TTT)*XX(M,J)
RETURN
END

C   THIS SUBROUTINE GIVES THE WAVELET TO BE USED
    COMPLEX FUNCTION PSI(IIP,DI,BII,W)
    COMPLEX G,TT1
    PI = 4.*ATAN(1.)
    IF(IIP.LT.1.OR.IIP.GT.7) RETURN
    GO TO (1,2,3,4,5,6,7), IIP
1   XK1 = PI*(2./LOG(2.))**.5
    PSI=PI**(-.25)*(EXP((-W-XK1)**2/2.)-EXP(-XK1**2/2.)
& *EXP(-W**2/2.))
    RETURN
2   PSI = 2./(3.)**(.5)*PI**(-.25)*(W)**2*EXP(-W**2/2.)
    RETURN
3   PSI = .011238*PI**(-.25)*(W)**8.*EXP(-W**2/2.)
    RETURN
4   XL = 2.*PI/(BII*(DI**2-1.))
    F = DI*XL
    FF = DI**2*XL
    IF(W.LT.XL.OR.W.GT.FF) PSI=0
    IF(W.GE.XL.OR.W.LT.F) GO TO 8
    IF(W.GE.F.OR.W.LT.FF) GO TO 9
    RETURN
8   Q = (W-XL)/(XL*(DI-1.))
    IF(Q.LT.1.0.OR.Q.GT.0) GO TO 62
    IF(Q.LE.0) V=0
    IF(Q.GE.1) V=1.
    GO TO 57
62  V = Q

```

```

57  PSI = (LOG(DI))**(-.5)*SIN(PI/2.*V)
    RETURN
9   Q = (W-DI*XL)/(DI*XL*(DI-1.))
    IF(Q.LT.1.0.OR.Q.GT.0) GO TO 55
    IF(Q.LE.0) V=0
    IF(Q.GE.1) V=1.
    GO TO 57
55  V = Q
57  PSI = (LOG(DI))**(-.5)*COS(PI/2.*V)
    RETURN
5   X1 = 5.+30.*(COS(W/2.))**2 + 30.*(SIN(W/2.))**2*(COS(W/2.))**2
    X2 = 2.*(COS(W/2.))**2*(SIN(W/2.))**4 + 70.*(COS(W/2.))**4
    &   + 2./3.*(SIN(W/2.))**6
    SIGMA8 = (X1+X2)/(105.*(SIN(W/2.)))
    X3 = 5. + 30.*(COS(W/4.))**2 + 30.*(SIN(W/4.))**2*(COS(W/4.))**2
    X4 = 2.*(COS(W/4.))**2*(SIN(W/4.))**4+70.*(COS(W/4.))**4
    &   + 2./3.*(SIN(W/4.))**6
    SIGMA7 = (X3+X4)/(105.*(SIN(W/4.)))
    X7 = 5.+30.*(COS(W/4+PI))**2+30.*(SIN(W/4+PI))**2*(COS(W/4+PI))**2
    X8 = 2.*(COS(W/4+PI))**2*(SIN(W/4+PI))**4+70.*(COS(W/4+PI))**4
    &   + 2./3.*(SIN(W/4+PI))**6
    SIGMA6 = (X7+X8)/(105.*(SIN(W/4+PI)))
    PSI = EXP(TP)/W**4.*(SIGMA6/(SIGMA8*SIGMA7))
    RETURN
6   XL = 2.*PI/(BII*(DI**2-1.))
    F = DI*XL
    FF = DI**2*XL
    IF(W.LT.XL.OR.W.GT.FF) PSI=0
    IF(W.GE.XL.OR.W.LT.F) GO TO 18
    IF(W.GE.F.OR.W.LT.FF) GO TO 19
    RETURN
18  Q = (W-XL)/(XL*(DI-1.))
    IF(Q.LT.1.0.OR.Q.GT.0) GO TO 17
    IF(Q.LE.0) V=0
    IF(Q.GE.1) V=1.
    GO TO 58
17  V = Q
58  PSI1 = (LOG(DI))**(-.5)*SIN(PI/2.*V)

```

```

V = -Q
PSI2 = (LOG(DI))**(-.5)*SIN(PI/2.*V)
GO TO 12
19  Q = (W-DI*XL)/(DI*XL*(DI-1.))
    IF(Q.LT.1.OR.Q.GT.0) GO TO 77
    IF(Q.LE.0) V=0
    IF(Q.GE.1) V=1.
    GO TO 59
77  V = Q
59  PSI1 = (LOG(DI))**(-.5)*COS(PI/2.*V)
    V = -Q
    PSI2 = (LOG(DI))**(-.5)*COS(PI/2.*V)
12  TT1 = CMPLX(0.,(W/2.))
    PSI = (2.*PI)**(-.5)*EXP(TT1)*(PSI1+PSI2)
    RETURN
7   PSI = (2.)**(.5)/PI*CMPLX(0.,SIN(PI*W)/(1.-W**2))
    RETURN
    END

C   THIS SUBROUTINE FINDS 1D FFT AND ITS INVERSE
C   X = 2**M COMPLEX ARRAY
C   N = 2**M POINTS
C   INV = 0 FLAG FOR DIRECT TRANSFORM
C   INV = 1 FLAG FOR INVERSE TRANSFORM
SUBROUTINE FFTC(X,N,INV)
COMPLEX*16 X(-525:-525,8900),U,W,T,CMPLX
M = LOG(DBLE(N)) / LOG(2.)+.1
NV2 = N/2
NM1 = N-1
J = 1
DO 40 I = 1,NM1
IF (I.GE.J) GO TO 10
T = X(1,J)
X(1,J) = X(1,I)
X(1,I)=T
10  K=NV2
20  IF (K.GE.J)GO TO 30
    J=J-K

```

```
W1(M,2)=VXW1(M,1)
      DO 6 J=3,NOS+1
W1(M,J)=W1(M,J-1)+VXW1(M,J-1)
6 CONTINUE
RETURN
END
```

APPENDIX C

CHAOS COMPUTER PROGRAMS

```

C CCCCCCCCCCCCCCCCCCCCCCCCCCCCCCCCCCCCCCCCCCCCCCCCCCCCCCCCC C
C           THIS PROGRAM DO THE NECESSARY STEPS OF                C
C   INTEGRATION AND THUS ENABLING THE CONSTRUCTION                C
C           OF A PHASE PLOT PORTRAIT.                               C
C CCCCCCCCCCCCCCCCCCCCCCCCCCCCCCCCCCCCCCCCCCCCCCCCCCCCCCCCC C
      DIMENSION DDX(2500),DX(2500),X0(2500)
      OPEN(UNIT=11,FILE='C:\V12S1.TXT',STATUS='OLD')
      OPEN(UNIT=12,FILE='DX12.TXT',STATUS='NEW')
C   NOS IS THE NUMBEER OF SAMPLES
C   SF IS THE SAMPLING FREQUENCY
C   READ(*,*)NOS
C   READ(*,*)SF
      SF = 4000
      NOS= 2030
      DT = 1./SF
      SUM1=0.
      DO 10 I = 1,NOS
          READ(11,*)DDX(I)
          SUM1 = SUM1 + DDX(I)
10  CONTINUE
      SMEAN = SUM1/NOS
      DO 15 I = 1,NOS
          DDX(I) = DDX(I) - SMEAN
15  CONTINUE

      CALL INTEGRAL(NOS,DT,DDX,DX)
      SUM2 = 0
      DO 16 I = 1,NOS
          SUM2 = SUM2 + DX(I)
16  CONTINUE
      SMEAN = SUM2/NOS

      DO 17 I=1,NOS
          DX(I) = DX(I) - SMEAN
17  CONTINUE

      CALL INTEGRAL(NOS,DT,DX ,X0)
      SUM3 = 0

```

```

DO 18 I = 1,NOS
    SUM3 = SUM3 + X0(I)
18 CONTINUE
SMEAN = SUM3/NOS
DO 19 I = 1,NOS
X0(I) = X0(I) - SMEAN
19 CONTINUE

DO 20 I = 1,NOS
DX(I)=DX(I)*10**6
X0(I)=X0(I)*10**8
WRITE(12,5)DDX(I),DX(I),X0(I)
5 FORMAT(1X,F5.3,3X,F15.9,3X,F16.8)
20 CONTINUE
STOP
END

SUBROUTINE INTEGRAL(NOS,DT,X,Y)
DIMENSION X(0:2500),Y(0:2500)
X(0)=X(1)
X(NOS+1)=X(NOS)
DO 10 I=1,NOS
SUM = 0.
DO 20 J=1,I
SUM = SUM + ( X(J-1) + 4*X(J) + X(J+1) ) *DT
20 CONTINUE
Y(I) = (1/6.) * SUM
10 CONTINUE
RETURN
END

```